People's Democratic Republic of Algeria

Ministry of Higher Education and Scientific Research

University of 20 août 1955 Skikda
Faculty of Sciences
Department of Chemistry

Thesis

Submitted to the Department of Chemistry

of the Requirement for PhD Degree (LMD) in Chemistry

Specialty: Materials chemistry

Presented by

REHIMI ZEHOUA

Preparation and characterization of Fe_3O_4/MWCNTs nanocomposite. Application for the removal of organic dyes from aqueous solution.

Élaboration et caractérisation d'un nanocomposite Fe_3O_4/MWCNTs. Application dans l'élimination des colorants organiques en solution aqueuse.

Presented publicly on: 17/01/2022

Jury composed of:

Chettah Abd Elhak	Full Professor	President	University of Skikda.
Halladja Sabrina	Full Professor	Supervisor	University of Skikda.
Ayadi Hassan	MCB	Co-supervisor	University of Skikda.
Chiha Mahdi	Full Professor	Examiner	University of Skikda.
Maouche Naima	Full Professor	Examiner	University of Ferhat Abbes Setif-1.
Hammouda Nadia	MCA	Examiner	University of Skikda.

Journal of New Technology and Materials (JNTM)
J. New Technol. Mater.
Vol. 10, N°01 (2020)31-37

OEB Univ. Publish. Co.

Synthesis and characterization of Fe_3O_4–MWCNTs adsorbent: application for bromocresol purple dye removal in aqueous medium

Zehoua Rehimi[a], Hassan Ayadi[b] and Sabrina Halladja[a,c]

[a] *Laboratory of Anticorrosion-Materials, Environment and Structures, Faculty of Technology, University of 20 Août 1955, Skikda 21000, Algeria*
[b] *Laboratory of Physico-Chemistry Research of Surfaces and Interfaces, Faculty of Sciences, University of 20 Août 1955, Skikda 21000, Algeria*
[c] *Laboratory of Innovative Techniques for the Environment Preservation, Faculty of Exact Sciences, University of Mentouri, Constantine 25000, Algeria*

Corresponding author, email: z.rehimi@univ-skikda.dz

Received date: Oct. 31, 2019 ; revised date: Feb. 24, 2020 ; accepted date: Apr. 24, 2020

Abstract

Magnetic nanocomposite was synthesized from iron salts and multi-walled carbon nanotubes (Fe_3O_4–MWCNTs) using the chemical coprecipitation method. The characterization of Fe_3O_4–MWCNTs adsorbent was carried out using X-Ray diffraction (XRD); Fourier transform infrared spectroscopy (FTIR); Brunauer-Emmett-Teller (BET) and scanning electron microscopy (SEM). The prepared material has exhibited a higher adsorption capacity 296.52 mg.g^{-1} to remove the Bromocresol purple (BCP) dye from aqueous solutions. Kinetic study shows that the equilibrium time reached after 80 minutes and the pseudo second order best suited this adsorption. Isotherm models indicate that the adsorption represented perfectly by the Langmuir. Thermodynamic study suggests that the sorption process is spontaneous, exothermic and physisorption type. This work focused on the efficiency of nanocomposite Fe_3O_4–MWCNTs as a magnetically separable adsorbent compared with pure multi-walled carbon nanotubes.

Keywords: Carbon nanotubes; magnetite; composite; dye; adsorption.

1. Introduction

Aquatic pollution is one of the most serious issues facing the humanity today, several contaminants like heavy metals [1], metalloids, pesticides and dyes invaded wastewater and caused health hazards [2]. About 7×10^5 tons / year of pigments and dyes are synthesized [3], and used in many fields like industrials, cosmetic, pharmaceutical, painting, textile and food [4]. Dyes whatever acidic or basic can be carcinogenic, mutagenic and toxic due to their complex aromatic structures, stability to biological degradation, and persistent nature in effluents [3,5]. Bromocresol purple is one of the organic dyes that can be produced from textile, paper, industries and pharmaceutical. Consequently, the disposal of such product could be harmful to the environment and human health by causing several diseases [6]. Nowadays, the removal of dyes in aqueous medium captivates the interest of many researchers around the world. Various methods are using in water remediation like conventional techniques which become not efficient enough for recalcitrant contaminants [7], adsorption [8], extraction [6], advanced oxidation processes [9], ozonation and photocatalysis, etc [10]. Only few studies have focused on the removal of Bromocresol Purple [6]. As reported by Farida M. S. E. El-Dars et al , the adsorption of BCP was carried out by using bentonite carbon composite at high temperature T= 313 K, the maximum adsorption capacity estimated to (Q_{max} = 0.1463 mg.g^{-1}) and equilibrium time achieved in 60 minutes [11]. Photochemical degradation of BCP dye was investigated also by Bousnoubra et al [12]; the present work studies the adsorption of BCP using a nanocomposite of commercial (MWCNTs) modified with magnetite (Fe_3O_4). The multi-walled carbon nanotubes adsorbent have an outstanding performance could be ascribed to its high adsorption capacity, unique structure, chemical stability [13] and huge specific surface area, etc [14]. Until now, the use of MWCNTs as adsorbent for BCP removal is very scarce in literature. To improve the performance of the dye removal by MWCNTs, magnetite lends support and enhances the adsorption process by faster and easier separation compared with boring filtration or centrifugation; the Fe_3O_4 may contribute as well in the adsorption process for dye removal [15]. In this context the Fe_3O_4–MWCNTs adsorbent was prepared using the coprecipitation method and characterized by X-ray diffraction, Fourier transform infrared spectroscopy, the Brunauer-Emmett-Teller and scanning electron microscopy analysis. Kinetics and equilibrium experiments of BCP dye adsorption onto the synthesized adsorbent studied in batch system.

2. Experimental

2.1. Materials

MWCNTs (Nanocyl 7000, diameter 1−10 nm, length 60−100 nm, purity >90%) were purchased from Nanocyl. Nitric acid 53% were purchased from Montplet & Esteban SA. Sodium was purchased from Prolabo (purity 98%); Hydrochloric acid was purchased from Sigma Aldrich. Ferrous sulfate heptahydrate ($FeSO_4.7H_2O$), ferric chloride hexahydrate ($FeCl_3.6H_2O$) and Bromocresol purple BCP dye were purchased from Biochem, these reagents were used without further purifications, all aqueous solutions were prepared using distilled water. The spectrophotometric measurements were performed with UV-visible Shimadzu 1605; X-ray Diffractometer system XPERT-PRO was utilized to identify the existing phases in nanocomposite. Analysis morphological examination of the nanocomposite was carried out by scanning electron microscopy (SEM) (model DSM 962; Carl Zeiss Meditec AG, Jena, Germany) ; Fourier Bruker infrared microscope "Hyperion 2000" This equipment is coupled with a Vertex 70 interferometer and optimized for Mid-IR (4000-400 cm^{-1}); specific surface area was obtained through a micromeritics ASAP- 2020.

2.2. Samples preparation

To improve the adsorption efficiency of the MWCNTs, it is necessary that an oxidation step be performed to purify, open and cut extremities; in order to facilitate their functioalization to their composites by the enhancement of interfacial adhesion [16]. The most common method is to add carboxylic acid groups onto the surface of MWCNTs by chemical oxidation using nitric acid [17]. Therefore, a small amount equal to 1g of MWCNTs was oxidized by 200 mL of HNO_3 (3M) then sonicated for 1 h to disperse the sample very well in the solution. After that at 100°C the mixture was stirred for 4 h then it was rinsed and filtrated with distilled water until the filtrate became neuter, the obtained material was dried at 80°C and calcined at 450 °C for 4h. The modification of oxidized MWCNTs by magnetite was occurred by coprecipitation method; in 75 mL of mixture containing 1.49 g $FeCl_3.6H_2O$ and 0.76g $FeSO_4.H_2O$; 0.5g of oxidized carbon nanotubes were added into the solution and stirred at 70°C under inert gas N_2. The precipitation of Fe_3O_4 required basic medium so, 15 ml of NaOH (0.5 M) was added by dropwise until pH=11. The mixture was stirred and heated at 70°C for 3 h to realize the following reaction:

$$Fe^{2+}+2Fe^{3+}+8OH^-+MWCNTs \rightarrow Fe_3O_4-MWCNTs+4H_2O$$

The nanocomposite obtained was washed several times and dried at 100°C for 4 h [15]. The magnetite was prepared using the coprecipitation method as described by Poedji Loekitowati Hariani et al [18].

2.3. Adsorption process

The Fe_3O_4−MWCNTs nanocomposite (20 mg) was added to 200 mL of BCP (10 $mg.L^{-1}$). The mixture was stirred at intervals of time ranging from 1 min to 120 min. After that, the residual dye concentration was determined by spectrophotometer using suitable calibration curves at appropriate wavelengths corresponding to λ_{max} = 431 nm the maximum absorbance. A simple separation was carried out using the permanent magnet (fig. 1). The amount of dye adsorbed per unit of mass has been calculated using the following formula [19].

$$Q_t = \frac{(C_0 - C_t)V}{m} \quad (1)$$

Q_t: Adsorption capacity given by ($mg.g^{-1}$).
C_0: The initial concentration of dye ($mg.L^{-1}$).
C_t: The residual concentration of dye ($mg.L^{-1}$).
V: The volume of the solution (L).
m: The mass of the adsorbent used (g).

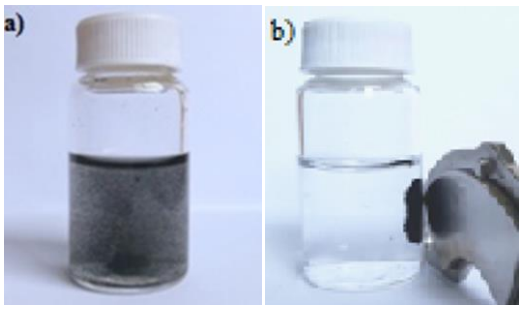

Figure1. (a). Before magnetic separation (b). After magnetic separation.

3. Results

3.1. Characterization of samples

The XRD patterns of both commercial MWCNTs (red color) and nanocomposite (black color) are represented in (fig. 2). The peaks At 2θ values about 26° indicate the presence of carbon nanotubes before and after modification, the presence of magnetite in the Fe_3O_4−MWCNTs spectra is confirmed by the appearing of new peaks at different 2θ values 30.1°, 35.5°, 43.1°, 53.5°, 57.0° and 62° [20]. To estimate the average size of the Fe_3O_4−MWCNTs composite, Debyee Scherrer formula was applied [21]:

$$D = \frac{0.9\lambda}{\beta cos\theta} \quad (2)$$

Where β (rad): The full width at half maximum (FWHM) of the diffraction; θ (rad): The Bragg's diffraction angle and λ=1.54060 A^0 the X-Ray wavelength of the copper (Cu) radiation used in XRD. The size of particles was found to be about 19±1 nm. The MWCNTs, Fe_3O_4 and Fe_3O_4− MWCNTs were analyzed by FTIR. As shown in (fig. 3), the peak at 580 cm^{-1} in both Fe_3O_4− MWCNTs and Fe_3O_4 curves is attributed to Fe−O bond; while 3398 cm^{-1} is referred to O-H in the magnetite and the nanocomposite. In the Fe_3O_4−MWCNTs pattern new peaks are slightly appear at 1393 cm^{-1} and 1587 cm^{-1} which

are indicated the presence of COO-Fe bond [22], 1651 cm^{-1} is referred to C=O stretching. The peak at 3450 cm^{-1} is appropriated to O-H stretching [15]. Surface Area analysis of Fe_3O_4– MWCNTs was carried out using the BET technique; (fig. 4) represents the isotherms of adsorption/desorption of N_2 onto Fe_3O_4 and Fe_3O_4–MWCNTs nanoparticles, these last are of type II. The isotherm of the Fe_3O_4 is less than that of nanocomposite indicates a lower specific surface area and lower adsorption quantity due to the porosity and high adsorbability of oxidized–MWCNTs [23]; the (Table 1) reveals some textural properties of the corresponding samples Fe_3O_4 and Fe_3O_4–MWCNTs. The SEM screened in (fig.5) the morphology of MWCNTs, Fe_3O_4 and Fe_3O_4–MWCNTs in images A, B and C, respectively. A homogenous surface of curly hair-like structure was shown in (image A) [24]; large quantities of spherical-shaped magnetite were observed in (image B) which were almost coated homogenously the multi-walled carbon nanotubes in the (image C) and the surface was relatively uniform.

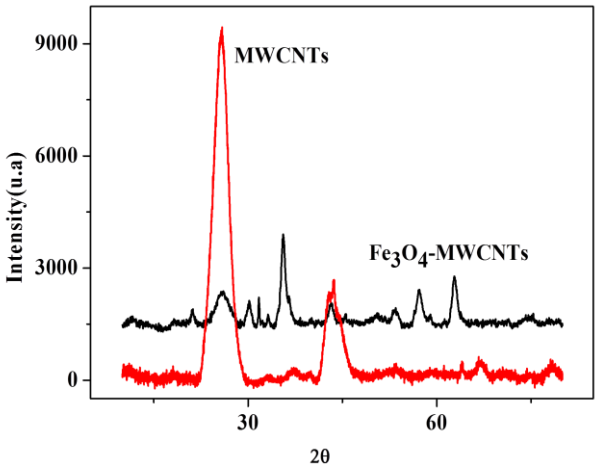

Figure 2. XRD patterns of MWCNTs and Fe_3O_4–MWCNTs

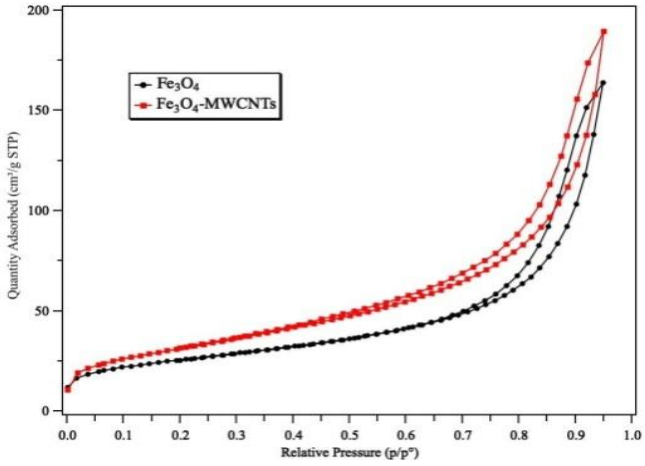

Figure 4. Nitrogen adsorption/desorption isotherm of the Fe_3O_4 and Fe_3O_4–MWCNTs samples

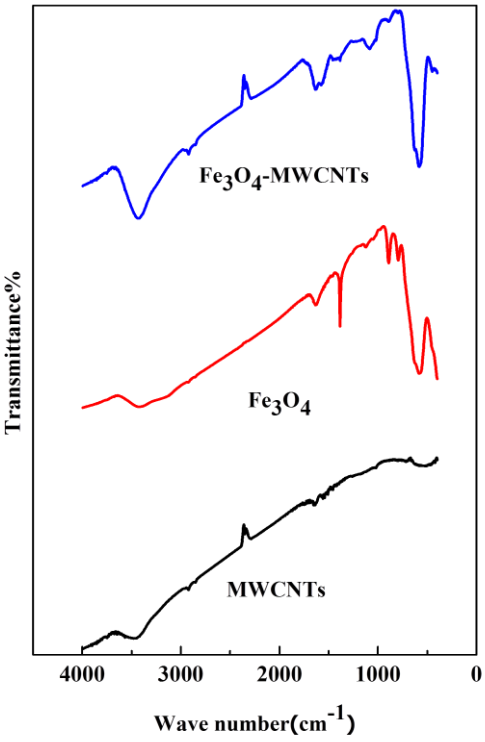

Figure 3. FTIR spectra of pure MWCNTs, Fe_3O_4 and Fe_3O_4–MWCNTs

Table1: Textural property of Fe_3O_4 and Fe_3O_4–MWCNTs samples

Sample	Mean specific surface area $S_{BET}(m^2.g^{-1})$	Mean Total pore volume $V_{Total}(cm^3.g^{-1})$	Mean pore size (nm)
Fe_3O_4	90.026	0.241	13.171
Fe_3O_4–MWCNTs	113.264	0.273	11.195

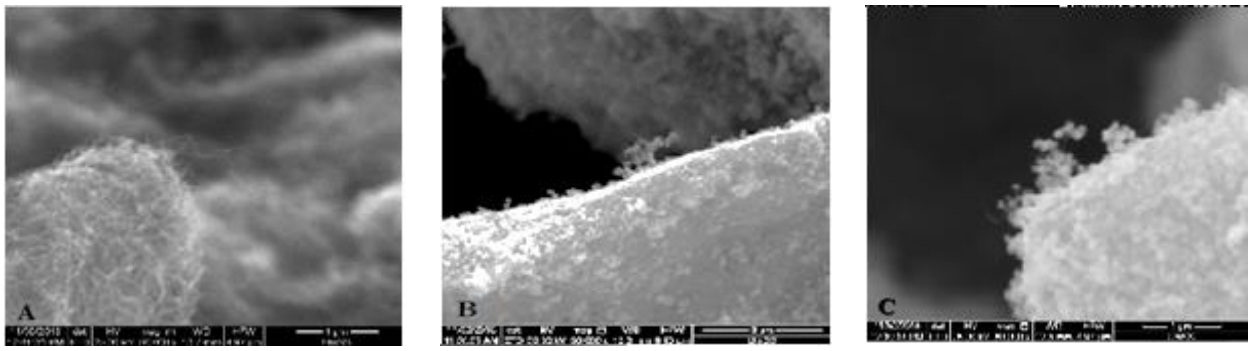

Figure 5. SEM images: (A) MWCNTs, (B) Fe_3O_4 and (C) Fe_3O_4–MWCNTs nanocomposite

3.2. Effect of initial pH

The optimization of pH is very required because it can control both the surface charge of the adsorbent and adsorbate [25]. In this part of study, the effect of initial pH of solution onto the adsorption of BCP was investigated; 20 mg of Fe_3O_4–MWCNTs was added to dye solution (200 mL, 10 mg.L^{-1}) at room temperature and different pH ranging from 5 to 11. (fig.6) shows a slight increase of adsorption capacity in acidic medium until pH = 8 as an optimum value followed by a careless decreasing at pH = 11. The zeta potentials of the adsorbent particles were previously discussed; OH and COOH groups were introduced onto the surface of Fe_3O_4–MWCNTs after the chemical treatment by nitric acid. This leads to the protonation of nanocomposite surface where a positive charge can be dominated in acidic medium [15]. The pH value correlates to Zeta potential of composite Fe_3O_4–MWCNTs was estimated to 6.6 as seen in (fig.6 inset). After this value the negative charges dominated the adsorbent surface in alkaline medium [26]. The Bromocresol purple characterized by acid dissociation constant pK_a equal to 6.3 [11]. Thus the dye molecules are negatively charged in acidic medium and positively charged in basic medium [27, 6]. Hence, a favorable electrostatic attraction occurred between the Fe_3O_4–MWCNTs surface and BCP molecules at all the pH range. Therefore, we can consider the effect of initial pH neglected and carry out the rest of experiments at free pH which was close to 6.

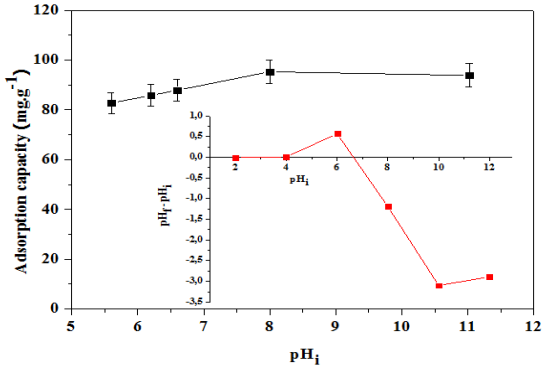

Figure 6. Effect of pH on the adsorption of BCP onto composite (m=20 mg of Fe_3O_4–MWCNTs; 200 mL and 10 mg.L^{-1} of BCP; at room temperature). (Inset) Zeta potential of Fe_3O_4–MWCNTs

3.3. Kinetic study

The interest of this study is to determine the contact time necessary to reach the adsorption equilibrium of BCP dye onto the Fe_3O_4–MWCNTs. As shown in (fig.7), the graph of adsorption capacity Q_t as function of time depicts the adsorption mechanisms as follow, rapid increase of Q_t at the initial stage (20 minutes). After that, a slow adsorption took place (from 20 to 80 minutes); in the last phase (from 80 to 120 minutes) the equilibrium achieved wherein a plateau was observed. As a result, the maximum adsorption capacity and equilibrium time were estimated to be about 90.28 mg.g^{-1} and 80 minutes, respectively. The kinetic models provide us by information about adsorption mechanism and the mode of solute transfer from the liquid phase to the solid phase [28]. For this purpose, the literature reported a number of models such as the Lagergren model or pseudo-first-order model (PFO) [29], the Blanchard model or pseudo-second order kinetic model (PSO) [30] and Weber and Morris model or intraparticle diffusion model [31]. The nonlinear plots of data regression of PFO and PSO were represented in order to determine kinetics using the following expressions in succession [2]:

$$\frac{dq}{dt} = k_1(Q_e - Q_t) \quad (3)$$

$$\frac{dq}{dt} = k_2(Q_e - Q_t)^2 \quad (4)$$

Where k_1 and k_2 are the rate constants for pseudo first and second order kinetics (min^{-1}); Q_t: amount adsorbed at time t (mg. g^{-1}); Q_e: amount adsorbed at equilibrium (mg.g^{-1}) and t: time (min). The equation of intraparticle diffusion model allows the determination of the diffusion rate in pores using the following equation [32]:

$$Q_t = k_d t^{\frac{1}{2}} + C_d \quad (5)$$

k_d (mg.g^{-1}.$min^{-1/2}$) : is the intraparticle diffusion rate constant and C_d(mg.g^{-1}): is the intercept. According to the data summarized in (Table 2), the pseudo second-order is favorable in this adsorption attributed to both of the correlation coefficient and adsorption capacity Q_e. (fig.8) screened that the curve was not linear over the whole time range, it is indicated that not only one process affected the adsorption. As seen from plot pattern there is two stages, the first one is characterized by rapid increase of Q_t at the initial process stage due to the adsorption of dye molecules on the external surface of adsorbent. A slow adsorption

took place referred to the second phase attributed to a slow diffusing of BCP particles into porous structure of nanocomposite because the external sites were occupied very quickly in the first stage.

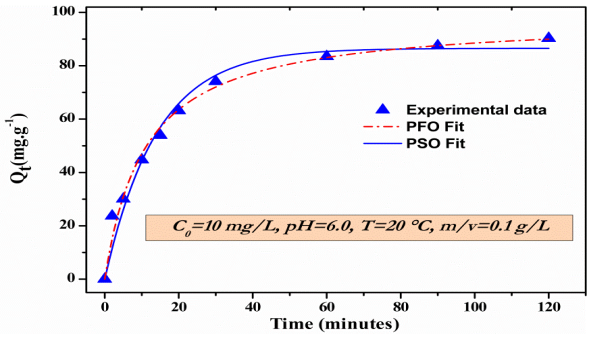

Figure 7. Adsorption kinetic of BCP using Fe_3O_4–MWCNTs

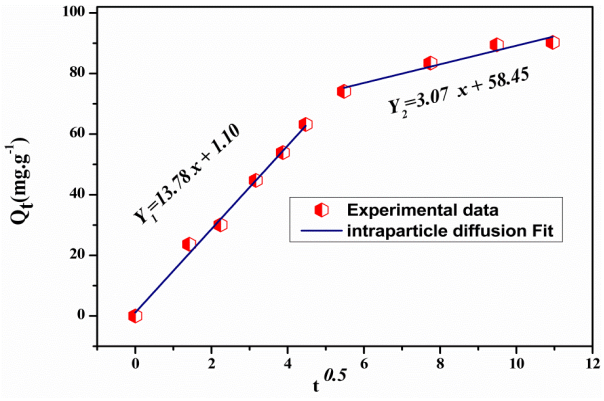

Figure 8. Intra-particle diffusion plot for BCP dye adsorption onto Fe_3O_4–MWCNTs adsorbent

Table 2: Kinetic parameters of PFO, PSO and intraparticle diffusion models.

Kinetic model	$q_{e(exp)}$ (mg.g^{-1})	$q_{e(cal)}$ (mg.g^{-1})	k_1 (L.min^{-1})	R^2	S.E
PFO model	90.28	86.53	0.071	0.972	2.94
PSO model	$q_{e(exp)}$ (mg.g^{-1})	$q_{e(cal)}$ (mg.g^{-1})	k_2 (g.min	R^2	S.E
	90.28	91.12	0.009	0.988	2.91
Intraparticle diffusion model	First step	K_{ip1} (mg.g^{-1}.min$^{-1/2}$)	C_1(mg.g^{-1})	R_1^2	S.E
		13.78	1.10	0.993	1.52
	Second step	K_{ip2} (mg.g^{-1}.min$^{-1/2}$)	C_2(mg.g^{-1})	R_2^2	S.E
		3.07	58.45	0.913	4.66

To conclude, the significant deviation of the line revealed that intra-particle diffusion was not the only rate limiting stage for this process [33].

3.4. Adsorption isotherm models

The modeling of experimental isotherm plays a critical role to understand the sorption process. The isotherm of BCP dye adsorption material was obtained by varying the initial concentration of BCP (from 5 to 50 mg.L^{-1}) at 293±1K. The plot of $Q_e = f(C_e)$ at equilibrium presents the isotherm of BCP adsorption onto Fe_3O_4–MWCNTs which corresponds to isotherm type I according to the Brunauer classification [34]. Among the most used theoretical models, the equilibrium data were fitted to the Langmuir, Freundlich and Dubinin-Radushkevich equations. The Langmuir model suggests that the adsorption takes place on a homogeneous phase, the nonlinear form of Langmuir equation is given by [35]:

$$Q_e = \frac{Q^0_{max}.k_L.C_e}{1+k_L.C_e} \quad (6)$$

Where Q^0_{max} (mg.g^{-1}) represents the maximum monolayer adsorption capacity; k_L(L.mg^{-1}) is the Langmuir constant. The favorability of adsorption can be confirmed using the dimensionless parameter, which is defined as

$$R_L = \frac{1}{1+K_L.C_0} \quad (7)$$

The value of R_L indicates that the type of isotherm can be irreversible if (R_L = 0), unfavorable if (R_L>1), linear if (R_L=1) and favorable while (0<R_L<1) [36].

The Freundlich model assumes that the multilayer adsorption takes place on a heterogeneous surface of adsorbent. This model is given as follows [37]:

$$Q_e = k_F.C_e^n \quad (8)$$

Where k_F is the Freundlich constant associated with adsorption capacity, n indicates the adsorption intensity.

The Dubinin-Radushkevich model is applied to evaluate the free adsorption energy that determines the nature of interactions adsorbent-adsorbate. The nonlinear equation of D-R model is outlined as follows [38]:

$$Q_e = Q_{DR}e^{-k_{DR}.\varepsilon^2} \quad (9)$$

Where Q_{DR} (mg.g^{-1}) is the maximum adsorption capacity; k_{DR}(mol^2.kJ^{-2})constant related to the sorption energy. ε is the Polanyi potential given by:

$$\varepsilon = RT\ln(1+\frac{1}{c_e}) \quad (10)$$

Where R is the gas constant (8.314 J.mol^{-1}.K^{-1}). The mean sorption energy E can be calculated using the following equation:

$$E = \frac{1}{\sqrt{2k_{DR}}} \quad (11)$$

The nature of sorption could be discussed according to the E value; if the magnitude of E is between 8 and 16 kJ.mol^{-1}, the adsorption process is occurred by ion exchange, while the values of E<8 kJ.mol^{-1} reveal the physical nature of interactions [39]. As shown in (fig.9), the data of aforementioned isotherms were plotted using nonlinear forms. According to the outcomes summarized in

(Table.3), the Langmuir model was selected as an optimum adsorption isotherm due to its highest correlation value corresponding to R^2=0.998; the prepared nanocomposite exhibited a high maximum adsorption capacity Q^0_{max}(mg.g^{-1}) estimated to be about 296.52 mg.g^{-1}. In addition, the mean adsorption energy E was found to be about 2.06 kJ.mol^{-1}; it demonstrates the physical nature of dye adsorption onto Fe_3O_4–MWCNTs.

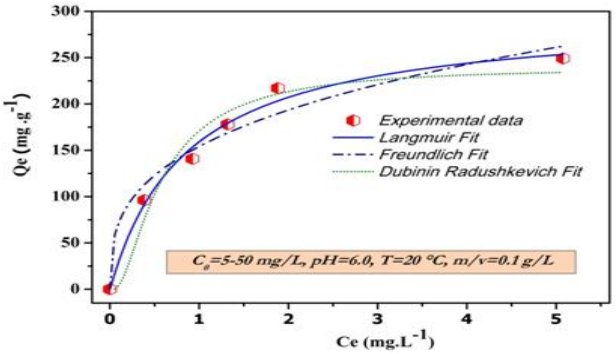

Figure 9. Isotherm models of BCP adsorption onto Fe_3O_4–MWCNTs adsorbent

3.5. *Thermodynamic study*

The thermodynamic study was carried out to estimate standard Gibbs free energy change (ΔG^0), standard enthalpy change (ΔH^0), and standard entropy change (ΔS^0). The different energies can be related with each other by equation (13) as follows [2]:

$$\Delta G^0 = -RTLnK_e \quad (12)$$

$$\Delta G^0 = \Delta H^0 - T\Delta S^0 \quad (13)$$

$$K_e = \frac{Q_e}{C_e} \quad (14)$$

To find the magnitudes of aforementioned energies, the Van'tHoff equation (15) was plotted (fig.10):

$$LnK_e = -\frac{\Delta H^0}{RT} + \frac{\Delta S^0}{R} \quad (15)$$

Where R is the universal gas constant, Q_e is the adsorption capacity at the equilibrium thermodynamic (mg.g^{-1}),C_e is the concentration at the equilibrium, T is the temperature (K), and K_e is the equilibrium thermodynamic constant [40]. (Table.4) shows that exothermic nature of the adsorption phenomena was confirmed by negative value of standard enthalpy change ΔH^0, besides the value of that parameter can give an idea about the type of interactions between adsorbate and adsorbent, therefore 15.45kJ.mol^{-1} is lower than 20 kJ.mol^{-1} indicates that van der Waals interactions occurred between BCP molecules and Fe_3O_4–MWCNTs particles, so then the physisorption type took place in this case. The negative values of standard Gibbs free energy change ΔG^0 show that the adsorption process was favorable, spontaneous and enthalpy controlled, where the negative value of ΔS^0 exhibites the decrease of randomness at the interface solid-liquid when the adsorption occurred [2,41].

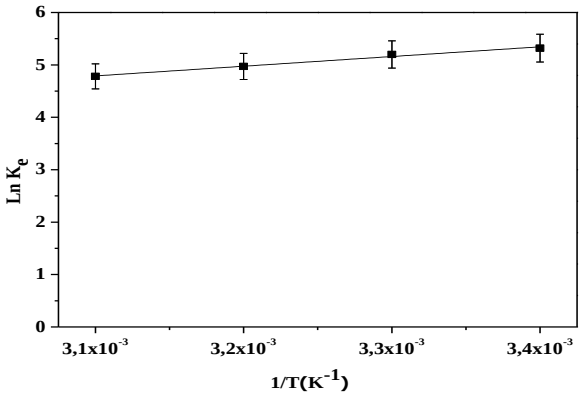

Figure 10. Effect of temperature on the equilibrium thermodynamic constant

Table 3: Isotherm constant parameters for the BCP adsorption onto Fe_3O_4–MWCNTs adsorbent

Models	Parameter				
Langmuir	Q^0_{max}(mg.g^{-1}) 296.52	k_L(L.mg^{-1}) 1.160	R^2 0.988	SE 16.3	R_L 0.079
Freundlich	k_F(mg.g^{-1}) 154.22	n 0.327	R^2 0.957	SE 9.55	-
Dubinin–Radushkevich	Q_{max}(mg.g^{-1}) 239.47	k_{DR}(mol^2.K^{-1}J^{-2}) 1.18×10^{-7}	R^2 0.956	SE 14.51	E(kJ.mol^{-1}) 2.06

Table 4: Thermodynamic parameters of BCP adsorption onto Fe_3O_4–MWCNTs adsorbent

ΔG^0 (kJ.mol^{-1})				ΔH^0(kJ.mol^{-1})	ΔS^0(J.mol^{-1}.K^{-1})	R^2
293 K	303 K	313 K	323 K	-15.45	-8.09	0.981
-13.08	-13.00	-12.66	-12,84			

4. Conclusion

Efficiently, a small amount of nanocomposite Fe_3O_4–MWCNTs exhibited a high adsorption capacity of BCP from aqueous solution 296.52 $mg.g^{-1}$; without high energy or complicated devices. This study highlights the modification of MWCNTs by magnetite which offers a simple separation and low cost adsorbent compared with pristine multi-walled carbon nanotubes. Kinetic study indicated that the pseudo second order fitted well the process. Meanwhile, the Langmuir isotherm best suited the experimental data. Results suggest that the adsorbent can have a potential application in industry.

Acknowledgments

The authors thank Pr. Plinio Innocenzi, Dr. Luca Malfatti, Róbert Ludmerczki (Materials Science and Nanotechnology Laboratory, Sassari, Italy) for their technical supports.

References

[1] M. Larakeb, L. Youcef, S. Achour, J. New Technol. Mater. 6 (2016) 19.
[2] A. Bonilla-Petriciolet, D. I. Mendoza-Castillo, H. E. Reynel-Ávila, Eds., Adsorption Processes for Water Treatment and Purification, Springer International Publishing, Cham, 2017.
[3] M. A. Al-Ghouti, M. A. M. Khraisheh, S. J. Allen and M. N. Ahmad, Journal of Environmental Management. 69 (2003) 229.
[4] P. B. Biru, D. R. Oren and Y. Diquarternasi, Malaysian Journal of Analytical Sciences 13 (2009) 185.
[5] V. Hernández-Montoya, M. A. Pérez-Cruz, D. I. Mendoza-Castillo, M. R. Moreno-Virgen and A. Bonilla-Petriciolet , Journal of Environmental Management. **116** (2013) 213.
[6] L. Aljerf, Journal of Environmental Management. 225 (2018) 120.
[7] R. Shrivastava, V. Christian and B. R. M. Vyas, Enzyme and Microbial Technology. 36 (2005) 333.
[8] L. C. Morais, O. M. Freitas, E. P. Gonçalves, L. T. Vasconcelos and C. G. González Beça, Water Research. 5 (1999) 979.
[9] M. C. Pereira, L. C. A. Oliveira and E. Murad, Clay miner. 47 (2012) 285.
[10] S. G. de Moraes, R. S. Freire and N. Dura, Chemosphere . 40 (2000) 369.
[11] F. El-dars, MSE, Ibrahim, H.M., Farag, Int. J. Sci. Eng. Res. 6 (2015) 6188.
[12] I. Bousnoubra, K. Djebbar, A. Abdessemed and T. Sehili, Desalination and Water Treatment, (2016) 1.
[13] S. Mallakpour, V. Behranvand, F. Mallakpour, Carbohydrate Polymers. 224 (2019) 115.
[14] H. Gao, S. Zhao, X. Cheng, X. Wang and L. Zheng, Chemical Engineering Journal. 223 (2013) 84.
[15] N. Dalali, M. Habibizadeh, K. Rostamizadeh and S. Nakisa, Asia-Pac. J. Chem. Eng. (2014).
[16] W. Yan, G. Lian, S. Jing et al, Chemical physics letters. 432 (2006) 205.
[17] R. M. Lago, S. C. Tsang, K. L. Lu, Y. K. Chen and M. L. H. Green, J. Chem. Soc., Chem. Commun. (1995) 1355.
[18] P. L. Hariani, M. Faizal, R. Ridwan, M. Marsi and D. Setiabudidaya, IJESD (2013) 336.
[19] N. Fayoud, S. A. Younssi, S. Tahiri and A. Albizane, J. Mater. Environ. Sci. *6* (2015) 12.
[20] V. Cleveland, J.-P. Bingham and E. Kan, Separation and Purification Technology. 133 (2014) 388.
[21] L. Houcine, L. Sonia, R. Schneider and T. B. Chaabane, Chemistry Africa. 1 (2018) 37.
[22] W.Yan, H.Bing, H. Xiaoyang, Procedia Engineering. 27 (2012) 632.
[23] X. Hu, B. Liu, Y. Deng, H. Chen, S. Luo, C. Sun, P. Yang and S. Yang, Applied Catalysis B: Environmental. 107 (2011) 274.
[24] M. H. Razali, A. Ahmad, M. A. Azaman and K. A. M. Amin. Inter J of app chem. 12(2016)273.
[25] A. T. Vo, V. P. Nguyen, A. Ouakouak, B. T. Nieva, A., Doma, H. N. Tran, H. P. Chao, Water. 11(2019) 1164.
[26] X. Bai, Liu, Y.L. Yu, Z. Hua, Scientific reports. *6* (2016) 32845.
[27] H. Tavakkoli, A. Ghaemi, M. Mostofizadeh, Int. J. Sci. Resin Knowledge. 2 (2014) 340.
[28] Y. Ho, Journal of Hazardous Materials. 136 (2006) 681.
[29] A. S. Özcan, B. Erdem, A. Özcan, Colloids and Surfaces A: Physicochemical and Engineering Aspects. 226 (2005) 73.
[30] Y. S. Ho and G. McKay, Wat Res. **33** (1999) 578.
[31] W. J. Weber and J. C. Morris, Journal of the Sanitary Engineering Division . 89 (1963) 31.
[32] N. Rouahna, D. Barkat, A. Ouakouak and E. Srasra, Journal of Environmental Chemical Engineering. 6 (2018) 1226.
[33] L.M.SUN and F. Meunier, Techniques de l'ingénieur Génie des procédés. 2 (2003) 2730.
[34] I. Langmuir, J. Am. Chem. Soc. 40(1918)1361.
[35] K. R. Hall, L. C. Eagleton, A. Acrivos and T. Vermeulen, Industrial & Engineering Chemistry Fundamentals. 5(1966)212.
[36] O. Hamdaoui and E. Naffrechoux, Journal of Hazardous Materials. 147 (2007) 381.
[37] H. Freundlich, Zeitschrift für Physikalische Chemie. 57 (1907) 385.
[38] K. O. Adebowale, B. I. Olu-Owolabi and E. C. Chigbundu, JEAS. 04 (2014) 89.
[39] A. S. Özcan, B. Erdem and A. Özcan, Colloids and Surfaces A: Physicochemical and Engineering Aspects. 266 (2005) 73.
[40] A. S. Özcan and A. Özcan, Journal of Colloid and Interface Science. 276 (2004) 39.
[41] G. Crini and P.-M. Badot, Progress in Polymer Science. 33 (2008) 399.

DEDICATION

This thesis is dedicated to

Dear Dad Abdelazize & Mom Nassima, my sweet sisters Rim, Loubna and Farida my little brothers Omar and Mehdi, my lovely angels Zine, Adem, Chames, Hanine and Flyne.....

To my second family Mrs. Halladja Sabrina and Mr . Ayadi Hassane, to all my friends and colleagues...

Zehoua

Acknowledgments

It is with great pleasure and enthusiasm that I am writing this page. Much more than the final point of the scientific writing, this page represents a meditation on a period relating, five years of life very rich in events.

From the bottom of my heart, I would like to thank God for his great blessing and his immense mercy which accompanied me throughout my school to a university career, and for the strength, he gave me to complete this thesis.

I would like to express my deepest gratitude to my supervisor Professor Halladja Sabrina and her co-supervisor Doctor Ayadi Hassane who honored me by directing this work, as well as for their availability, their passion, their patience, and all the attention they have given to me along with the realization of this work.

I would also like to thank Professor Chettah Abd Elhak, who kindly gave me the honor of chairing the jury.

I wish to express my gratitude to the members of the jury who have kindly devoted part of their time to my thesis: Professor Maouche Naima, Doctor Hammouda Nadia and Professor Chiha Mahdi.

I am pleased to express my sincere thanks to all the teachers of the Department of Chemistry for the richness and quality of their teaching and for the great efforts they make to provide their students with up-to-date training.

A special thanks are addressed to Doctor Boudraa Issam for his relevant advice, his moral and scientific support, his listening, his encouragement throughout this work and his sympathy. I would like to express my gratitude from the bottom of my heart.

Acknowledgments

This work was carried out in the laboratory of Hall technology, University of Skikda. I would like to thank Linda, Fulla , Houda, Nawal, Nora and Samira for their help.

Finally, I will not forget my friends for their encouragement over the years especially Khaoula Kerbouche, Hayoune Asma, Bouchareb Imane, Satouh Sara and Kabir Hamza. Thank you for keeping me entertained and supporting me to the end.

List of tables

N°	Title	Page
Chapter I: Carbon nanotubes, magnetite and nanocomposite		
Table.I.1	Structures and characteristics of SWCNTs and MWCNTs	05
Table.I.2	CNTs as adsorbent/catalyst support for water treatment	11
Table.I.3	Comparison of different chemical methods used in the preparation of magnetite nanoparticles	20
Table.I.4	Magnetite properties	22
Chapter II: Wastewater treatment		
Table.II.1	Types of dyes	40
Table.II.2	Effect of pH medium on different dye adsorption using Fe_3O_4/MWCNTs adsorbent	44
Table.II.3	Thermodynamic parameters	47
Table.II.4	SRP of most common oxidizing agents	48
Chapter III: Materials and methods		
Table.III.1	Manufacturer and quality of reagents used	57
Table.III.2	Physical-chemical characteristics of BCP and CV dyes	58
Chapter IV: Results and discussion		
Table.IV.1	The average size of nanoparticles	78
Table.IV.2	SSA of samples	81
Table.IV.3	Concentration values and their corresponding absorbance of the calibration curve	81
Table.IV.4	Kinetic parameters of PFO, PSO and intraparticle diffusion models	87
Table.IV.5	Isotherm constant parameters for the adsorption of BCP onto Fe_3O_4/MWCNTs nanocomposite	89
Table.IV.6	Thermodynamic parameters	91
Table.IV.7	Concentration values and their corresponding absorbance of the calibration curve	93
Table.IV.8	Effect of weight ratio on dye removal and rate constant	94
Table.IV.9	Effect of hydrogen peroxide concentration on dye removal and rate constant	96
Table.IV.10	Effect of temperature on removal and rate constant	99
Table.IV.11	The rate constant of CV dye degradation	105

N°	Title	Page
Chapter I: Carbon nanotubes, magnetite and nanocomposite		
Figure.I.1	Methods have been developed previously for producing CNTs	06
Figure.I.2	Most current types of CNTs functionalization	08
Figure.I.3	Unit cell and structure of Fe_3O_4	14
Figure.I.4	Chemical oxidation and preparation of Fe_3O_4/MWCNTs via hydrothermal route	25
Chapter II: Wastewater treatment		
Figure.II.1	AOPs types	48
Chapter III: Materials and methods		
Figure.III.1	(a) and (b) the two forms of BCP molecule structures, (c) molecule structure of CV	58
Figure.III.2	Representation of nitric acid oxidation of CNTs	60
Figure.III.3	Illustration of Fe_3O_4/MWCNTs preparation steps	61
Figure.III.4	X-ray diffraction	62
Figure.III.5	FTIR Spectrometer diagram	64
Figure.III.6	Diagram of SEM	65
Figure.III.7	Representation of a cell traversed by an incident beam of intensity $I_{0\lambda}$, and beam of intensity $I_{t\lambda}$ is transmitted	67
Figure.III.8	Operating principle of a single-beam spectrophotometer	68
Figure.III.9	Illustration of BCP adsorption onto Fe_3O_4 /MWCNTs nanocomposite	70
Figure.III.10	Illustration of CV degradation using Fe_3O_4/MWCNTs catalyst via heterogeneous Fenton process	71
Figure.III.11	Illustration of CV degradation using Fe_3O_4/MWCNTs catalyst via heterogeneous photo-Fenton process	73
Chapter IV: Results and discussion		
Figure.IV.1	XRD patterns of pure MWCNTs, Fe_3O_4/MWCNTs nanocomposites and magnetite	78
Figure.IV.2	FTIR spectra of (a) oxidized-MWCNTs, (b) Fe_3O_4 and (c) Fe_3O_4/MWCNTs	79

Figure.IV.3	SEM images of A. pure MWCNTs, B. magnetite and C. Fe_3O_4/MWCNTs nanocomposite	80
Figure.IV.4	Calibration curve for BCP standards	82
Figure.IV.5	Plot showing the pH_{PZC} of Fe_3O_4/MWCNTs nanocomposites	83
Figure.IV.6	Effect of pH on the BCP adsorption onto nanocomposite (pH= 5.5-11; m=20 mg of Fe_3O_4/MWCNTs; 200 mL; 10 $mg.L^{-1}$ of BCP and ±293 K)	84
Figure.IV.7	Adsorption kinetic of BCP using Fe_3O_4/MWCNTs and fitting curves of kinetic models (pH= 6; m=20 mg of Fe_3O_4/MWCNTs; 200 mL; 10 $mg.L^{-1}$ of BCP and ±293 K)	86
Figure.IV.8	Intra-particle diffusion plot for BCP dye adsorption onto Fe_3O_4/MWCNTs adsorbent (pH=6; m=20 mg of Fe_3O_4/MWCNTs; 200 mL; 10 $mg.L^{-1}$ of BCP and ±293 K)	86
Figure.IV.9	Isotherms model of BCP adsorption onto Fe_3O_4/MWCNTs nanocomposites (pH=6; m=20 mg of Fe_3O_4/MWCNTs; 200 mL; 5-50 $mg.L^{-1}$ of BCP and 293 K)	89
Figure.IV.10	Effect of temperature on the adsorption of BCP dye onto Fe_3O_4/MWCNTs nanocomposites (pH=6; m=20 mg of Fe_3O_4/MWCNTs; 200 mL; 10 $mg.L^{-1}$ of BCP)	90
Figure.IV.11	Temperature effect on the equilibrium thermodynamic constant (pH=6; m=20 mg of Fe_3O_4/MWCNTs; 200 mL; 10 $mg.L^{-1}$ of BCP)	91
Figure.IV.12	The UV-visible absorption spectrum of crystal violet (CV) [CV]= 6$mg.L^{-1}$	92
Figure.IV.13	Calibration curve of Crystal violet	93
Figure.IV.14	Effect of weight ratio on dye removal ($m_{catalyst}$ =20 mg; pH=2.5, $[H_2O_2]$ = 0.2 $mol.L^{-1}$; [CV] = 4 $mg.g^{-1}$; V=200 mL; 298 K)	95
Figure.IV.15	Linearization of the first order kinetic at different weight ratio	95
Figure.IV.16	Effect of hydrogen peroxide concentration onto dye removal ($m_{catalyst}$ =20 mg; pH=2.32; [CV] = 4 $mg.g^{-1}$; V=200 mL; 298 K)	97
Figure.IV.17	Linearization of the first order kinetic at different H_2O_2 concentrations	97
Figure.IV.18	Effect of temperature on dye removal ($m_{catalyst}$ =20 mg; $[H_2O_2]$=0.14 $mol.L^{-1}$; pH=2; V=200 mL; $[CV]_0$ = 4 $mg.L^{-1}$)	98

Figure.IV.19	Linearization of the first order kinetic at different temperature	99
Figure.IV.20	Determination of activation energy	100
Figure.IV.21	Reuse of the catalyst ($m_{catalyst}$ =20 mg; [CV] = 6 $mg.L^{-1}$; [H_2O_2] =0.14 $mol.L^{-1}$; pH=2.3; V=200 mL; 318 K; t=210 min)	101
Figure.IV.22	The influence of different systems onto the degradation of CV dye (293 K; V=100 mL; $[CV]_0$=4 $mg.L^{-1}$; pH = 2.5 ; m = 10 mg, [H_2O_2]=0.14 $mol.L^{-1}$)	103
Figure.IV.23	Linearization of the first order kinetic at different systems	104
Figure.IV.24	Comparison between the removal rates under polychromatic light obtained by different catalysts	104

Abbreviations and acronyms

3D	Three Dimensional
AC	Arc Discharge
AFM	Atomic Force Microscope
AOPs	Advanced Oxidation Processes
BCP	Bromocresol Purple
BET	Brunauer, Emmett, and Teller
C_e	Equilibrium Concentration of dye in solution
CFSE	Crystal Field Stabilization Energy
CNTs	Carbon Nanotubes
CoMoCat	Co–Mo Catalysis
CV	Crystal Violet
CVD	Chemical Vapor Deposition
DIPA	Disopropanolamine
DLS	Dynamic Light Scattering
D-R	Dubinin–Radushkevich
EDX	Energy Dispersive X-rays analysis
E_g	Band Gap Energy
FCC	Face Centered Cubic
Fe_3O_4/MWCNTs	Multi-Walled Carbon Nanotubes functionalized by magnetite
FTIR	Fourier Transform Infrared Spectroscopy
GPa	Giga Pascal
HiPco	High-Pressure Co

I_0	Incident light
JCPDS	Joint Committee on Powder Diffraction Standards
K_1	Pseudo-First-Order Rate Constant
K_2	Pseudo-Second-Order Rate Constant
K_e	Equilibrium Thermodynamic Constant.
K_i	Intraparticle Diffusion Rate Constant
K_L	Isotherm Constant of Langmuir
LA	Laser Ablation
MB	Methylene Blue
MIPA	Mono-Isopropanolamine
MR	Magnetic Resonance
Ms	Magnetization Saturation
MWCNTs	Multi Walled Carbon Nanotubes
NIR	Near Infra-Red
NoCNTs	Ndoped Carbon Nanotubes
Ohm.cm	Ohm.centimeter
PAA	Poly(acrylic acid)
PET	Positron Emission Tomography
PFO	Pseudo-First-Order
pH_{pzc}	Point of Zero Charge
PSO	Pseudo-Second-Order
q_e	Adsorption Capacity at eEquilibrium

q_{max}	Maximum Adsorption Capacity
q_{D-R}	D-R constant ($mg.g^{-1}$);
q_t	Adsorption Capacity at any Time
R	Gas Constant (8.31 $J \cdot K^{-1} \cdot mol^{-1}$).
SE	Standard Error
SEM	Scanning Electron Microscope
SQUID	Superconducting Quantum Interference Device
SRP	Standard Reduction Potentials
SSA	Specific Surface Area
SWCNTs	Single Walled Carbon Nanotubes
T	Temperature (K).
t	Time
T_C	Curie Temperature
TEM	Transmission Electron Microscope
TPa	Tera Pascal
UV	Ultra-Violet
VSM	Vibrating Sample Magnetometer
wt%	Weight Percent
XRD	X-Ray Diffraction
β	Mean Sorption Free Energy
ΔG^0	Standard Gibbs Free Energy Change
ΔG_f^0	Standard Gibbs Free Energy of Formation

Abbreviations and acronyms

ΔH^0	Standard Enthalpy Change
ΔS^0	Standard Entropy Change
ε	Adsorption Potential

Contents

Introduction……..……..1

Chapter I : Carbon nanotubes, magnetite and nanocomposite

I.1. Introduction……...4

I.2. Carbon nanotubes……4

I.2.1. Types of carbon nanotubes and their structures……4

I.2.1.1. Single walled carbon nanotubes (SWCNTs)……4

I.2.1.2. Multi walled carbon nanotubes (MWCNTs)……4

I.2.2. Synthesis methods of CNTs……5

I.2.3. Properties of CNTs……...6

I.2.3.1. Chemical reactivity……6

I.2.3.2. Adsorption properties……6

I.2.3.3. Electronic properties……7

I.2.3.4. Mechanical properties……7

I.2.3.5. Thermal properties……7

I.2.3.6. Dispersion of CNTs……8

I.2.3.6.1. Non-covalent functionnalization……..……8

I.2.3.6.2. Covalent functionnalization……..8

I.2.3.6.3. Dispersion using surfactants.....8

I.2.3.6.4. Physical dispersion using ultrasonication……9

I.2.4. Application of CNTs……9

I.2.4.1. Application of CNTs for environmental remediation……9

I.2.4.1.1.CNTs and CNTs-based composites as sorbents……..……...….9

I.2.4.1.2. CNTs for catalysis reaction..……..……..……10

I.2.4.2. Application of CNTs in electronics……11

I.2.4.3. Application of CNTs in biomedicine……...12

I.2.4.4. Application of CNTs in gas storage……12

I.2.5. Advantages of CNTs…….....12

I.2.6. Toxicity…….....12

I.3. Magnetite……13

I.3.1. Structure of magnetite……13

I.3.2. Origin and Synthesis methods of magnetite…….....14

I.3.2.1. Chemical co-precipitation method……...14

I.3.2.2. Sol-gel method……16

Contents

I.3.2.3. Hydrothermal method……..17

I.3.2.4. Thermal decomposition method…….. 18

I.3.3. Comparison between the synthesis methods…….. 19

I.3.4. Characterization techniques for Fe_3O_4 nanoparticles…….. 21

I.3.5. Properties……21

I.3.5.1. Physical properties……...21

I.3.5.2. Thermal properties……...21

I.3.5.3. Magnetic properties……. 21

I.3.6. Applications……22

I.3.6.1. Lithium-ion batteries……23

I.3.6.2. Wastewater treatment…….. 23

I.3.6.3. Biomedical applications……...23

I.4. Fe_3O_4/MWCNTs nanocomposite…….. .23

I.4.1. Preparation techniques for functionalizing MWCNTs with Fe_3O_4..... 23

I.4.1.1. Chemical coprecipitation……23

I.4.1.2. Sol-gel method……24

I.4.1.3. Hydrothermal method……24

I.4.2. Application of Fe_3O_4/MWCNTs…….....25

I.4.2.1. Biosensors……25

I.4.2.2. Batteries……... 25

I.4.2.3. Drug delivery……... 25

I.4.2.4. Water remediation……26

I.5. Conclusion…….....26

References…….....27

Chapter II: Wastewater treatment

II.1. Introduction…...…….……..…… 39

II.2. Water pollution……... 39

II.2.1. Heavy metals…….. 39

II.2.2. Organic pollutants…… ..39

II.2.2.1. Cationic dyes.....…….....…….40

II.2.2.2. Anionic dyes…….....……..41

II.3. Wastewater treatment techniques for organic dyes using Fe_3O_4/MWCNTs nanocomposite…. 42

II.3.1. Adsorption…….. 42

Contents

II.3.1.1. Adsorption mechanism……..42

II.3.1.2. Types of adsorption……43

II.3.1.2.1. Chemical sorption……...43

II.3.1.2.2. Physical sorption……43

II.3.1.3. Factors affecting the adsorption of organic dyes……...43

II.3.1.3.1. Effect of pH……..43

II.3.1.3.2. Effect of initial dye concentration.....……44

II.3.1.3.3. Effect of temperature……44

II.3.1.3.4. Effect of adsorbent amount ……44

II.3.1.4. Adsorption kinetics……45

II.3.1.4.1. Pseudo-first-order……45

II.3.1.4.2. Pseudo-second-order……45

II.3.1.4.3. Intraparticule diffussion……....45

II.3.1.5. Adsorption isotherms……45

II.3.1.5.1. Langmuir isotherm model……45

II.3.1.5.2. Freundlich isotherm model……...46

II.3.1.5.3. Dubinin-Radushkevich (D-R)……..46

II.3.1.6. Thermodynamic study of adsorption……..46

I.3.1.7. Desorption……...47

II.3.2. Advanced oxidation processes (AOPs)…… ….....48

II.3.2.1. Heterogeneous Fenton-like reaction……..49

II.3.2.1.1. pH effect……49

II.3.2.1.2. H_2O_2 dosage effect……49

II.3.2.1.3. Initial dye concentration effect……50

II.3.2.1.4. Temperature effect……50

II.3.2.2. Heterogeneous photo-Fenton like reaction……...50

II.4. Conclusion……..51

References……..52

Chapter III: Materials and methods

III.1. Introduction…….. 57

III.2. Chemical products…….. 57

III.3. Physical and chemical characteristics of BCP and CV dyes…….58

III.4. Synthesis of Fe_3O_4/MWCNTs nanocomposite.……59

III.4.1. Activation of MWCNTs…….....59
III.4.2. Functionalization of MWCNTs by Fe_3O_4 via coprecipitation method.. 60
III.5. Synthesis of Fe_3O_4 iron oxide…… 61
III.6. Experimental methods of analysis and characterization…….....61
III.6.1. X-ray diffraction (XRD)…….....61
III.6.2. Fourier transform infrared spectroscopy (FTIR)….. 63
III.6.3. Scanning electron microscopy (SEM)….. 64
III.6.4. Brunauer, Emmett and Teller analysis (BET)…….....65
III.6.5. UV-visible spectrophotometer analysis for organic dyes…….....67
III.7. Efficiency of Fe_3O_4/MWCNTs nanocomposite on the removal of BCP by adsorption process69
III.7. 1. Determination of point of zero charge…… 69
III.7. 2. Preparation of standards and simple solutions…….....69
III.7. 3. Optimization of adsorption parameters.....69
III.7. 3.1. Effect of contact time on BCP adsorption…….69
III.7. 3.2. Effect of pH on BCP adsorption……...69
III.7. 3.3. Effect of temperature on BCP adsorption……..70
III.7. 4. Effect of initial dye concentrations and isotherms model for BCP adsorption…….. 70
III.8. Efficiency of Fe_3O_4/MWCNTs nanocomposite in the removal of CV dye via …… heterogeneous Fenton process……..70
III.8.1. Preparation of standards and sample solutions……... ...70
III.8.2. Optimization of degradation parameters……....70
III.8.2.1. Weight ratio effect on the degradation of CV dye……...70
III.8.2.2. Effect of hydrogen peroxide dose on the degradation of CV dye……71
III.8.2.3. Effect of temperature on the degradation of CV dye ……...71
III.8.2.4. Effect of initial concentration of CV dye on its degradation……...71
III.8.3. Reuse of the catalyst Fe_3O_4/MWCNTs.....71
III.9. Efficiency of Fe_3O_4/MWCNTs catalyst in the removal of CV under polychromatic light… 72
III.9.1. Preparation of Standards and Sample Solutions…….72
III.9.2. Removal of CV dye under polychromatic light …….....72
III.9.2.1. Photolysis of CV…….....72
III.9.2.2. Degradation of CV in the presence of H_2O_2 and light irradiation……..72
III.9.2.3. Degradation of CV in the presence of Fe_3O_4/MWCNTs and light irradiation 72
III.9.2.4. Photo-Fenton of CV using Fe_3O_4…….....72
III.9.2.5. Photo-Fenton of CV using Fe_3O_4/MWCNTs…….....73
III.10. Conclusion…….....73

References……...74

Chapter IV: Results and discussion

IV.1. Introduction…… 77

IV.2. Analysis and characterization of nanoparticles…….. 77

IV.2.1. XRD characterization…….....77

IV.2.2. FTIR characterization…….....78

IV.2.3. Morphology of the samples…… 79

IV.2.4. BET characterization…….....80

IV.3. Efficiency of Fe_3O_4/MWCNTs nanocomposites on the removal of BCP by adsorption process ……...81

IV.3.1. Analysis of BCP dye using UV-visible spectrophotometer…… ……. .81

IV.3.2. Optimization parameters…….....82

IV.3.2.1. The point zero charge of Fe_3O_4/MWCNTs nanocomposites and pH effect ...82

IV.3.2.1.1. The point zero charge of Fe_3O_4/MWCNTs nanocomposites.....82

IV.3.2.1.2. Effect of pH….....83

IV.3.2.2. Effect of contact time and kinetic study……84

IV.3.2.2.1.. Effect of contact time…….....84

IV.3.2.2.2 Kinetic models…….....84

IV.3.2.3. Effect of initial BCP concentrations and isotherm models……...87

IV.3.2.3.1. Effect of initial BCP concentrations……87

IV.3.2.3.2. Adsorption isotherm models ……87

IV.3.2.4. Effect of temperature and thermodynamic study……..89

IV.3.2.4.1. Effect of temperature……...89

IV.3.2.4.2. Thermodynamic study…….90

IV.4. Efficiency of Fe_3O_4 /MWCNTs nanocomposite in the removal of CV via heterogeneous Fenton process……. 92

IV.4.1. Spectrophotomtric analysis of Crystal Violet (CV)… ….....92

IV.4.1.1. Determination of the maximum absorption wavelength……...92

IV.4.1.2. Calibration curve……...92

IV.4.2. Optimization parameters…. 93

IV.4.2.1. Effect of Fe_3O_4/MWCNTs weight ratio……94

IV.4.2.2. Effect of hydrogen peroxide concentration……96

IV.4.2.3. Effect of temperature……..98

IV.4.3. Determination of activation energy……. 99

IV.4.4. The reuse of Fe_3O_4/MWCNTs nanocomposite…….. 100
IV.5. Efficiency of Fe_3O_4/MWCNTs catalyst in the removal of CV under polychromatic light.....101
IV.5.1. Photolysis of CV system……. 101
IV.5.2. Degradation of CV in the presence of H_2O_2 and light irradiation …….....101
IV.5.3. Degradation of CV in the presence of Fe_3O_4/MWCNTs and light irradiation …….. ...102
IV.5.4. Photo-Fenton of CV using Fe_3O_4…….....102
IV.5.5. Photo-Fenton of CV using Fe_3O_4/MWCNTs …….....102
IV.6. Conclusion……....105
References……...……..…106
Conclusion……...……111

Introduction

Nowadays the world faces a horrible issue which is water pollution, so the control of this problem becomes a priority and a necessity. Numerous contaminants are present in water like organic dyes, which can cause diseases and serious damage in environment **[1]**.

Various techniques are developing everyday to find the best way to the safe drinking water and save the planet. The most effective processes should be characterized by their simplicity, flexibility, low-energy and low cost requirements **[2]**.

Adsorption of organic dyes has been widely discussed in literature; it is recognized as an efficient technology for water treatment. Many nanocomposites have been used as new adsorbents. In this context, carbon nanotubes with their unique properties have attracted the attention of many researchers worldwide as a promising adsorbent, in particular, carbon nanotubes modified with iron oxide such as magnetite, which offer further advantages to adsorption process **[3]**.

Advanced oxidation processes are widespread methods used for the degradation of organic dyes. Heterogeneous Fenton and photo-Fenton are considered as effective methods due to their great oxidative power towards large scale of contaminants. Multi-walled carbon nanotubes functionalized with magnetite nanocomposites represent a good catalyst for heterogeneous Fenton reaction owing to their high stability, huge surface area and fast separation **[4, 5]**.

In this work, we investigated the capacity of the synthesized Fe_3O_4/MWCNTs as an adsorbent for the removal of Bromocresol Purple (BCP), and the degradation of Crystal Violet (CV) dye via heterogeneous Fenton and photo-Fenton reactions in aqueous solution.

Crystal Violet is a cationic dye which has large application in biology, transistors, batteries, detergents, printer industries and so on [3]. Bromocresol Purple is another dye which is anionic and has numerous applications in: tanneries, biology, printing activities, textile industries, etc. The uncontrolled release of these dyes leads to serious environmental problems and can cause several diseases **[6]**.

The targets of the present work are to synthesis nanocomposite made of MWCNTs and magnetite, to characterize the properties of this nanomaterial and to evaluate its adsorption capacity in the removal of Bromocresol Purple as a model of anionic dye.

Furthermore, we used Fe_3O_4/MWCNTs to investigate its efficiency in the degradation of Crystal Violet contaminant as a model of cationic dyes using heterogeneous Fenton and photo-Fenton reaction. The effect of the most important parameters onto adsorption and heterogeneous Fenton reaction was studied as well in order to obtain the optimal conditions.

This thesis consists of four chapters:

- The first chapter represents short literature review on :
  - Carbon nanotubes: (types; structure; synthesis methods; properties and applications);
  - Magnetite: (structure; origin and synthesis methods; characterization techniques available for Fe_3O_4; properties and application);
  - Fe_3O_4/MWCNTs nanocomposite: (preparation techniques and its application);
- The second chapter summarizes background information about:
  - Water pollution: (organic dyes and their types);
  - Wastewater treatment techniques for organic dyes using Fe_3O_4/MWCNTs nanocomposite: (adsorption; heterogeneous Fenton and photo-Fenton processes).
- In the third chapter, we described the experimental aspect by presenting:
  - Chemical products;
  - Physical and chemical characteristics of BCP and CV dyes;
  - Preparation method of Fe_3O_4/MWCNTs nanocomposite and magnetite;
  - Characterization of Fe_3O_4/MWCNTs nanocomposite by different techniques;
  - UV-visible spectrophotometer for dye analysis;
  - Preparation of standards and simple solutions;
  - Optimization of adsorption parameters;
  - Optimization of degradation parameters.
- The fourth chapter covers the obtained results of this study and their discussions which are:
  - Analysis and characterization of nanocomposite results;
  - Optimization parameters for the adsorption of BCP dye onto Fe_3O_4/MWCNTs;
  - Kinetic study of the adsorption;
  - Isotherm modeling of the adsorption;
  - Thermodynamic study of the adsorption;
  - Optimization parameters of the degradation of CV using heterogeneous Fenton oxidation;
  - Efficiency of Fe_3O_4/MWCNTs catalyst in the removal of Crystal Violet under polychromatic light.

Finally, we finished with general conclusion which highlighted the objective of this thesis and most important results obtained during the study with a proposal of some perspectives.

References

[1] R. Das, Carbon Nanotubes for Clean Water, Carbon Nanostructures, Springer, 2018, doi : https://doi.org/10.1007/978-3-319-95603-9_11

[2] A. Bonilla-Petriciolet, D. I. Mendoza-Castillo, et H. E. Reynel-Ávila, Éd., Adsorption Processes for Water Treatment and Purification. Springer, 2017, doi : 10.1007/978-3-319-58136-1

[3] N. Dalali, M. Habibizadeh, K. Rostamizadeh, et S. Nakisa, « Synthesis of magnetite multi-walled carbon nanotubes composite and its application for removal of basic dyes from aqueous solutions: REMOVAL OF BASIC DYES », Asia-Pacific Journal of Chemical Engineering, vol. 9, n° 4, p. 552-561 , 2014, doi: 10.1002/apj.1784.

[4] V. Cleveland, J.-P. Bingham, et E. Kan, « Heterogeneous Fenton degradation of bisphenol A by carbon nanotube-supported Fe_3O_4 », Separation and Purification Technology, vol. 133, p. 388‑395, sept. 2014, doi: 10.1016/j.seppur.2014.06.061.

[5] M. C. Pereira, L. C. A. Oliveira, et E. Murad, « Iron oxide catalysts: Fenton and Fenton like reactions – a review », Clay minerals., vol. 47, n° 3, p. 285‑302, sept. 2012, doi: 10.1180/claymin.2012.047.3.01.

[6] I. Bousnoubra, K. Djebbar, A. Abdessemed, et T. Sehili. «Decolorization of methyl green and Bromocresol Purple in mono and binary systems by photochemical processes: direct UV photolysis, Acetone/UV and H_2O_2/UV. A comparative study », Desalination and Water Treatment, vol. 57, n° 57 p. 27710-27725. 2016, doi: 10.1080/19443994.2016.1174741

Chapter I

Carbon nanotubes, magnetite and nanocoposite

I.1. Introduction

This chapter underlines the most important information about carbon nanotubes (CNTs), magnetite and the synthesis methods of the nanocomposite Fe_3O_4/MWCNTs (multi-walled carbon nanotubes functionalized by magnetite) followed by the various applications of Fe_3O_4/MWCNTs in many fields and on the top of them water treatment.

I.2. Carbon nanotubes

Carbon nanotubes (CNTs) have been one of the most amazing nanomaterials over the last years. In this context, it can contribute in solving the century difficulties, especially in water treatment field **[1]**. CNTs can be described as one or several graphene planes rolled up and closed on themselves, thus forming one or several co-axial cylinders consisting only of carbon atoms. They have been observed for the first time at transmission electron microscope (TEM) in 1991 by S. Iijima during his work on fullerenes **[2]**.

I.2.1. Types of carbon nanotubes and their structures

CNTs have a cylindrical shape comprising of graphene layers which consisting only of carbon atoms located in hexagonal form, and connected among themselves by strong covalent bonds **[1]**. Mainly, there are two types of this nanomaterial: single and multi walled carbon nanotubes **[3]**.

I.2.1.1. Single walled carbon nanotubes (SWCNTs)

SWCNTs are simpler to picture as a single shell composed of graphene sheet rolled up to form a tubular conformation **[1]**. Their diameter ranges between 0.4 and 2 nm, whereas their length can achieve several micrometers depending on the synthesis conditions **[3, 4]**; SWCNTs may have arm chair, chiral, zigzag or helical structures **[5]**.

I.2.1.2. Multi walled carbon nanotubes (MWCNTs)

MWCNTs comprise of several coaxial cylinders, each one consisting of a single sheet of graphene surrounding a hollow core. The nanotubes have an outer diameter varies from 2-100 nm, and an inner diameter between 1-3 nm, while their length ranges from 1 to several micrometers **[6]**. MWCNTs are the third carbon allotrope hybridized sp^2 like the fullerenes; the delocalized electron cloud onto the wall ensures the interactions between two successive layers in multi carbon nanotubes **[7]**. We can distinguish two structures of MWCNTs depending on their layer arrangements: the first structure is parchment-like which consists of layer of graphene rolling around it; the second one is the Russian doll model in which the graphene layers are arranged in concentric structure **[8]**. Table I.1 shows the structures and some characteristics of SWCNTs and MWCNTs.

Table.I.1. Structures and characteristics of SWCNTs and MWCNTs **[1, 9-11]**.

	SWCNTs	**MWCNTs**
Structure		
Young's Modulus (GPa)	1054.0	1200.0
Tensile strength (GPa)	75.0	150.0
Cost	Higher price	lower price

I.2.2. Synthesis methods of CNTs

Mainly, there are three common methods to produce carbon nanotubes: arc discharge (AC), laser ablation (LA) and chemical vapor deposition (CVD). Furthermore, researchers are trying everyday to find cheaper techniques to synthesize them. Figure.I.1 summarizes the most available methods used in carbon nanotubes production. It is interesting to note that almost of these techniques use prevalent experimental parameters like carbon feedstock, temperature and metal catalysts. Some of those methods are for the synthesis of SWCNTs such as LA and template/ bottom up, and others are more appropriate to produce MWCNTs such as CVD, hydrothermal and electrolysis. While AC considered as an old method that can be applied for the two types of carbon nanotubes. Furthermore, some studies proved the efficiency of domestic microwave oven as a fast and cheap technique use several methods like: mixture, metal complex, nickel nanoparticles and nano-fiber in producing the carbon nanotubes **[1]**.

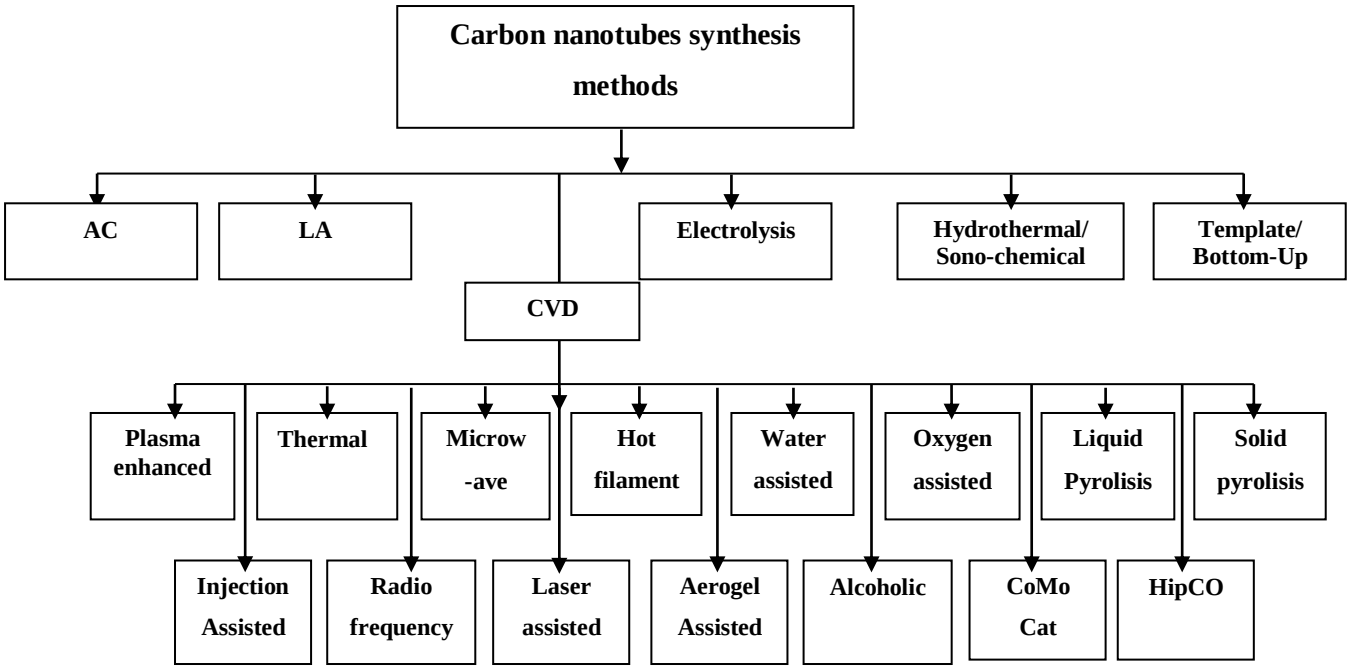

Figure.I.1. Methods have been developed previously for producing CNTs **[1]**.

I.2.3. Properties of CNTs

CNTs have outstanding properties which make them much needed in various fields, like huge surface area, high mechanical strength besides a good thermal and electrical conductivity **[12]**.

I.2.3.1. Chemical reactivity

CNTs exhibit a better chemical reactivity than that of graphene layers due to their curvature surfaces. Basically, the reactivity of nanotubes depend on the mismatch of orbital π which occurred by the increasing of curvature. So, a distinction should be made between a nanotubes sidewall and end caps. For the same cause, shorter diameter of the tubes leads to higher reactivity **[10]**. CNTs have a hydrophobic character; as a result they do not exhibit wetting behavior with the majority of aqueous solvents **[13]**. Furthermore, it is possible to obtain a covalent chemical modification at sidewalls and the end caps of nanotubes **[10]**.

I.2.3.2. Adsorption properties

Carbon nanotubes can interact with gases or other species and adsorb them either onto external or internal surfaces, this property besides their high surface area and huge pore volumes make gas storage significant **[14]**. The curvature of graphene layers can decrease adsorption heat if we compared it with planar graphite layers. Actually, graphene sheets rolling up around themselves in order to create the tubes which resulting rehybridization of the atom orbital, leading to a change of the density of π orbital in graphene sheet **[10]**.

I.2.3.3. Electronic properties

Many studies have demonstrated that CNTs showed unique electronic properties which can be affected by various parameters such as the degree of crystallinity, chirality, defects and different diameters **[12, 13]**. The resistivity of SWCNTs as a metal ranges from 0.34×10^{-4} to 1.0×10^{-4} Ohm.cm **[14]**. Taking into account carbon atoms in nanotubes located in hexagonal structure, where each atom is bonded through sp^2 molecular orbitals to three neighboring carbons covalently. So, in each unit the fourth valence electron stays free and delocalizes over the entire lattice which add an electric character to CNTs. This allows CNTs to be conductors or semi-conductors according to their chirality type **[11, 15]**. The electronic properties of SWCNTs and MWCNTs have been relatively investigated because of their great applications in the last decade **[11, 16]**.

I.2.3.4. Mechanical properties

Literature considered CNTs as extremely strong materials, particularly in the axial direction **[17]**, despite many studies have suggested that CNTs in radial direction are relatively soft **[12]**. They possess a high Young's modulus varies from 1000 to 5000 GPa, when the steel exhibits only 208 GPa which is lower five times than CNTs **[10]**. Their tensile strength as well has very high values **[12]**. Nanotubes are considered as extremely flexible material due to their good length. These compounds are therefore potentially suitable for use in composite materials which require anisotropic properties **[10, 18, 19, 20]**.

I.2.3.5. Thermal properties

Besides their unique electronic and mechanical properties CNTs also have important thermal properties. Embedding pristine or functionalized carbon nanotubes even in small loading (only 1 %) added to various materials can improve the thermal conductivity. Therefore, literature considered nanocomposites based on carbon nanotubes as a useful material that can be applied in thermal management **[12]**. Kim et al, 2001 reported that the measurements of the thermal conductivity at room temperature are higher than that of graphite (3000 W/K) for individual MWCNTs **[21]**. Such properties depend mainly on various factors like: structure, diameter, length, morphology, the structure defects number and impurities **[12]**.

I.2.3.6. Dispersion of CNTs

One of the issues related to CNTs is the tubes agglomeration, caused by weaker intermolecular forces, resulting lower dispersion in various polymeric matrices and also in different solvents. The CNTs can be functionalized to overcome the bundle formation, which even improves their dispersion in such mediums. Therefore, it is very important to purify or

functionalize CNTs to boost their homogeneous dispersion and degree of reactivity. Purification eliminates impurities that be left after the synthesis of CNTs, whereas functionalization produces a new functional groups onto the surface of the tubes **[22]**. Hence, to functionalize and disperse carbon nanotubes particles researchers use different methods. Figure.I.2 represents the most current methods of functionalization.

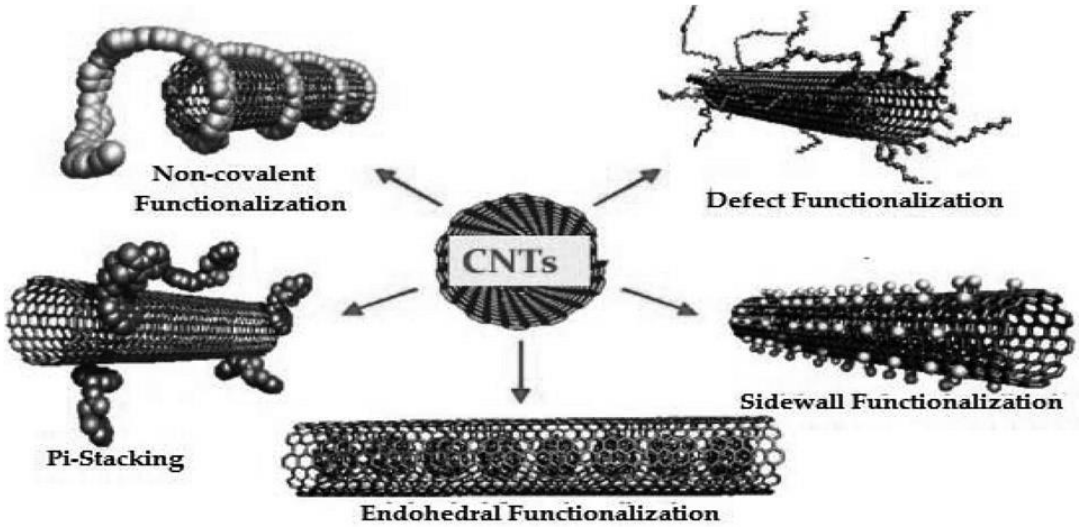

Figure.I.2. Most current types of CNTs functionalization **[23]**.

I.2.3.6.1. Non-covalent functionalization

This functionalization method is dependent on Van der Wall's forces besides hydrophobic or π-π interactions. Among the applications of such type of functionalization we find: non-covalent protein interactions, the use of surfactant especially with SWCNTs wrapping. Literature has considered non-covalent functionalization as an important and nondestructive method due to the fact that this type does not significantly modify or cause damage to the CNTs structure **[23]**.

I.2.3.6.2. Covalent functionalization

In this kind of functionalization, the chemical groups are introduced onto the sidewall of carbon tubes with an irreversible manner and permanently. After a covalent functionalization, various desired groups like carboxylic are attached to the ends or the side chains of CNTs. This chemical functionalization has a great important because it can be attached with polymeric particles covalently and well dispersed in many solvents. Despite, it can produce defects in the CNTs structure **[12]**.

I.2.3.6.3. Dispersion using surfactants

The application of surfactants was also reported for the reason of CNTs dispersion in polymers **[24]**. The most common surfactants used to reduce the aggregative tendency and

bundle formation of CNTs in different solvents are the following: polyethylene glycol, dodecyl-benzene sodium sulfonate and sodium dodecyl sulfate **[12]**.

I.2.3.6.4. Physical dispersion using ultrasonication

The physical dispersion is also an effective method to reduce the agglomeration of CNTs using an ultrasonication technique, which provides the bundles of CNTs by certain vibrational energies that can overcome the interactions within the nanoparticles and dispersed them **[12]**.

I.2.4. Application of CNTs

There are several potential applications of CNTs and their nanocomposites, owing to their unique properties. They are considered as promising materials in different fields including water remediation, electronics, biomedicine, energy, sensors and in actuators **[12]**. Due to their diverse applications, CNTs are developing rapidly in nanotechnology. Many researchers have focused on the creation of new properties in order to expand the number of applications **[25]**; some of these interest applications are described with further detail.

I.2.4.1. Application of CNTs for environmental remediation

Water remediation using CNTs is also a fast growing field, especially in adsorption studies. Researchers have considered carbon nanotubes as an innovative technology in wastewater treatment, regarding to their efficiency in the removal of several contaminants such as organic pollutants, arsenic, heavy metals and fluoride **[26]**. Carbon nanotubes possess specific properties which make them an attractive material, such as huge surface area, hydrophobic character, hollow structure and high length. In addition, it can be simple to functionalize the CNTs surface. This nanomaterial and its composite can be used in water purification as a sorbent or rather as a catalyst **[27]**.

I.2.4.1.1. CNTs and CNTs-based composites as sorbents

In literature, carbon nanotubes are considered as a better adsorbent comparing with the most common materials using in water treatment such as clay, activated carbon and zeolite. They possess stronger interactions, high adsorption efficiency, suitable surface area and rapid equilibrium for the elimination of a large range of organic and inorganic pollutants **[28]**. In the following study, contribution of CNTs in water purification is discussed. Adsorption process of organic compounds onto carbon nanotubes has been widely studied. Simultaneously, various mechanisms are occurred onto the surface of nanotubes such as electrostatic, hydrogen bonds and π-π interactions **[29]**. This kind of adsorption is principally affected by functional groups, active sites, defects and morphology of CNTs and even the molecules of organic contaminant **[30]**. Raw CNTs have a hydrophobic surface that makes

them more suitable to adsorb hydrocarbons (e.g., benzene, hexane and cyclohexane), alcohols also (e.g., ethanol and 2-propanol). The functionalization of CNTs surface can increase the oxygen content, decrease the hydrophobicity and reduce the surface area; which leads to lower adsorption capacity of nonpolar hydrocarbons and planar chemicals as a consequence of weak contact between adsorbent and contaminant molecules. As a result, carbon nanotubes have proved their worth in environment remediation, by their high adsorption capacity towards a large number of pollutants including organic dyes, heavy metal, radioactive cesium and strontium ions **[27]**.

I.2.4.1.2. CNTs for catalysis reaction

Water pollution remains as a serious issue facing the humanity, which needs large interest to save the planet. In this context, researchers since 1976 have been investigated the efficiency of semiconductors in water remediation using photocatalytic oxidation/reduction method. Multiple semiconductors such as titanium dioxide, iron oxides and zinc oxide have been extremely discussed since then **[31]**. Despite, the efficiency of those semiconductors is not high enough, and their ultraviolet photoresponse speed is not significant. Hence, the modification of TiO_2 properties to develop them is necessary in order to reach higher photocatalytic activity for the removal of organic contaminants. In the other hand, carbon nanotubes seem like the best candidate to play the role of a catalyst ; regarding to their notable chemical stability, special electronic behavior, small size and hollow shape, good absorbability and large surface area that expand the light adsorption zone and improve the quantum efficiency **[27]**. Table.I.2 summarizes few studies of CNTs and CNTs based-composites used in water purification.

Table.I.2. CNTs as adsorbent/catalyst support for water treatment.

Catalyst	Method	contaminant	Important observations	Ref
SWCNTs/TiO_2	Photocatalysis	Oil	-Excellent antifouling -High separation efficiency -High-self-cleaning performance	**[32]**
TiO_2/SWCNT aerogel	Photocatalysis	MB	-Significant visible light photoactivity	**[33]**
Fe_3O_4-MWCNT	Photo-Fenton	Rhodamine B	-Rapid and efficient removal of Rhodamine B	**[34]**
MWCNT/TiO_2	Photocatalysis	MB	-High improvent in visible light photocatalysis	**[35]**
Fe_3O_4/CNT	Adsorption	Organophosp-horus Pesticides	-Simple separation - Good reproducibility	**[36]**
Fe_3O_4/CNT	Adsorption	Copper ions	-Effective adsorbent -Simple and fast removal	**[37]**
MWCNTs-OH-PbO_2	Electrocatalysis	Pyridine	-High removal efficiency	**[38]**
CNT sponge	Electrocatalysis	Antibiotic tetracycline	-High degradation efficiency >88%	**[39]**
NoCNTs	Catalysis	Phenol	-Excellent stability -High catalytic activity	**[40]**

I.2.4.2. Application of CNTs in electronics

Carbon nanotubes are already used as field-emission sources by applying a potential between the anode and CNTs surface. Due to the curvature shape of CNTs, electrons can be easily emitted from tips of the tubes **[41, 42]** or since oxidized tips are present. As a result, carbon nanotubes can be applied to produce several electronic devices, such as flat panel displays, bright lamps, intense light and X-ray sources. However, they are excellent emitters, CNTs-based composites also considered as good electron-emission surfaces. Furthermore, the application of CNTs in this field has a lot of advantages such as the stability of the field emission for an extended duration, high current densities, and prolonged lifetimes of the devices and absence of ultra-high vacuum requirement **[12]**.

I.2.4.3. Application of CNTs in biomedicine

In the field of biomedicine, there are many applications of carbon nanotubes including biomedical imaging, biosensors and drug delivery **[43]**.

I.2.4.4. Application of CNTs in gas storage

CNTs can operate as efficient containers for gas or metals regarding to their hollow cylindrical structure. Researchers found that multiple necessary species (e.g. metals, oxides, metal carbides) can be inserted into CNTs structure using various processes such as arc-discharge, chemical treatment, electrochemical and solidstate techniques **[44]**. The main issue relating to these methods is that CNTs can not encapsulate gaseous compounds. Literature indicated that SWCNTs is able to store both hydrogen and Argon gases and the same results were revealed concerning MWCNTs. Furthermore, experiments proved that nitrogen gas can be introduced into MWCNTs using only one process. The essential advantage offered by the storage of chemical species is the fuel cells fabrication, which can feed electric vehicles. However, there are few problems facing the storage using CNTs, thereby literature may not consider this material as the best container for hydrogen. Nevertheless, further studies and measurements should be carried out with a view to clarifying these outcomes **[12]**.

I.2.5. Advantages of CNTs

Literature has documented numerous advantages of carbon nanotubes which is summarized as follow, outer and inner surfaces that can be easily functionalized, large inner volume depend on their diameter, two open ends which make the incorporation of chemical species relatively easier inside the tubes, ultra-light weight and unbreakable during their manipulation, excellent elastic nature, the ability to enter cells through spontaneous mechanism regarding to their tiny size and tubular shape, may represent relatively lower cytotoxicity, they can be excreted through urine 96% and 4 % by faeces, non-biodegradable, non-immunogenic nature and biocompatible **[45, 46]**.

I.2.6. Toxicity

Recently, carbon nanotubes are widely used in various areas because of their outstanding properties. However, there are few issues related with their application, particularly the toxicity problem. CNTs may have serious impact on pulmonary system of human being, which is the principle route of exposure **[47]**. Oxidative stress and inflammation can be caused after an over-exposure to the dust of CNTs. In order to minimize this toxicity, preventive techniques must be respected **[48]**. Previous study indicated that both rigidity and length of CNTs can affect the pro-inflammatory resulted by the exposure to them **[49]**. Further work is therefore required to establish the potential effect of certain physiochemical

properties **[50]**. As the characteristics of CNTs surface are the main influencers on the pro-inflammatory **[51]**, researchers expected that the modification of CNTs through their incorporating in polymeric matrices in order to modify their surface characteristics, can be led to lower toxicity without the loss of their unique properties and keep using them in numerous applications. Thus, a strict strategy focused on the developing of inherently safer nanoparticles, seems to be the best way to overcome the toxicity problem of such materials. Various studies interested on CNTs toxicity revealed that modification of their surface is the key to minimize their danger **[12]**.

I.3. Magnetite

Currently, there are broad studies on magnetic nanoparticles in various fields including both applications and fundamental research. Magnetite (Fe_3O_4) has been attracted the eyeballs of scientists due to its outstanding properties that can meet the critical needs of numerous applications **[52]**. Magnetite is among the known iron oxides easily obtained and synthesized **[53]**. Briefly, the magnetic Fe_3O_4 can be described as a hard nanomaterial with black color. This shiny iron oxide possess a ferromagnetic character, it exists in nature and can even be synthesized through several methods in order to achieve specific nanoparticles **[54]**.

I.3.1. Structure of magnetite

Magnetite particles are consisted of two oxidation states of iron Fe (II) and Fe (III), generally identified as Fe_3O_4 but its more accurate formula is Fe (II)$Fe(III)_2O_4$. This iron oxide is one of the minerals class elements, well known as spinels with the general formula of $A^{2+}B_2{}^{+3}O_4{}^{2-}$, where A and B can also take other oxidation states as the divalent, trivalent and quadrivalent or be other cations such as zinc, magnesium, manganese, titanium, chromium, silicon and aluminum. In the case of magnetite the A and B are the same cations with a variation in their charges **[55]**. Actually, the crystal structure of magnetite fits an inverse spinel trend with alternating layers of tetrahedral-octahedral and octahedral. Figure.I.3 shows that ferrous Fe (II) species are occupied half of the octahedral sites, owing to their large crystal field stabilization energy (CFSE).While, ferric Fe (III) atoms are occupied alternatively the other half of the octahedral lattice and all the sites of tetrahedral lattice. In addition, the face centered cubic (FCC) adhere to the unit cell of magnetite **[56]**.

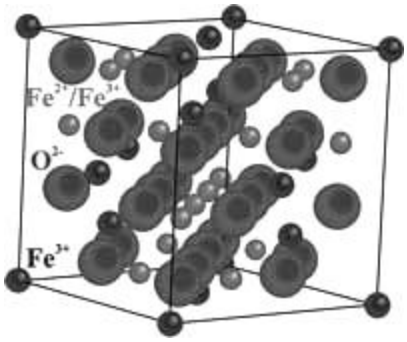

Figure.I.3. Unit cell and structure of Fe_3O_4 **[56]**.

I.3.2. Origin and synthesis methods of magnetite

Among the various iron oxides, magnetite is considered as the most available ferromagnetic materials on the earth. Fe_3O_4 particles are commonly formed in terrestrial environments extending from metamorphic rock and igneous to all types of sedimentary. Furthermore, magnetite is also present in the intracellular of several lineages like animals, protozoa and bacteria **[57]**. In addition, it has been existed in materials suspected to have extraterrestrial origin such as the Martian meteorite ALH84001 **[58]**. Recently, many studies have focused on synthesize of magnetic magnetite with a view to reach sufficient control on its properties, size, shape and crystallinity. Nowadays, there are numerous routs for the preparation of Fe_3O_4 iron oxide, which can divide onto chemical, physical and biological techniques. In terms of simplicity, performance and reproducibility, the chemical technique is preferable comparing with other routs **[59]**. In shorter time and lower cost, Chemical route can offer new materials with great homogeneity by changing the precursor combination. Even so, this technique suffers from few drawbacks such as agglomeration of nanoparticles during the synthesis procedure and the formation of impurities and intermediates. To obtain specific properties of magnetite nanomaterial, researchers should study deeply the synthesis method in order to know the process details, the mechanism and especially the influencing factors that can affect size, structure, magnetic character and size distribution of the nanoparticles **[52, 60]**.There are variety of synthesis methods such as co-precipitation **[61]**, sol-gel **[62]**, hydrothermal **[63]**, thermal decomposition and so on **[64]**.

I.3.2.1. Chemical co-precipitation method

Chemical co-precipitation technique is considered as the best candidate for Fe_3O_4 producing, because it is simple and requires less chemicals and equipments **[65]**. Generally, this process depends on the precipitation of iron ions using an alkaline solution added to the mixture under specific conditions as an inert atmosphere and a desired temperature **[66]**. Mainly, there are two different routes to synthesis Fe_3O_4 molecules through co-precipitation

method in aqueous solution. The first one includes the oxidation of ferrous hydroxide suspensions partially, followed by co-precipitation. The synthesizing of magnetite using this method was successful, Sugimoto and Matijevic, 1980 obtained spherical nanoparticles with narrow size and mean diameter ranges from 30 to 100 nm, by the oxidation of Ferrous salt with an oxidant agent and a base **[67]**. Other researchers have succeed in the preparation of Fe_3O_4 with mean size of about 58 nm through the partial oxidation of ferrous sulfate with potassium hydroxide (KOH as a base) and potassium nitrate (KNO_3 as oxidant). Equations bellow represents the reaction mechanism of this route. Where, (eq.1) demonstrates the partial oxidation of iron (II) sulfate to iron hydroxide. The last equations summarize the possible reactions between oxidant and iron hydroxide to yield magnetite precipitate, the intermediate steps are included **[53, 68]**.

$$FeSO_4 + 2OH^- \rightarrow Fe(OH)_2 + SO_4^{2-} \quad \text{(eq.1)}$$
$$3Fe(OH)_2 + NO_3^- \rightarrow Fe_3O_4 + NO_2^- + 3H_2O \quad \text{(eq.2)}$$
$$3Fe(OH)_2 + 2NO_2^- \rightarrow Fe_3O_4 + 2NO + 2H_2O + 2OH^- \quad \text{(eq.3)}$$
$$15Fe(OH)_2 + 2NO \rightarrow 5Fe_3O_4 + 2NH_3 + 12H_2O \quad \text{(eq.4)}$$

In the second method, stoichiometric ferric and ferrous hydroxides mixtures are aged in aqueous solution in order to obtain spherical magnetite. Additionally, it has been shown that the adjustment of pH and ionic strength of solution can control the particles mean size over the value of one order (2 to 15 nm) **[53]**. The (eq.5) shows the reaction mechanism of this method, which includes the iron hydroxides precipitation, accompanied by the formation of Fe_3O_4 due to the low water activity. The whole reaction mechanism depends mainly on the concentration of Fe^{2+}, Fe^{3+} and OH^- species, it can be considered as a dynamic equilibrium equation **[69]**. Generally, the precipitation method based on the mix of Fe^{3+} and Fe^{2+} and requires taking into account the molar ratio (Fe^{3+}/ Fe^{2+}: 2/1); which is the necessary and exact stoichiometry for the formation of Fe_3O_4. Furthermore, the pH value and the quantity of alkaline solution is related to the final concentration of OH^-, so to complete the precipitation, pH value should be range from 8 to 14 **[53]**.

$$Fe^{2+} + 2Fe^{3+} + 8OH^- \leftrightarrow Fe(OH)_2 + 2Fe(OH)_3 \rightarrow Fe_3O_4 + 4H_2O \quad \text{(eq.5)}$$

In this method, the magnetite concentration and its size are mainly related to the following factors, the nature of iron salt reactants (e.g., nitrates, chlorides and sulfates), the molar ratio of Fe (III) to Fe (II) ions, the pH of the solution, temperature of the reaction and ionic strength. In addition to other parameters such as the stirring rate and the dropping amount of alkaline in aqueous medium **[70]**. It is possible to produce superparamagnetic particles with small size, if the aforementioned factors well controlled. Likewise, it is necessary to carry out the reaction under inert gas flow, in order to decrease the nanoparticles

size and prevent Fe_3O_4 formation from critical oxidation **[71]**. Literature revealed that an increase in pH value and base amount can inhibit the growth of magnetite nanoparticles, which resulted smaller particles and lower magnetization saturation (Ms). On the other hand, reaction temperature also can affect the particles size, thus lower temperature can yield smaller particles because of the expedition movement of species which slow down the growth rate. Moreover, the stirring rate is one of the influencing factors of co-precipitation route, researchers on this context proved that small Fe_3O_4 nanoparticles can be obtained by the increasing of stirring rate, which boost the agitation degree. Accordingly, the energy resulted by the agitation can be transferred effectively and disperse the media components into tiny droplets **[72]**. Furthermore, Pereira et al, 2012 found that both isopropanolamine (MIPA) and diisopropanolamine (DIPA) can be used not only as alkaline but also as complexing agents in the synthesizing of iron oxide, in order to reduce nanoparticles growth and enhance surface spin order **[73]**. To conclude, smaller size of magnetite can be obtained via co-precipitation method by controlling the pH of the solution (around 12), temperature of the reaction (25 to 45 °C) and good stirring (600 to 800 rpm) **[53]**.

I.3.2.2. Sol-gel method

Sol-gel is one of the commonly chemical methods used in the synthesizing of metal oxides nanomaterial; it is also known as wet process. In this conventional method, the precursor is hydrolyzed and condensed in order to prepare the nanoparticles or as called in this route the 'sol' **[70]**. After the aging of the dispersed sol, nanoparticles are growing up then a dimensional (3D) network of metal oxide is dominated as a gel. To reach the final crystalline structure of iron oxide, heat treatment of the gel is a very important step in the synthesis procedure. To clarify the mechanism of sol-gel route, the (eq.6) and (eq.7) show the hydroxylation and condensation reactions of Fe (III) ions, respectively **[74]**.

$$Fe^{3+} + 3H_2O \rightarrow Fe(OH)_3 + 3H^+ \quad \text{(eq.6)}$$

$$12Fe(OH)_3 \rightarrow 4Fe_3O_4 + 18H_2O + O_2 \quad \text{(eq.7)}$$

The precursor used before in the sol-gel method was the metal alkoxides of the required metal oxides, which has excellent endurance against hydrolysis process and offer uniform size with better crystalline structure. Despite, metal alkoxides are not the promising precursors of sol-gel route due to their toxicity, complicated procedures and high cost **[75]**. In this fact, researchers have replaced the metal alkoxides by metal salts as nitrates, chlorides or acetates **[76]**. After that, they discovered that iron (III) chloride as an inexpensive precursor did not yield pure magnetite **[77]**. Later, many researchers succeed in producing pure magnetite using ethylene glycol and iron (III) nitrate using sol-gel coupled with annealing process under

vacuum, which considered as an additional treatment depends on the heat of nanoparticles in order to overcome the restrictions of previous results and prevent magnetite against the oxidation to maghemite or hematite **[78]**. Influencing parameters are investigated as well to control dispersion, size distribution and volume fraction of the nanoparticles. Literature reported that the precursor concentration has a great effect onto particle size **[53]**, Sundar and Piraman, 2013 confirmed that an increase of precursor concentration can improve the nucleation rate and enhance particles growth. Moreover, the crystallinity was tailored by higher temperature and longer period of annealing treatment which greatly decrease the agglomeration of the nanoparticles **[79]**. Consequently, smaller size of magnetite synthesized via sol-gel method can be obtained by reducing annealing time under vacuum (1-2 hours), decreasing annealing temperature (200-250 °C) and increasing the concentration of precursor (1M in solution) **[53]**.

I.3.2.3. Hydrothermal method

Hydrothermal process is considered as an effective method to synthesize plenty types of single crystals with specific characters and morphologies. It is mainly depended on high temperature and high pressure ensured by the autoclave, which offer fast nucleation, rapid growth and resulting smaller nanoparticles **[80]**. Deng et al, 2005 synthesized single crystal of ferrite microspheres through hydrothermal route; they used ethylene glycol as reducing agent and solvent in the same time, this method is very easy to manipulate because it did not require inert gas or complicated devices. Both chemical and physical properties of the obtained nanoparticles are extremely affected by the condition process such as Fe^{+3} concentration, quantity of the sodium acetate and aging time **[81]**. Previous study revealed that the aging time has a great impact on morphological properties and the size of synthesized nanomaterial. Moreover, the ratio of Ferric to sodium acetate must be lower than the third ($FeCl_3/CH_3COONa < 1/3$) **[80]**.

$$FeCl_3 + 3CH_3COONa \rightarrow Fe(CH_3COO)_3 + 3NaCl \quad \text{(eq.8)}$$

$$Fe(CH_3COO)_3 + 3H_2O \rightarrow 3CH_3COOH + Fe(OH)_3 \quad \text{(eq.9)}$$

$$2HOCH_2CH_2OH \rightarrow HOCH_2 - CH = C = CH_2 + 3H_2O \quad \text{(eq.10)}$$

$$HOCH_2CH_2OH \rightarrow CH \equiv CH + 2H_2O \quad \text{(eq.11)}$$

$$Fe(OH)_3 + HOCH_2CH_2OH \rightarrow Fe(OH)_2 + CH_2CHO + 2H_2O \quad \text{(eq.12)}$$

$$2Fe(OH)_3 + Fe(OH)_2 \rightarrow Fe_3O_4 + 4H_2O \quad \text{(eq.13)}$$

Due to the long time required in conventional hydrothermal method, researchers revealed that nanoparticles synthesized under microwave-assisted exhibited smaller size (about 25 nm) of magnetite with no impurities phases **[63]**. Yang et al, 2012 in their experiments used 1.5 mmol of iron acetylacetonate $Fe(acac)_3$ as an environmental precursor

and poly(acrylic acid) PAA (0.00 -3.00 wt%) as stabilizer and coating material in parallel; with the aim to investigate the effect of some factors on the average particle size of magnetite nanoparticles. Briefly, the chosen precursor is $Fe(acac)_3$ in order to reach better size distribution instead of ferric chloride hexahydrate usually used in hydrothermal process. Considering the solvent ethylene glycol was the preferable one, due to its higher reduction beside it resulted better morphology control. The reaction temperature is mainly dependent on the boiling point of the solvent which can affect by high pressure; as a result the suitable temperature for this reaction was adjusted at 200 °C during reaction time estimated to be about 16 hours **[82].**

I.3.2.4. Thermal decomposition method

Thermal decomposition is another chemical process aimed to produce narrow size and highly crystalline nanoparticles, despite it required superior temperature. There are two categories of precursors used in this method, iron organometallic (eg., iron (III) N-nitrosophenylhydroxylamine and iron (III) acetylacetonate), in addition to the solvents and organic surfactant (eg,. oleylamine, oleic acid, phenyl ether, 1-octadecene and benzyl ether). In order to stabilize the synthesis reaction a mixture of one or several solvents and surfactants would be added to yield monodispersed magnetite. So, the stabilizers can slow down the nucleation step and influence adsorption of additives onto nuclei, which can limit the growth of nanoparticles and promote the formation of smaller Fe_3O_4 **[83]**. This magnetic nanomaterial prepared through thermal decomposition process is typically well controlled in shape and size, because of its high crystallinity and excellent saturation moment resulted at higher temperature **[84]**. Moreover, the desirable characters such as narrow size distribution, high crystallinity and monodispersed are mainly related to the nucleation and the growth steps of nanoparticles at high temperature **[85]**. Hence, the adjustment of temperature, time, concentration and ratio of the mixture solvent/surfactant play a critical role in the control of magnetic propriety as well as the morphology of the magnetic product **[71]**. Literature revealed that the improving of Ms, size and size distribution can be achieved easily by increasing temperature and time of the reaction. Whereas, large size distribution is obtained at high temperature and long time of the process; this result indicated that another phenomenon is occurred during the synthesizing of Fe_3O_4. It is 'Ostwald ripening' process by which the small particles reduced while the large ones increased with prolonging the reaction time. As a result, Maity et al, 2008 succeed to overcome this phenomenon and produce magnetite with the desired characters by using solvent and surfactant. Particularly, they discovered that despite high temperature and extending time oleic acid can improve the size distribution of

Fe_3O_4 particles, because the magnetite surface may exhibit selective adsorption toward coordinating surfactant **[86]**. To sum up, thermal decomposition can be an effective method to synthesize smaller particles of magnetic iron oxide with high Ms and suitable distribution through the decomposing of $Fe(acac)_3$ with oleic acid and oleylamine mixture at higher temperature (300 to 330˚C) and prolonged time (2 to 4 hours) **[53]**.

I.3.3. Comparison between the synthesis methods

There is no ideal method and each one has some weaknesses beside its advantages .The approaches aforementioned (co-precipitation, sol-gel, hydrothermal and thermal decomposition) are applied for the preparation of Fe_3O_4 nanoparticles with desired characters. Firstly, chemical co-precipitation seems to be the most efficient technique, owing to its simplicity, low cost as well as its high and scalable yield. However, it suffers from agglomeration, while also can hinder the interfacial area of the nanoparticles and reduce their dispersibility and magnetism. Therefore, it is hard to produce small nanoparticles with high crystalline via this method. Secondly, sol-gel is considered as an alternative technique characterized by ambient condition and excellent control of the nanoparticles size. Despite, this synthesis procedure requires safety consideration due to the large quantity of ethanol released during the process. Additionally, annealing under high temperature and vacuum seems to be an expensive post treatment due to the high consumption of energy. Thirdly, hydrothermal method exhibits higher Ms (80-90 $emu.g^{-1}$) at 100 nm. Meanwhile, the smaller size (lower than 50 nm) are obtained at higher temperature (200-300°C) and under high pressure, despite hydrothermal technique still need developed facilities. Finally, small size distribution of Fe_3O_4 with high crystalline structure and highly monodispersed can be obtained through thermal decomposition route. Nevertheless, it is also considered as an expensive method because of the increased temperature required during the process **[53, 63]**. Table.I.3 summarizes the drawbacks and advantages of each method.

Table.I.3. Comparison of different chemical methods used in the preparation of magnetite nanoparticles [**53, 63]**.

Method	**Co-precipitation**	**Sol-gel**	**Hydrothermal**	**Thermal decomposition**
Conditions	Easy, inert atmosphere	Complicated, ambient	Relatively easy, higher pressure	Complicated, inert atmosphere
Temperature	25 to 70 °C	25 to 80°C	130 to 250 °C	100 to 350°C
Time	Minutes/hours	Minutes/ hours	Hours	Hours/days
Size distribution	Relatively narrow	Narrow	Very narrow	Very narrow
Shape control	Not well	well	Very well	Very well
Output	Superior and scalable	good	Medium	Superior and scalable
Drawbacks	-Wide size distribution - The use of strong base	-Release a large quantity of alcohol during the calcination -Consumption of high energy during annealing treatment -Low wear-resistance -Weak bonding -High permeability	- Consumption of high energy due to the higher temperature required. - High pressure required (ranging from 0.3 to4 MPa) -Relatively long reaction time of synthesis process	-Consumption of high energy -Products can dissolve in non polar solvents - Relatively expensive -Relatively long time of synthesis process
Advantages	-Easy and efficient - Safer procedure -High efficiency - Lower cost	-High control of microstructure; internal structure homogeneity; size; shape and aspect ratio	- High Control of size and shape.	-High crystallinity - Simple control of shape and particle size

I.3.4. Characterization techniques for Fe_3O_4 nanoparticles

Characterization methods are applied for a deeper understanding of the surface properties, morphology and composition of nanomaterial. The main techniques used to characterize magnetic Fe_3O_4 are the following, Fourier-transform infrared spectroscopy (FTIR); energy dispersive x-rays analysis (EDX); X-ray diffraction (XRD); scanning electron microscope (SEM); transmission electron microscope (TEM); dynamic light scattering (DLS); vibrating sample magnetometer (VSM) and superconducting quantum interference device (SQUID) **[53]**.

I.3.5. Properties

The application of Fe_3O_4 nanoparticles in water remediation is mainly dependent to their unique magnetic characteristics. Moreover, magnetite has large application areas owing to their useful properties [87].

I.3.5.1. Physical properties

The electronic configurations of iron (II) and iron (III) ions are: $[Ar]3d^6$ and $[Ar]3d^5$, respectively. So, the electron of 3d orbital is the controller of the particular properties of iron atom. As mentioned above, magnetite posses a crystalline structure (cubic inverse spinel), the Fe^{2+} and Fe^{3+} situate in octahedral lattice and Fe^{3+} occupies tetrahedral sites. The conductivity of magnetite could simulate by the hopping of brisk electrons between Fe^{2+} and Fe^{3+} on the octahedral lattice. Concerning the Fe_3O_4 physical properties, the jet-black colour characterize the pure powder of magnetite and their colloidal solutions **[88]**.

I.3.5.2. Thermal properties

Magnetite has various kinetic based properties, the behavior of magnetic nanoparticles change according to three distinct temperature phases. The first phase is called temperature (0 to 119 K), in which Fe_3O_4 transforms from semiconductor to metal **[89]**. The next phase represents the Curie temperature (120-840 K), which takes place during the transition of magnetisation from ferromagnetic to superparamagnetic at a critical temperature **[90]**. The last phase represents higher temperatures (above 840 K), in which magnetite acts as a paramagnetic metal **[91]**.

I.3.5.3. Magnetic properties

Magnetic property is also related to Fe_3O_4 structure, the cubic unit cell of the inverse spinel structure is estimated to 8.396 A˚. Where, 32 ions of oxygen are occupied roughly close packed array. Particularly, eight Fe^{2+} and eight Fe^{3+} are occupied the octahedral (B) coordination and they are surrounded by six O^{2-} ions; other eight ions of Fe^{3+} are occupied the tetrahedral (A) coordination and other four oxygen ions surrounded them. To sum up, the

ratio Fe^{3+}/ Fe^{2+}/: 2/1kepts the charge neutrality in correlation with the oxygen ions. The magnetic moment of Fe^{3+} and Fe^{2+} are 5 and $4\mu_B$, respectively. There are magnetic exchange interactions between the neighboring Fe (II) and Fe (III), where the ions arranged in (A) site exhibited an antiparallel orientation to the ions of B site. As consequence, the orientations of magnetic spin of all the (A) site ions are arranged in opposite and parallel directions to the orientation of magnetic spin of all the (B) site ions. As Fe^{3+} occupy both of A and B sites equally, which make their spin states delete each other and result no net magnetization. This results in a net magnetization owing to the Fe^{2+} ions in the (B) site, which is stated for bulk magnetite as (92 $Am^2.kg^{-1}$). As a conclusion, the variations in the Fe^{3+}/ Fe^{2+} ratio may have a major effect on the magnetite's bulk magnetic characteristics **[92]**.

Table.I.4. Magnetite properties **[88]**.

Molecular formula	**Fe_3O_4**
Colour	Jet black
Density	5.18 $g.cm^{-3}$
Melting point	1583-1597 ˚C
Crystallographic system	Cubic
Structure type	Inverse spinel
Lattice parameter	a=b=c=0.8396 nm
Lattice angles	α=β=γ=90˚
Magnetism type	Ferrimagnetic
Curie temperature	858 K
Saturation magnetisation (at 300K)	92-100 $emug^{-1}$
Standard Gibbs free energy of formation (ΔG_f^0)	-1012.6 $kJ.mol^{-1}$
Band gap energy (E_g)	2.6 eV

I.3.6. Applications

Magnetite nanomaterials have been used in several applications like drug delivery, catalyst, metal chemosensor and so on. In this section we tried to summarize the potential applications of these nanoparticles **[93]**.

I.3.6.1. Lithium-ion batteries

In the aim to improve the energy density and the power of lithium-ion batteries, magnetite nanomaterials have been used as an anode owing to their higher theoretical capacity (900-1000 $mA.h.g^{-1}$), lower cost and other specific properties **[94]**.

I.3.6.2. Wastewater treatment

Recently, the water pollution has attracted great attention which paths the way to the development of nanomaterials. Magnetite has been used as an adsorbent for heavy metals in several studies. Moreover the nanocomposites based on Fe_3O_4 have been widely used as catalysts to remove various organic contaminants via different methods **[78, 87, 92, 95]**.

I.3.6.3. Biomedical applications

Magnetic nanomaterials have been widely explored in biomedical field, among the various applications we can cite: bio imaging, diseases local treatment, hyperthermia cancer therapy, dental application, and so on **[96]**.

I.4. Fe_3O_4/MWCNTs nanocomposite

Immobilized magnetite species on MWCNTs as a solid support can be considered as promising material owing to their unique properties, in addition to their large application and especially in wastewater treatment. Therefore, numerous techniques have been developed for the preparation of Fe_3O_4/MWCNTs nanocomposite **[97]**.

I.4.1. Preparation techniques for Fe_3O_4/MWCNTs nanocomposite

Recently, researchers have been focused on the development of efficient and simple synthetic methods in order to achieve controlled shape and higher stability of well defined magnetic nanocomposites made of carbon nanotubes **[98]**. Therefore, various common routes were developed including chemical vapor deposition **[99]**, microwave irradiation method **[100]**, sonochemical route **[101]**, solvothermal **[102]**, sol-gel **[103]**, hydrothermal **[104]**, chemical coprecipitation **[105]** and so on. In the following, summary of the main important synthesis routes is presented.

I.4.1.1. Chemical coprecipitation

Coprecipitation method is considered as a direct, simple and effective route for the functionalization of MWCNTs by magnetite. It mainly aims to control both of size and size distribution of Fe_3O_4 on the MWCNTs surface **[106]**.Briefly, chemical oxidation using an acid as HNO_3 (nitric acid) is required before its modification. So, the desirable amount of MWCNTs should be dispersed into appropriate volume of concentrated acid under heating at high temperature (between 80 and 120 °C) for few hours (4-5 hours). After that, the solid was separated from the acidic solution, well rinsed and dried in oven at 80 °C for 4 hours; the

obtained material was calcined in furnace for 4 hours at 450°C. Iron salts were well dissolved in distilled water in order to obtain two different solutions rich on iron (II) and iron (III) ions. These solutions were added onto oxidized-MWCNTs nanoparticles under inert atmosphere (N_2) at 70 °C, and NaOH dropwise (until pH reach 11-12) to precipitate the iron oxide for 4 hours. We noticed that some experimenters synthesized Fe_3O_4 nanoparticles then dispersed them with oxidized-MWCNTs instead of iron salts solutions. Finally, the obtained solid was separated from the mixture using an external magnetic field, washed several times and dried in oven at 100°C for few hours. (eq.14) shows the corresponding chemical reaction **[95, 105, 106]**:

$$MWCNTs + Fe^{2+} + 2Fe^{3+} + 8OH^- \rightarrow Fe_3O_4/MWCNTs + 4H_2O \quad \text{(eq.14)}$$

I.4.1.2. Sol-gel method

Chemical oxidation step was effectuated before the modification of MWCNTs by Fe_3O_4 in order to remove amorphous carbon, purify and functionalize the carbon nanotubes surface by active groups. As reported by Ali et al **[103]**, who has succeeded in the preparation of magnetic nanocomposite through sol-gel route. First of all, the chemical reagents were dried and iron nitrate was stirred over night under N_2 gas; acid treated carbon was added to nona-hydrate ferric solution under nitrogen gas and agitation for 15 minutes. Ammonium hydroxide was added to the solution by dropwise in order to reach alkaline medium (pH around 9) under 60 °C and mechanical stirring for 25 minutes. The obtained gel was separated then rinsed with distilled water and ethanol, respectively. Finally, the solid was dried in oven overnight and calcined at 350°C in hot air for 10 munities **[103]**.

I.4.1.3. Hydrothermal method

After the purification of the CNTs nanoparticles, very simple step was carried out to obtain the magnetic nanocomposite. The acidifying MWCNTs were dispersed in ethylene glycol solution and ultrasonically agitated for 30 minutes. In parallel, grinded iron salt and sodium acetate in addition to the ethidene diamine were introduced into dried Teflon-lined stainless-steel autoclave. After that the dispersed MWCNTs solution was added into autoclave slowly and stirred using a glass rod. Next, the autoclave was maintained at 200°C in the oven for 4 hours. At last, the residue was collected using an external magnetic field, washed several times and dried at 50°C for 24 hours. Figure.I.4 shows the preparation of Fe_3O_4/MWCNTs process **[107]**.

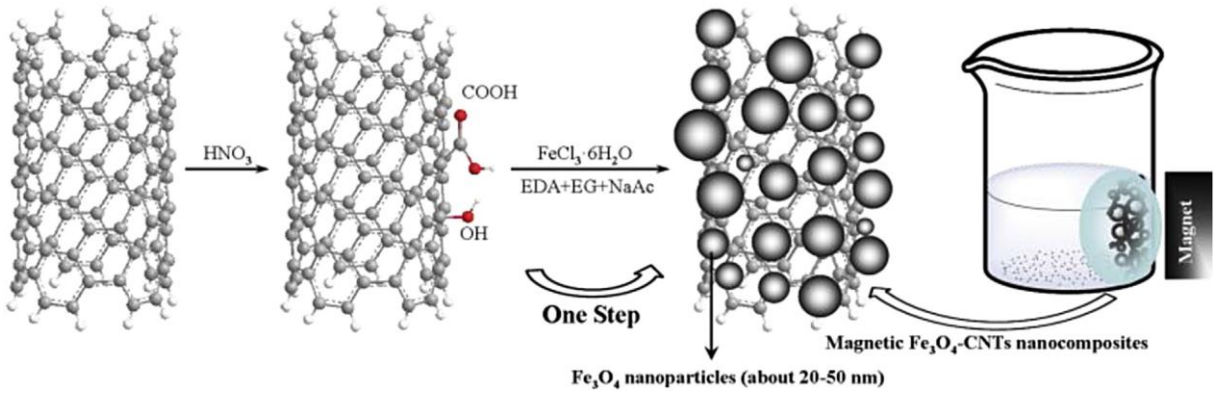

Figure.I.4. Chemical oxidation and preparation of Fe_3O_4/ MWCNTs via hydrothermal route **[107]**.

I.4.2. Application of Fe_3O_4/MWCNTs

The nanocomposite Fe_3O_4/MWCNTs is considered as a novel material with large application areas, due to the unique properties of both MWCNTs and magnetite **[108]**. This nanomaterial is recommended and used in various fields such as bioapplication **[93]**, functional magnetic printing ink **[99]**, Li-ion batteries **[109]**, screening of nasopharyngeal carcinoma **[110]**, electrochemical immunoassay **[111]**, hyperthermia and drug delivery **[112]** and so on. In the last decades, the nanocomposite Fe_3O_4/MWCNTs has attracted the attention of many researchers, owing to its high adsorption capacity and removal efficiency of contaminants from water **[34, 87]**.

I.4.2.1. Biosensors

Nanocomposite made of CNTs and iron oxide was applied in biosensors field. M.Kundu et al., 2019 have been developed an electrochemical biosensor (CNTs-Fe_3O_4) to evaluate formaldehyde adulteration in sample of orange juice **[113]**. This nanocomposite is used in many other works as an effective sensor **[96]**.

I.4.2.2. Batteries

Nanocrystals consisting of magnetite and MWCNTs can be utilized as high-performance Li-ion batteries anode, this nanocomposite electrodes show a significant improvement in lithium storage efficiency and syclablity. Furthermore, the reversible capacity was estimated to 850 $mAh.g^{-1}$ maintained until 100 cycles of charge/discharge at a current rate of 0.1 C for 100 cycles, which can be considered as impressive results **[109]**.

I.4.2.3. Drug delivery

Recently, magnetic nanoparticles are considered as promising materials for drugs delivery with an efficient loading. P.Ghoderao et al., 2019 have studied the efficiency of this material in Doxycycline delivery, the results indicated that the application of

Fe_3O_4/MWCNTs improve the drug delivery by extending the drug releasing time and reducing the dosing frequency at various pH **[115]**.

I.4.2.4. Water remediation

Fe_3O_4/MWCNTs nanocomposite has been widely used as promising adsorbent for heavy metals **[116]**, dyes **[117]**, pesticides **[36]**, and so one. It is not only used in adsorption, literature has reported numerous studies on the removal of recalcitrant pollutants from aqueous medium using magnetic nanocomposite as a catalyst due to its unique properties and simple separation **[118]**. This topic will be discussed with details in the next section.

I.5. Conclusion

During this chapter, we have seen that MWCNTs modified with magnetite have a great potential in wastewater treatment which makes them a promising adsorbent and catalyst at the same time; due to their outstanding properties and huge specific surface area of the MWCNTs. In literature, we have found that the preparation of magnetite via different routs is very simple and low cost. Furthermore, the functionalization of MWCNTs surface with iron oxide by co-precipitation method has great advantages.

The next chapter will describe water pollution and some organic pollutants like cationic and anionic dyes, the different techniques used in the present work for wastewater treatment using Fe_3O_4/MWCNTs nanocomposite which are adsorption, heterogeneous Fenton and photo Fenton oxidation.

References

[1] R. Das, Carbon Nanotubes for Clean Water, Carbon Nanostructures, Springer, 2018, doi: https://doi.org/10.1007/978-3-319-95603-9-11.

[2] T. T. Nguyen, « Utilisation de nanotubes de carbone pour la préparation de catalyseurs confinés », 2013. p. 63.

[3] P.Pandey, et M. Dahiya, «Carbon nanotubes: Types, methods of preparation and applications», Carbon NY, vol. 1, no 4, 2016.

[4] C. Klumpp, K. Kostarelos, M. Prato, et A. Bianco, « Functionalized carbon nanotubes as emerging nanovectors for the delivery of therapeutics », Biochimica et Biophysica Acta (BBA) - Biomembranes, vol. 1758, n° 3, p. 404-412, mars 2006, doi: 10.1016/j.bbamem.2005.10.008.

[5] D. Danailov, P. Keblinski, S. Nayak, et P. M. Ajayan, « Bending Properties of Carbon Nanotubes Encapsulating Solid Nanowires », journal of nanosciences and nanotechnolgy, vol. 2, n° 5, p. 503-507, oct. 2002, doi: 10.1166/jnn.2002.132.

[6] V. Rastogi, P. Yadav, P., Bhattacharya, S. S., Mishra, A. K., Verma, N., Verma, A., & Pandit, J. K, « Carbon Nanotubes: An Emerging Drug Carrier for Targeting Cancer Cells », Journal of Drug Delivery, vol.2014, p.23. avr. 24, 2014, doi: http://dx.doi.org/10.1155/2014/670815

[7] Z. H. Xia, P. R. Guduru, et W. A. Curtin, « Enhancing Mechanical Properties of Multiwall Carbon Nanotubes via Interwall Bridging », Physical review letters., vol. 98, n° 24, p. 245501, juin 2007, doi: 10.1103/PhysRevLett.98.245501.

[8] S. Y. Madani, N. Naderi, O. Dissanayake, A. Tan, et A. M. Seifalian, « A new era of cancer treatment: carbon nanotubes as drug delivery tools », Int J Nanomedicine, vol. 6, p. 2963-2979, 2011, doi: 10.2147/IJN.S16923.

[9] Y.-L. Zhao et J. F. Stoddart, « Noncovalent Functionalization of Single-Walled Carbon Nanotubes », vol. 42, no 8, p. 1161-1171 mai 22, 2009, doi: https://pubs.acs.org/doi/10.1021/ar900056z.

[10] F. H. Hussein, A. Kamil « Wastewater Treatment using Carbon Nanotubes», LAP LAMBERT Academic Publishing, 2015.

[11] B. Zhang et al., « Characterization of and biomolecule immobilization on the biocompatible multi-walled carbon nanotubes generated by functionalization with polyamidoamine dendrimers », Colloids and Surfaces B: Biointerfaces, vol. 80, no 1, p. 1825, oct. 2010, doi: 10.1016/j.colsurfb.2010.05.023.

[12] K. S. Ibrahim, « Carbon nanotubes-properties and applications: a review », Carbon letters, vol. 14, no 3, p. 131-144, juill. 2013, doi: 10.5714/CL.2013.14.3.131.

[13] Y. Xiang, L. Kong, P. Xie, T. Xu, J. Wang, et X. Li, « Carbon Nanotubes and Activated Carbons Supported Catalysts for Phenol in Situ Hydrogenation: Hydrophobic/Hydrophilic Effect » Industrial & engineering chemistry research, vol. 53, no 6, p. 2197-2203., janv. 31, 2014, doi: https://doi.org/10.1021/ie4035253.

[14] M. Barberio, P. Barone, F. Stranges, R. A. Romano, F. Xu, et A. Bonanno, « Adsorption of Molecular Gases on Silver/Carbon Nanotube Composites at Low Temperatures and Low Pressures », Journal of Chemistry, vol. 2014, p. 1-7, 2014, doi: 10.1155/2014/816193.

[15] H. Dai, E. W. Wong, et C. M. Lieber, « Probing Electrical Transport in Nanomaterials: Conductivity of Individual Carbon Nanotubes », Science, vol. 272, no 5261, p. 523-526, avr. 1996, doi: 10.1126/science.272.5261.523.

[16] B. Chandra et al., « Molecular-scale quantum dots from carbon nanotube heterojunctions », Nano Lett., vol. 9, no 4, p. 1544-1548, avr. 2009, doi: 10.1021/nl803639h.

[17] T. W. Ebbesen, H. J. Lezec, H .Hiura , J. W Bennett, H. F. Ghaemi, & T. Thio, « Electrical conductivity of individual carbon nanotubes».,Nature, 382(6586), 54-56, 1996, doi: https://doi.org/10.1038/382054a0.

[18] R. Saito, M. Fujita, G. Dresselhaus, et M. S. Dresselhaus, « Electronic structure of chiral graphene tubules », Appl. Phys. Lett., vol. 60, no 18, p. 2204-2206, mai 1992, doi: 10.1063/1.107080.

[19] J. Hone et al., « Electrical and thermal transport properties of magnetically aligned single wall carbon nanotube films », Appl. Phys. Lett., vol. 77, no 5, p. 666-668, juill. 2000, doi: 10.1063/1.127079.

[20] M. Yu, « Strength and Breaking Mechanism of Multiwalled Carbon Nanotubes Under Tensile Load », Science, vol. 287, no 5453, p. 637-640, janv. 2000, doi: 10.1126/science.287.5453.637.

[21] P. Kim, L. Shi, A. Majumdar, et P. L. McEuen, « Thermal Transport Measurements of Individual Multiwalled Nanotubes », Phys. Rev. Lett., vol. 87, no 21, p. 215502, oct. 2001, doi: 10.1103/PhysRevLett.87.215502.

[22] V. Georgakilas, K. Kordatos, M. Prato, D. M. Guldi, M. Holzinger, et A. Hirsch, « Organic Functionalization of Carbon Nanotubes », J. Am. Chem. Soc., vol. 124, no 5, p. 760-761, févr. 2002, doi: 10.1021/ja016954m.

[23] A. Hirsch, « Functionalization of Single-Walled Carbon Nanotubes », Angewandte Chemie International Edition, vol. 41, no 11, p. 1853-1859, 2002, doi: https://doi.org/10.1002/1521-3773.

[24] H. Wang, « Dispersing carbon nanotubes using surfactants », Current Opinion in Colloid & Interface Science, vol. 14, no 5, p. 364--71, oct. 2009, doi: 10.1016/j.cocis.2009.06.004.

[25] R. H. Baughman, « Carbon Nanotubes--the Route Toward Applications », Science, vol. 297, no 5582, p. 787-792, août 2002, doi: 10.1126/science.1060928.

[26] S. Kar, R. C. Bindal, S. Prabhakar, P. K. Tewari, K. Dasgupta, et D. Sathiyamoorthy, « Potential of carbon nanotubes in water purification: an approach towards the development of an integrated membrane system », IJND, vol. 3, no 2, p. 143, 2008, doi: 10.1504/IJND.2008.020221.

[27] Y. Wang, C. Pan, W. Chu, A. Vipin, et L. Sun, « Environmental Remediation Applications of Carbon Nanotubes and Graphene Oxide: Adsorption and Catalysis », Nanomaterials, vol. 9, no 3, p. 439, mars 2019, doi: 10.3390/nano9030439.

[28] V. K. K. Upadhyayula, S. Deng, M. C. Mitchell, et G. B. Smith, « Application of carbon nanotube technology for removal of contaminants in drinking water: a review », Sci. Total Environ., vol. 408, no 1, p. 1-13, déc. 2009, doi: 10.1016/j.scitotenv.2009.09.027.

[29] B. Pan et B. Xing, « Adsorption Mechanisms of Organic Chemicals on Carbon Nanotubes », Environ. Sci. Technol., vol. 42, no 24, p. 9005-9013, déc. 2008, doi: 10.1021/es801777n.

[30] Y. Liu et al., « Excellent Microwave Absorbing Property of Multiwalled Carbon Nanotubes with Skin–Core Heterostructure Formed by Outer Dominated Fluorination », J. Phys. Chem. C, vol. 122, no 11, p. 6357-6367, mars 2018, doi: 10.1021/acs.jpcc.7b10819.

[31] J. H. Carey, J. Lawrence, et H. M. Tosine, « Photodechlorination of PCB's in the presence of titanium dioxide in aqueous suspensions », Bull. Environ. Contam. Toxicol., vol. 16, no 6, p. 697-701, déc. 1976, doi: 10.1007/BF01685575.

[32] S. J. Gao, Z. Shi, W. B. Zhang, F. Zhang, et J. Jin, « Photoinduced Superwetting Single-Walled Carbon Nanotube/TiO2 Ultrathin Network Films for Ultrafast Separation of Oil-in-Water Emulsions », ACS Nano, vol. 8, no 6, p. 6344-6352, juin 2014, doi: 10.1021/nn501851a.

[33] H.-A. Park, S. Liu, P. A. Salvador, G. S. Rohrer, et M. F. Islam, « High visible-light photochemical activity of titania decorated on single-wall carbon nanotube aerogels », RSC Adv., vol. 6, no 27, p. 22285-22294, févr. 2016, doi: 10.1039/C6RA03801H.

[34] Kim, Min Il, 임지선, In, Se Jin, Kim, Hyuk, Kim, Jong-Gyu, et Lee, Young-Seak, « Improved Photo Degradation of Rhodamine B Dye using Iron Oxide/Carbon Nanocomposite by Photo-Fenton Reaction », Carbon letters, vol. 9, no 3, p. 195-199, sept. 2008, doi: 10.5714/CL.2008.9.3.195.

[35] W. J. Lee et al., « Biomineralized N-Doped CNT/TiO2 Core/Shell Nanowires for Visible Light Photocatalysis », ACS Nano, vol. 6, no 1, p. 935-943, janv. 2012, doi: 10.1021/nn204504h.

[36] B. Maddah et M. Hasanzadeh, « Fe_3O_4/CNT Magnetic Nanocomposites as Adsorbents to Remove Organophosphorus Pesticides from Environmental Water », international journal of nanoscience and nanotechnology, vol. 13, n° 2, p 139-149, 2017.

[37] Z.-F. Yang, L.-Y. Li, C.-T. Hsieh, et R.-S. Juang, « Co-precipitation of magnetic Fe_3O_4 nanoparticles onto carbon nanotubes for removal of copper ions from aqueous solution », Journal of the Taiwan Institute of Chemical Engineers, vol. 82, p. 56-63, janv. 2018, doi: 10.1016/j.jtice.2017.11.009.

[38] Z. Xu, H. Liu, J. Niu, Y. Zhou, C. Wang, et Y. Wang, « Hydroxyl multi-walled carbon nanotube-modified nanocrystalline PbO_2 anode for removal of pyridine from wastewater », Journal of Hazardous Materials, vol. 327, p. 144-152, avr. 2017, doi: 10.1016/j.jhazmat.2016.12.056.

[39] Y. Liu et al., « Conductive 3D sponges for affordable and highly-efficient water purification », Nanoscale, vol. 10, no 10, p. 4771-4778, 2018, doi: 10.1039/C7NR09435C.

[40] X. Duan, H. Sun, Y. Wang, J. Kang, et S. Wang, « N-Doping-Induced Nonradical Reaction on Single-Walled Carbon Nanotubes for Catalytic Phenol Oxidation », ACS Catalysis., vol. 5, no 2, p. 553-559, févr. 2015, doi: 10.1021/cs5017613.

[41] J.-M. Bonard et al., « Field-Emission-Induced Luminescence from Carbon Nanotubes », Physical. Review. Letters., vol. 81, no 7, p. 1441-1444, 1998, doi: 10.1103/PhysRevLett.81.1441.

[42] A. De Vita, J.-C. Charlier, X. Blase, et R. Car, « Electronic structure at carbon nanotube tips », Applied Physics A: Materials Science & Processing, vol. 68, no 3, p. 283-286, mars 1999, doi: 10.1007/s003390050889.

[43] S. Beg, M. Rizwan, A. M. Sheikh, M. S. Hasnain, K. Anwer, et K. Kohli, « Advancement in carbon nanotubes: basics, biomedical applications and toxicity: Biomedical applications of carbon nanotubes », Journal of Pharmacy and Pharmacology, vol. 63, no 2, p. 141-163, févr. 2011, doi: 10.1111/j.2042-7158.2010.01167.x.

[44] F. Banhart, N. Grobert, M. Terrones, J.-C. Charlier, et P. M. Ajayan, « METAL ATOMS IN CARBON NANOTUBES AND RELATED NANOPARTICLES », International Journal of Modern Physics B, vol. 15, no 31, p. 4037-4069, déc. 2001, doi: 10.1142/S0217979201007944.

[45] H. He, L. A. Pham-Huy, P. Dramou, D. Xiao, P. Zuo, et C. Pham-Huy, « Carbon nanotubes: applications in pharmacy and medicine », Biomed Research International, vol. 2013, p. 578290, 2013, doi: 10.1155/2013/578290.

[46] N. K. Mehra, A.K. Jain, N. Lodhi, R. Raj, V. Dubey, D. Mishra & N.K. Jain, « Challenges in the Use of Carbon Nanotubes for Biomedical Applications », Critical Reviews in Therapeutic Drug Carrier Systems , vol. 25, no 2. p.169- 206, 39, 2008, doi: 10.1615/CritRevTherDrugCarrierSyst.v25.i2.20

[47] P. P. Simeonova, « Update on carbon nanotube toxicity », Nanomedicine, vol. 4, no 4, p. 373-375, juin 2009, doi: 10.2217/nnm.09.25.

[48] A. Nemmar, H. Vanbilloen, M. F. Hoylaerts, P. H. M. Hoet, A. Verbruggen, et B. Nemery, « Passage of Intratracheally Instilled Ultrafine Particles from the Lung into the Systemic Circulation in Hamster », Am J Respir Crit Care Med, vol. 164, no 9, p. 1665-1668, nov. 2001, doi: 10.1164/ajrccm.164.9.2101036.

[49] C. A. Poland, C.A. Poland, R. Duffin , I.Kinloch, A.Maynard, W.A. Wallace, A. Seaton & K. Donaldson « Carbon nanotubes introduced into the abdominal cavity of mice show asbestos-like pathogenicity in a pilot study », Nature Nanotechnology, vol. 3, no 7, p. 423-428, juill. 2008, doi: 10.1038/nnano.2008.111.

[50] C. Lam, J. T. James, R. McCluskey, S. Arepalli, et R. L. Hunter, « A Review of Carbon Nanotube Toxicity and Assessment of Potential Occupational and Environmental Health Risks », Critical Reviews in Toxicology, vol. 36, no 3, p. 189-217, janv. 2006, doi: 10.1080/10408440600570233.

[51] S. T. Stern et S. E. McNeil, « Nanotechnology Safety Concerns Revisited », Toxicol Sci, vol. 101, no 1, p. 4-21, janv. 2008, doi: 10.1093/toxsci/kfm169.

[52] A. Ali et al., « Synthesis, characterization, applications, and challenges of iron oxide nanoparticles », NSA, vol. Volume 9, p. 49-67, 2016, doi: 10.2147/NSA.S99986.

[53] K. N. Koo, A. F. Ismail, M. H. D. Othman, N. Bidin, et M. A Rahman, « Preparation and characterization of superparamagnetic magnetite (Fe_3O_4) nanoparticles: A short review », Mal. J. Fund. Appl. Sci., vol. 15, no 1, p. 23-31, févr. 2019, doi: 10.11113/mjfas.v15n2019.1224.

[54] C. DeArmitt, « Magnetite », in Encyclopedia of Polymers and Composites, S. Palsule, Éd. Berlin, Heidelberg: Springer Berlin Heidelberg, 2014, p. 1-11.

[55] J. R. Lloyd et al., « Biomineralization: linking the fossil record to the production of high value functional materials », Geobiology, vol. 6, no 3, p. 285-297, juin 2008, doi: 10.1111/j.1472-4669.2008.00162.x.

[56] L. Blaney, « Magnetite (Fe_3O_4): Properties, Synthesis, and Applications », p. 50.

[57] D. M. Angrove, Magnetite: Structure, Properties, and Applications. Nova Science Publishers, 2011.

[58] K. L. Thomas-Keprta et al., « Elongated prismatic magnetite crystals in ALH84001 carbonate globules: Potential Martian magnetofossils », Geochimica et Cosmochimica Acta, vol. 64, no 23, p. 4049-4081, déc. 2000, doi: 10.1016/S0016-7037(00)00481-6.

[59] A. Akbarzadeh, M. Samiei, et S. Davaran, « Magnetic nanoparticles: preparation, physical properties, and applications in biomedicine », Nanoscale research letters, vol. 7, no 1, p. 144, 2012, doi: 10.1186/1556-276X-7-144.

[60] M. R. Ghazanfari, M. Kashefi, S. F. Shams, et M. R. Jaafari, « Perspective of Fe_3O_4 Nanoparticles Role in Biomedical Applications », Biochemistry Research International, mai 12, 2016.

[61] J. Sun, J.Sun, S. Zhou, P. Hou, Y. Yang, J. Weng, X. Li, X & M.Li, M. « Synthesis and characterization of biocompatible Fe_3O_4 nanoparticles », journal of Biomedical materials research, vol. 80A, no 2, p. 333-341, févr. 2007, doi: 10.1002/jbm.a.30909.

[62] Z. I. Takai, M. K. Mustafa, S. Asman, et K. A. Sekak, « Preparation and Characterization of Magnetite (Fe_3O_4) nanoparticles By Sol-Gel Method », International jurnal of nanoelectron. Materials, vol. 12, p. 37-46. p. 11, Jan 2019.

[63] A. H. M. Yusoff, M. N. Salimi, et M. F. Jamlos, « A review: Synthetic strategy control of magnetite nanoparticles production », Advances in nano research, vol. 6, no 1, p. 1-19, mars 2018, doi: 10.12989/ANR.2018.6.1.001.

[64] D. Maity, S.-G. Choo, J. Yi, J. Ding, et J. M. Xue, « Synthesis of magnetite nanoparticles via a solvent-free thermal decomposition route », Journal of Magnetism and Magnetic Materials, vol. 321, no 9, p. 1256-1259, mai 2009, doi: 10.1016/j.jmmm.2008.11.013.

[65] Z. Cheng, A. L. K. Tan, Y. Tao, D. Shan, K. E. Ting, et X. J. Yin, « Synthesis and Characterization of Iron Oxide Nanoparticles and Applications in the Removal of Heavy Metals from Industrial Wastewater », International Journal of Photoenergy, vol. 2012, p. 1-5, 2012, doi: 10.1155/2012/608298.

[66] X. Chu et Y. Hou, « Overview of Synthesis of Magnetic Nanomaterials », in Magnetic Nanomaterials - Fundamentals, Synthesis and Applications, Y. Hou et D. J. Sellmyer, Éd. Weinheim, Germany: Wiley-VCH Verlag GmbH & Co. KGaA, 2017, p. 81-120.

[67] T. Sugimoto et E. Matijević, « Formation of uniform spherical magnetite particles by crystallization from ferrous hydroxide gels », Journal of Colloid and Interface Science, vol. 74, no 1, p. 227-243, mars 1980, doi: 10.1016/0021-9797(80)90187-3.

[68] J. C. Aphesteguy, G. V. Kurlyandskaya, J. P. de Celis, A. P. Safronov, et N. N. Schegoleva, « Magnetite nanoparticles prepared by co-precipitation method in different conditions », Materials Chemistry and Physics, vol. 161, p. 243-249, juill. 2015, doi: 10.1016/j.matchemphys.2015.05.044.

[69] M. C. Mascolo, Y. Pei, et T. A. Ring, « Room Temperature Co-Precipitation Synthesis of Magnetite Nanoparticles in a Large pH Window with Different Bases », Materials (Basel), vol. 6, no 12, p. 5549-5567, nov. 2013, doi: 10.3390/ma6125549.

[70] Y. Hou et D. J. Sellmyer, Magnetic Nanomaterials: Fundamentals, Synthesis and Applications. John Wiley & Sons, 2017.

[71] S. Laurent, D. Forge, M. Port, A. Roch, C. Robic, L. Vander Elst & R.N. Muller, « Magnetic Iron Oxide Nanoparticles: Synthesis, Stabilization, Vectorization, Physicochemical Characterizations, and Biological Applications », Chemical. Reviews., vol. 108, no 6, p. 2064-2110, juin 2008, doi: 10.1021/cr068445e.

[72] M. Mahdavi, M.B. Ahmad, M.J. Haron, F. Namvar, B. Nadi, L.Z.A. Rahman & J. Amin, « Synthesis, Surface Modification and Characterisation of Biocompatible Magnetic Iron Oxide Nanoparticles for Biomedical Applications », Molecules, vol. 18, no 7, p. 7533-7548, juin 2013, doi: 10.3390/molecules18077533.

[73] C. Pereira, A.M. Pereira, C. Fernandes, M. Rocha, R. Mendes, M.P. Fernández-García, & C. Freire, « Superparamagnetic MFe_2O_4 (M = Fe, Co, Mn) Nanoparticles: Tuning the Particle Size and Magnetic Properties through a Novel One-Step Coprecipitation Route », Chemestry of materials, vol. 24, no 8, p. 1496-1504, avr. 2012, doi: 10.1021/cm300301c.

[74] J. Xu, H. Yang, W. Fu, K. Du, Y. Sui, J. Chen, & G. Zou, « Preparation and magnetic properties of magnetite nanoparticles by sol–gel method », Journal of Magnetism and Magnetic Materials, vol. 309, no 2, p. 307-311, févr. 2007, doi: 10.1016/j.jmmm.2006.07.037.

[75] G. J. Owens, R.K. Singh, F. Foroutan, M. Alqaysi, C.M. Han, C. Mahapatra, & J.C. Knowles, « Sol–gel based materials for biomedical applications », Progress in Materials Science, vol. 77, p. 1-79, avr. 2016, doi: 10.1016/j.pmatsci.2015.12.001.

[76] A. E. Gash, T. M. Tillotson, J. H. Satcher, J. F. Poco, L. W. Hrubesh, et R. L. Simpson, « Use of Epoxides in the Sol−Gel Synthesis of Porous Iron(III) Oxide Monoliths from Fe(III) Salts », Chemistry of materials., vol. 13, no 3, p. 999-1007, mars 2001, doi: 10.1021/cm0007611.

[77] N. J. Tang, W. Zhong, H. Y. Jiang, X. L. Wu, W. Liu, et Y. W. Du, « Nanostructured magnetite (Fe_3O_4) thin films prepared by sol–gel method », Journal of Magnetism and Magnetic Materials, vol. 282, p. 92-95, nov. 2004, doi: 10.1016/j.jmmm.2004.04.022.

[78] A. Aftabtalab, H. Sadabadi, C. S. Chakra, et K. V. Rao, « Magnetite nanoparticles (Fe_3O_4) synthesis for removal of Chromium (VI) from waste water », international journal of scientific and engineering research,, vol. 5, no 1, p. 1419-1423.

[79] Tamilnadu, INDIA, S. Sundar, et S. Piraman, « Nanospheres of Fe_3O_4 Synthesis through Sol-gel Technique and Their Structural & Magnetic Characterization », Indian Journal of Applied Research, vol. 3, no 7, p. 123-126, oct. 2011, doi: 10.15373/2249555X/JULY2013/33.

[80] Y. Liang, K. Sun, et X. Sun, « Hydrothermal synthesis of magnetite: investigation of influence of aging time and mechanism », Micro & Nano Letters, vol. 10, no 2, p. 99-104, févr. 2015, doi: 10.1049/mnl.2014.0344.

[81] H. Deng, X. Li, Q. Peng, X. Wang, J. Chen, et Y. Li, « Monodisperse Magnetic Single-Crystal Ferrite Microspheres », Angewandte Chemie. Int. Ed., vol. 44, no 18, p. 2782-2785, avr. 2005, doi: 10.1002/anie.200462551.

[82] X. Yang, W. Jiang, L. Liu, B. Chen, S. Wu, D. Sun, & F. Li, « One-step hydrothermal synthesis of highly water-soluble secondary structural Fe_3O_4 nanoparticles », Journal of Magnetism and Magnetic Materials, vol. 324, no 14, p. 2249-2257, juill. 2012, doi: 10.1016/j.jmmm.2012.02.111.

[83] S. Majidi, F. Zeinali Sehrig, S. M. Farkhani, M. Soleymani Goloujeh, et A. Akbarzadeh, « Current methods for synthesis of magnetic nanoparticles », Artificial Cells, Nanomedicine, and Biotechnology, vol. 44, no 2, p. 722-734, févr. 2016, doi: 10.3109/21691401.2014.982802.

[84] W. Wu, Q. He, et C. Jiang, « Magnetic Iron Oxide Nanoparticles: Synthesis and Surface Functionalization Strategies », Nanoscale Res Lett, vol. 3, no 11, p. 397-415, nov. 2008, doi: 10.1007/s11671-008-9174-9.

[85] W. Wu, Z. Wu, T. Yu, C. Jiang, et W.-S. Kim, « Recent progress on magnetic iron oxide nanoparticles: synthesis, surface functional strategies and biomedical applications »,

Science and Technology of Advanced Materials, vol. 16, no 2, p. 023501, avr. 2015, doi: 10.1088/1468-6996/16/2/023501.

[86] D. Maity, J. Ding, et J.-M. Xue, « synthesis of magnetite nanoparticles by thermal decomposition: time, temperature, surfactant and solvent effects », functional materials letters, vol. 01, no 03, p. 189-193, déc. 2008, doi: 10.1142/S1793604708000381.

[87] F. I. El-Dib, D. E. Mohamed, O. A. A. El-Shamy, et M. R. Mishrif, « Study the adsorption properties of magnetite nanoparticles in the presence of different synthesized surfactants for heavy metal ions removal », Egyptian Journal of Petroleum, vol. 29, no 1, p. 17, mars 2020, doi: 10.1016/j.ejpe.2019.08.004.

[88] L. S. Ganapathe, M. A. Mohamed, R. Mohamad Yunus, et D. D. Berhanuddin, « Magnetite (Fe_3O_4) Nanoparticles in Biomedical Application: From Synthesis to Surface Functionalisation », Magnetochemistry, vol. 6, no 4, p. 68, déc. 2020, doi: 10.3390/magnetochemistry6040068.

[89] M. Bohra, N. Agarwal, et V. Singh, « A Short Review on Verwey Transition in Nanostructured Fe_3O_4Materials », Journal of Nanomaterials, vol. 2019, p. 1-18, mars 2019, doi: 10.1155/2019/8457383.

[90] S.-N. Sun, C. Wei, Z.-Z. Zhu, Y.-L. Hou, S. S. Venkatraman, et Z.-C. Xu, « Magnetic iron oxide nanoparticles: Synthesis and surface coating techniques for biomedical applications », Chinese Phys. B, vol. 23, no 3, p. 037503, janv. 2014, doi: 10.1088/1674-1056/23/3/037503.

[91] H. Liu et C. Di Valentin, « Band Gap in Magnetite above Verwey Temperature Induced by Symmetry Breaking », J. Phys. Chem. C, vol. 121, no 46, p. 25736-25742, nov. 2017, doi: 10.1021/acs.jpcc.7b09387.

[92] M. Usman, J.M. Byrne, A. Chaudhary, S. Orsetti, K. Hanna, C. Ruby, &S.B. Haderlein, « Magnetite and Green Rust: Synthesis, Properties, and Environmental Applications of Mixed-Valent Iron Minerals », Chemical Reviews, févr. 2018, doi: 10.1021/acs.chemrev.7b00224.

[93] X. Liu, Z. Zhong, Y. Tang, et B. Liang, « Review on the Synthesis and Applications of Fe_3O_4 Nanomaterials », Journal of Nanomaterials, vol. 2013, p. 1-7, 2013, doi: 10.1155/2013/902538.

[94] Y. Chen, H. Xia, L. Lu, et J. Xue, « Synthesis of porous hollow Fe_3O_4 beads and their applications in lithium ion batteries », Journal of materials Chemistry, vol. 22, no 11, p. 5006-5012, févr. 2012, doi: 10.1039/C2JM15440D.

[95] Z. Rehimi, H. Ayadi, et S. Halladja, « Synthesis and characterization of Fe_3O_4−MWCNTs adsorbent: application for Bromocresol Purple dye removal in aqueous medium », journal of New technology and materials, vo 10, n°1, p. 7, 2020.

[96] Wallyn, Anton, et Vandamme, « Synthesis, Principles, and Properties of Magnetite Nanoparticles for In Vivo Imaging Applications—A Review », Pharmaceutics, vol. 11, no 11, p. 601, nov. 2019, doi: 10.3390/pharmaceutics11110601.

[97] X. Hu et al., « Adsorption and heterogeneous Fenton degradation of 17α-methyltestosterone on nano Fe_3O_4/MWCNTs in aqueous solution », Applied Catalysis B: Environmental, vol. 107, no 3, p. 274-283, sept. 2011.

[98] M. Samadishadlou et al., « Magnetic carbon nanotubes: preparation, physical properties, and applications in biomedicine », Artificial Cells, Nanomedicine, and Biotechnology, vol. 46, no 7, p. 1314-1330, oct. 2018, doi: 10.1080/21691401.2017.1389746.

[99] E. Flahaut, F. Agnoli, J. Sloan, C. O'Connor, et M. L. H. Green, « CCVD Synthesis and Characterization of Cobalt-Encapsulated Nanoparticles », Chemistry of Materials., vol. 14, no 6, p. 2553-2558, juin 2002, doi: 10.1021/cm011287h.

[100] Y. Chen et H. Gu, « Microwave assisted fast fabrication of Fe_3O_4-MWCNTs nanocomposites and their application as MRI contrast agents », Materials Letters, vol. 67, no 1, p. 49-51, janv. 2012, doi: 10.1016/j.matlet.2011.09.042.

[101] R. Rahmawati, A. Melati, A. Taufiq, M. Diantoro, B. Yuliarto, S. Suyatman, & D. Kurniadi, D, « Preparation of MWCNT- Fe_3O_4Nanocomposites from Iron Sand Using Sonochemical Route », IOP Conf. Ser.: Materials science and engineering, vol. 202, p. 12-13, mai 2017, doi: 10.1088/1757-899X/202/1/012013.

[102] J. Deng, X. Wen, et Q. Wang, « Solvothermal in situ synthesis of Fe_3O_4-multi-walled carbon nanotubes with enhanced heterogeneous Fenton-like activity », Materials Research Bulletin, vol. 47, no 11, p. 3369-3376, nov. 2012, doi: 10.1016/j.materresbull.2012.07.021.

[103] A. ALI, « Synthesis of Magnetic MWCNTs Nanohybrids and Application in Remediation of Chromium Ions in Refinery Wastewater », Engineering and Technology Journal, vol. 35, no 8 Part A, 2017.

[104] T. Zhao, X. Ji, X. Guo, W. Jin, A. Dang, H. Li, & T. Li, « Preparation and electrochemical property of Fe_3O_4/MWCNT nanocomposite », Chemical Physics Letters, vol. 653, p. 202-206, juin 2016, doi: 10.1016/j.cplett.2016.04.083.

[105] N. Dalali, M. Habibizadeh, K. Rostamizadeh, & S. Nakisa, « Synthesis of magnetite multi-walled carbon nanotubes composite and its application for removal of basic dyes from aqueous solutions: removal of basic dyes », 2014, doi: 10.1002/apj.1784.

[106] H. Sadegh, R. Shahryari-ghoshekandi, et M. Kazemi, « Study in synthesis and characterization of carbon nanotubes decorated by magnetic iron oxide nanoparticles », International Nano Letters, vol. 4, no 4, p. 129-135, 2014.

[107] X. Zhou, C. Fang, Y. Li, N. An, et W. Lei, « Preparation and characterization of Fe_3O_4-CNTs magnetic nanocomposites for potential application in functional magnetic printing ink », Composites Part B: Engineering, vol. 89, p. 295-302, mars 2016, doi: 10.1016/j.compositesb.2015.11.041.

[108] Z. Y. Bai, Q. Yang, et J. L. Wang, « Fe_3O_4/multi-walled carbon nanotubes as an efficient catalyst for catalytic ozonation of p-hydroxybenzoic acid », Int. J. Environ. Sci. Technol., vol. 13, no 2, p. 483-492, févr. 2016, doi: 10.1007/s13762-015-0881-3.

[109] L. Yang, J. Hu, A. Dong, et D. Yang, « Novel Fe_3O_4-CNTs nanocomposite for Li-ion batteries with enhanced electrochemical performance », Electrochimica Acta, vol. 144, p. 235-242, oct. 2014, doi: 10.1016/j.electacta.2014.08.099.

[110] L. Chia-Ching, S. Subramaniam, S. Sivasubramanian, et L. Feng-Huei, « MWCNT-Fe_3O_4-based immuno-PCR for the early screening of nasopharyngeal carcinoma », Materials Science and Engineering: C, vol. 61, p. 422-428, avr. 2016, doi: 10.1016/j.msec.2015.12.055.

[111] H. Zarei, H. Ghourchian, K. Eskandari, et M. Zeinali, « Magnetic nanocomposite of anti-human IgG/COOH–multiwalled carbon nanotubes/ Fe_3O_4 as a platform for electrochemical immunoassay », Analytical Biochemistry, vol. 421, no 2, p. 446-453, févr. 2012, doi: 10.1016/j.ab.2011.12.031.

[112] A. Pistone et al., « Synthesis and magnetic properties of multiwalled carbon nanotubes decorated with magnetite nanoparticles », Physica B: Condensed Matter, vol. 435, p. 88-91, févr. 2014, doi: 10.1016/j.physb.2013.11.015.

[113] M. Kundu, H. Bhardwaj, M. Pandey, P. Krishnan, R. K. Kotnala, et G. Sumana, « Development of electrochemical biosensor based on CNT– Fe_3O_4 nanocomposite to determine formaldehyde adulteration in orange juice », Journal of Food Science and Technology, vol. 56, févr. 2019, doi: 10.1007/s13197-019-03635-7.

[114] H. Teymourian, A. Salimi, et R. Hallaj, « Low potential detection of NADH based on Fe_3O_4 nanoparticles/multiwalled carbon nanotubes composite: Fabrication of integrated dehydrogenase-based lactate biosensor », Biosensors and Bioelectronics, vol. 33, no 1, p. 60-68, mars 2012, doi: 10.1016/j.bios.2011.12.031.

[115] P. Ghoderao, S. Sahare, P. Alegaonkar, A. A. Kulkarni, et T. Bhave, « Multiwalled Carbon Nanotubes Decorated with F Fe_3O_4 Nanoparticles for Efficacious Doxycycline Delivery », ACS Applied Nano Materials, déc. 2018, doi: 10.1021/acsanm.8b02268.

[116] F. Elmi, T. Hosseini, M. S. Taleshi, et F. Taleshi, « Kinetic and thermodynamic investigation into the lead adsorption process from wastewater through magnetic nanocomposite Fe_3O_4/CNT », Nanotechnolgy for environment engineering, vol. 2, no 1, p. 13, juill. 2017, doi: 10.1007/s41204-017-0023-x.

[117] F. H. Malayeri, M. R. Sohrabi, et H. Ghourchian, « Magnetic Multi-Walled Carbon Nanotube as an Adsorbent for toluidine blue O removal from aqueous solution», international journal of nanoscience and nanotechnology, vol 8, n° 2, p. 79-87, 2012.

[118] V. Cleveland, J.-P. Bingham, et E. Kan, « Heterogeneous Fenton degradation of bisphenol A by carbon nanotube-supported Fe_3O_4 », Separation and Purification Technology, vol. 133, p. 388-395, sept. 2014, doi: 10.1016/j.seppur.2014.06.061.

Chapter II

Wastewater treatment

II.1. Introduction

In this chapter, water pollution and especially organic dyes are highlighted. Moreover, the three processes used in this work which are adsorption, heterogeneous Fenton and photo-Fenton are reviewed.

II.2. Water pollution

Literature reported that about 33% of the world population can be suffer from water pollution, which caused by the released chemicals from various sources either anthropogenic or natural. There are different groups of water pollutants that can affect environment and human health; they are divided on organic and inorganic micro-pollutants such as heavy metals and synthetic organic chemicals **[1]**.

II.2.1. Heavy metals

Heavy metals are natural elements that exist in earth's crust, but they are considered as toxic contaminants for living things and environment. Recently, they are widely used in various applications which make the human in their dangers. In which the principle source of human contact with those contaminants is derived from drinking water polluted by lead, arsenic, cadmium, nickel and mercury. Heavy metals can cause diseases that may lead to death. Therefore, care and caution must be taken and radical solutions should be found to solve this problem **[2]**.

II.2.2. Organic pollutants

As opposed to heavy metals which have a limited types of contaminants, organic pollutants are numerous (more than millions) with different functional groups, characteristics and applications. They are mainly divided into pharmaceuticals, cosmetics products, endocrine disruptors, detergents, pesticides, organic dyes, and so forth. In this study we highlight organic dyes due to their potential applications, uncontrolled release and carcinogenic effects **[3, 4]**. Prior to the discovery of synthetic pigments and dyes, a small range of natural colorants were obtained from animals, plants, and minerals. Organic dyes can be defined as synthetic aromatic components with high molecular weight and complex structure. They used in textile, paper industries, plastic, and so on. These dyes exhibit potential mutagenic and carcinogenic impacts on human health and living organisms due to their recalcitrant and persistent nature in water. The widespread of dyes imposed the specialists to classify them according to their application, structure, color, source and solubility. Therefore, we find in literature many classifications such as (acid, basic, reactive, disperse, direct) **[3-5]**. Table.II.1 shows classifications and some characteristics of dyes.

Table.II.1. Types of dyes **[6]**.

Dye class	Characteristics	Pollutants commonly associated with different dyes
Acid	Anionic; soluble in water	Color; unfixed dyes; organic acids.
Basic	Bright; soluble in water	/
Direct	Anionic; soluble in water	Color; unfixed dye; cationic fixing agents; salt; surfactant; leveling and retarding agents; diluents; defoamer.
Disperse	Insoluble in water	Color; carriers ; organic acids; leveling agents; defoamers; phosphates ; lubricants; diluents; dispersants; delustrants.
Reactive	Soluble in water; anionic	Color; alkali; salt; unfixed dye; diluents; surfactants; defoamer.
Sulfur	containing sulfur/sodium sulfide	Color; oxidizing agent; alkali; unfixed dye; reducing agent.
Vat	Oldest dyes; more complex dyes; insoluble in water.	Color; oxidizing agents; alkali; reducing agents.

II.2.2.1. Cationic dyes

Cationic dyes commonly exist in the form of zinc chloride or hydrochloride complexes. They are extensively applied in wool, acrylic, silk dyeing and nylon. Those colorants have various chemical structures depend on their substituted atomic groups. However, these kinds of colorants are viewed as toxic compounds that can provoke harmful impacts such as skin irritation, allergic dermatitis, mutations and even cancer. Cationic dyes are characterized by their positive charge, water solubility and they can result colored cations in aqueous mediums. They are extremely visible with great brilliance and intense color. The cationic functionality is available in various cationic dyes such as azo dyes, methane dyes, phthalocyanine dyes, polycarbocyclic, solvent dyes, anthraquinon, di- and tri-arylcarbenium. There are many examples of cationic dyes such as Crystal Violet, methylene blue, basic blue 41 and basic red 46 **[6]**. Crystal Violet (CV) is a triphenylmethane dye, it considered as an important cationic dye used in medicine (human and veterinary) as a biological stain, and

used also for textiles (cotton and silk), further, it gives printing ink and paints a bright and intense Violet color. Despite its many advantages and large applications, CV is reviewed as a recalcitrant pollutant that persists in water for a long while; it has negative effects on living organisms. Aggressive effects can occur to some fish species due to the exposure to CV which can act as a potent carcinogen, mitotic poison, and even promotes tumor growth. CV is reported as a biohazard compound. It can also provoke moderate eye problems such as: irritation, sensitization to light, permanent injury to conjunctiva and cornea. Acute exposure to CV can cause kidney and respiratory failures as well. Water containing basic dyes is regarded as unsuitable environment for plants to live and grow because contaminants disturb the plants photosynthetic activity due to the reduction of sunlight penetration, in addition to their toxicity to some other aquatic species **[7]**.

II.2.2.2. Anionic dyes

Anionic dyes are typically characterized by negatively charged ions, water solubility and ionic substituent. Anionic colorants comprise a wide variety of compounds from the most diverse dye groups, each with distinct structural differences such as (azoic, nitro dyes, triphenylmethane, anthraquinone and so on). Anionic dyes type also contains direct dyes, while literature reported that huge proportion of reactive colorants are included in anionic azo dyes group. The discharge of reactive dyes in environment has a negative impact, because in water medium, acid dyes have a low fixation degree owing to the hydrolysis of reactive groups. Anionic dyes are considered hydrophilic and applied with wool, silk, modified acrylic, polyamide, and polypropylene fibres **[6]**. Moreover, acidic colorants are used in paper, leather, and ink-jet printing. Despite, they are harmful to environment and human health and considered as carcinogenic. There are large examples of anionic dyes such as (acid orange 10, acid red 183, acid orange 12, acid orange 8, acid red 18, sunset yellow, methyl orange, indigo carmine and so forth) **[8]**. Bromocresol Purple (BCP) is one of the anionic dyes that utilized in medicinal laboratories for the quantification of albumin by spectrophotometric analysis. Furthermore, it is used for other applications like photographing microbiology, **[9]** textile and paper industries. Although manufacturing industries are used BCP colorants in some processes, this dye is soluble in water and consider as a harmful pollutant because it can cause various problems to aquatic organisms and human by itself or when it binds to heavy metals. Therefore, it is extremely recommended for environmental and economical reasons to eliminate and recycle BCP dye from industrial effluents **[10]**.

II.3. Wastewater treatment techniques for organic dyes using Fe_3O_4/MWCNTs nanocomposite

The application of organic dyes in industries has extremely increased in the last decades and has produced various environmental issues. Nowadays, numerous techniques are in practice for wastewater treatment. Effective treatment methods before the release of utilized water in environment are necessary and required **[11]**. Multiple techniques are existed for dye removal and countless scientific papers revealed the success of dye elimination processes. Suitable methods of organic dye removal should be efficient towards most dyes (non-selective), fast, simple, economical and without generating secondary contaminants. Available techniques for wastewater remediation can be divided into three different categories called biological, physical and chemical methods. Despite various dye elimination techniques have been studied in the past decades, only few routes are being implemented in reality nowadays by industries due to the limitations of these methods **[12]**. Numerous techniques and materials are used for the removal of anionic/cationic dyes from aqueous medium such as: adsorption **[13]**, coagulation-flocculation **[14]**, photocatalytic **[15]**, electrochemical **[16]**, Fenton oxidation **[17]**, and so on. In this study adsorption and advanced oxidation processes will be investigated and summarized in the next section owing to their efficiency and simplicity.

II.3.1. Adsorption

Adsorption process is regarded as a feasible technology for water remediation. It is applied for the treatment of wastewaters, industrial effluents and groundwater in order to obtain drinking water. The advantages of this treatment process are vast due to its simplicity, flexibility, versatile design, low-energy conditions, and cost-effectiveness. In general, the economic and feasibility of adsorption method are based on various factors notably the adsorbent type, contaminant properties, process configuration, operating conditions, waste disposal and regeneration **[5]**.

II.3.1.1. Adsorption mechanism

In the literature adsorption is considered as a unit operation, which occurs when a solid phase comes into contact with a fluid phase (gas/liquid) **[18]**. In this study, we focus on the solid–liquid adsorption. Solid phase is called adsorbent and the species which are dissolved in the solvent (normally water) to be adsorbed are called adsorbates. Due to unbalanced forces, the adsorbate compounds are attracted to the surface of adsorbent surface, thus, the surface free energy and freedom degrees are decreased **[19]**. The adsorbate is

transferred from the liquid towards solid until the equilibrium. The distribution in solid and liquid phases can be determined by the degree of affinity between adsorbate and adsorbent **[20]**.

II.3.1.2. Types of adsorption

Depending on the type of interactions between adsorbate and adsorbent, adsorption mainly divided into two types:

II.3.1.2.1. Chemical sorption

Chemical adsorption is known as chemisorption, it characterized by the strong chemical interactions between adsorbent surface and adsorbate molecules or ions with high energy (40-800 $kJ.mol^{-1}$). Typically, this type of sorption is caused by exchange of electrons and just monolayer adsorption is noted; in this case, desorption is challenging which makes chemical adsorption irreversible **[21]**.

II.3.1.2.2. Physical sorption

Physical adsorption is known as physisorption and illustrated by weak van der Waals bonds between the solid and liquid, hence most of physisorption are reversible and multilayer. It characterized by lower energies (5-40 $kJ.mol^{-1}$). The principle physical interactions controlling the adsorption besides the van der Waals forces are dipole–dipole (π–π)interactions, hydrogen bonds and polarity, and so on; with no electron exchange **[22, 23]**.

II.3.1.3. Factors affecting the adsorption of organic dyes

Numerous parameters can affect the adsorption of organic dyes and should be taken into consideration. The pH of the solution tops the list owing to its great importance in controlling dye adsorption; in addition to initial dye concentration, temperature, and so on. Obtaining the optimum values of such parameters can extremely improve the dye removal and contribute in the development of effective wastewater treatment **[24]**.

II.3.1.3.1. Effect of pH

The pH of solution controls both the adsorbent surface and adsorbate molecules. Several studies have discussed the effect of pH on the adsorption of organic pollutants; in order to find in which range the removal is optimum and adsorption is favorable **[25]**. Table.II.2 summarizes the effect of the solution pH on the adsorption of some organic dyes.

Table.II.2. Effect of pH medium on different dye adsorption using Fe_3O_4/MWCNTs adsorbent.

Dye	pH	Adsorption capacity ($mg.g^{-1}$)	References
Bromocresol Purple	8	296.520	**[26]**
Crystal Violet	9	38.000	**[27]**
Reactive Violet 2	6	52.356	**[28]**

Point of zero charge is an important parameter that characterizes the adsorbent and indicates at which the charge of its surface is equal to zero. Herein, the value of pH plays a critical role to understand the adsorption mechanism for solids contain functional groups on their surfaces. Therefore, the adsorption of cationic dyes is favorable in the presence of negative charge onto the adsorbent surface when $pH > pH_{PZC}$. And vice versa, adsorption of anionic dyes is favorable when the positive charge is dominated on the adsorbent surface, at which $pH < pH_{PZC}$ **[29, 30]**.

II.3.1.3.2. Effect of initial dye concentration

Initial dye concentration can affect the removal of dye by adsorption process, because when the initial dye concentration increases the amount of species increased in the solution, while the available active sites containing in the solid is limited at constant temperature. Typically, dye removal efficiency at higher concentrations decreases due to the saturation of active sites. But, it is not the same case for adsorption capacity because the increase of initial pollutant concentration can improve the mass transfer by high driving force **[31, 32]**.

II.3.1.3.3. Effect of temperature

Temperature has a significant and direct effect on the adsorption capacity, if the adsorption improved at higher temperatures. It can be explained by the stimulating of molecules mobility and increasing active site numbers, in this case adsorption exhibits endothermic nature. By contrast, the adsorption capacity can decrease by increasing temperature if the process is exothermic, because of reducing adsorptive forces between the active sites and dye species **[24]**.

II.3.1.3.4. Effect of adsorbent amount

The adsorption can be influenced by the solid amount, because the number of active sites increases, if the adsorbent dosage increases. As a result, dye removal percentage can be improved due to the rise on the active sites. This is a very important study from an economic point of view **[33]**.

II.3.1.4. Adsorption kinetics

The target of this study lays in the determination of rate constant by studying the adsorption kinetics **[34]**. Researchers are seeking for the adsorbent that can offer higher adsorption capacity with faster adsorption rate**.** Among various models the pseudo-first-order, pseudo-second-order and intraparticle diffusion are the most used models in literature **[5]**.

II.3.1.4.1. Pseudo-first-order

The pseudo-first-order (PFO) delivered by (Lagergren, 1898) is depended on the adsorption capacity of the solid **[35]**.

Various studies consider this model as the most suitable for representing adsorption kinetics. There are many linear equations of the PFO model; although, non linear is the best equation to minimize the standard errors **[5]**.

II.3.1.4.2. Pseudo-second-order

The pseudo-second-order model has been applied to describe adsorption of dyes, metal ions, and other organic compounds from aqueous medium **[5]**.

In general, kinetic adsorption is better fitted by PSO model for cationic and anionic dye adsorption **[36]**.

II.3.1.4.3. Intraparticle diffusion

Intraparticle diffusion model indicates that adsorption capacity 'q_t'is in correlation with $t^{0.5}$ the half-power of time. Typically, the plot of the model is linear at the initial stage if intraparticle diffusion is the rate limiting step.

Furthermore, the plot of q_t as function of $t^{0.5}$ may exhibit multi-linearity, which reveals that more than one rate controlling steps take a place in the adsorption mechanism **[37, 38]**.

II.3.1.5. Adsorption isotherms

The study of adsorption isotherm is necessary to understand the adsorption mechanism, the interactions between adsorbent and adsorbate and evaluate the adsorption capacity. In the literature, the solid surface can be monolayer or multilayer. Among various isotherm models Langmuir and Freundlich are commonly applied in addition to Dubinin, in order to describe dye adsorption phenomena **[24]**.

II.3.1.5.1. Langmuir isotherm model

The common isotherm model of Langmuir suggests that adsorption occurs onto specific homogeneous active sites of the adsorbent. This model has been applied effectively for monolayer adsorption studies **[39]**.

Furthermore, Langmuir isotherm assumes that one site cannot hold more than molecule, the surface is uniform, the sites are identical in terms of energy, and the competence of a site to adsorb molecules is independent with neighboring occupation **[40]**.

II.3.1.5.2. Freundlich isotherm model

Freundlich isotherm suggests that adsorption occurs in a heterogeneous surface, and the sites are not energetically equivalent.

This isotherm model aims to integrate the role of the interactions between the adsorbate molecules (adsorbate–adsorbate) on the surface.

II.3.1.5.3. Dubinin–Radushkevich (D-R)

Dubinin–Radushkevich (D-R) model assumes that the size of adsorbent is similar to micro-pore size.

II.3.1.6. Thermodynamic study of adsorption

Thermodynamic study provides us by essential information about the amount of energies, adsorption nature, interactions and so on. Table.II.3 summarizes the most important energies obtained by Van't Hoff plot ($\ln(k_e)$ as function of 1/T), with the appropriate interpretation for each result, which are previously discussed in literature **[5]**.

Table.II.3. Thermodynamic parameters **[5, 21, 23]**.

Energy ($kJ.mol^{-1}$)	Result	Interpretation
ΔG^0	$\Delta G^0 < 0$	Adsorption is spontaneous ,favorable and enthalpy controlled process
	$\Delta G^0 > 0$	adsorption is an entropy controlled process
ΔH^0	$\Delta H^0 < 0$	Adsorption is exothermic
	$\Delta H^0 > 0$	Adsorption is endothermic
	$\Delta H^0 < 20$	Physisorption (van der Waals interactions)
	$20 < \Delta H^0 < 80$	Electrosatic interaction
	$80 < \Delta H^0 < 450$	Chemisorption
ΔS^0	$\Delta S^0 < 0$	Dramatical decreases in the randomness at the liquid/ solid interface within the adsorption
	$\Delta S^0 > 0$	Possibility of some changes in adsorbent/adsorbate structure changes or readjustments in the adsorbate–adsorbent complex.

II.3.1.7. Desorption

Desorption process is aimed to regenerate the solid adsorbent, recuperate the dye compounds, and even help to understand well the adsorption mechanism. The rate of desorption depends on the driving force, and kinetic study of desorption is necessary for the pollutant transport modeling. Typically, desorption carried out by adding appropriate solvent to the adsorbent saturated by dye molecules under stirring for a certain time. When the dye molecules extracted from the adsorbent, this solid should be separated from the solution using external magnetic field (for Fe_3O_4/MWCNTs and other magnetic nanocomposites). After that, both of the adsorbent and adsorbate can be recovered by putting each one in oven to evaporate the solvents at suitable temperature **[33]**. Dalali et al, 2013 have been studied the desorption of Crystal Violet dye and the generation of Fe_3O_4/MWCNTs adsorbent using different solvents such as (acetone, ethanol, methanol, and hydrogen chloride). This study revealed that

ethanol was the best solvent for CV desorption at pH equal to 1. Hence, adsorbent was reused after its generation at the optimum conditions of desorption for eight times, without notable loss in the removal efficiency (approximately 96 %) **[27]**.

II.3.2. Advanced oxidation processes (AOPs)

The AOPs with their great oxidation power have attracted the fancy of the researchers worldwide. The ·OH radicals are generated by the reaction occurred within these processes, these species exhibit high oxidation efficiency towards organic pollutants in wastewater. Simple illustration in figure.II.1 highlights the most available methods including in AOPs. In order to compare other techniques with that of AOPs, table.II.4 summarizes standard reduction potentials (SRP) of most applied oxidizing agents. As shown in the table, hydroxyl radicals possesses higher potential (E°= 2.80 V), which make them very efficient and effective for the degradation of several contaminants **[42]**. Despite, fluorine has the highest SRP (E°=3.03 V) and considered as an extremely electronegative and reactive element, it has great affinity with positively charged ions like calcium which can affect the bone and provoked serious diseases in the case of its presence in drinking water **[43]**.

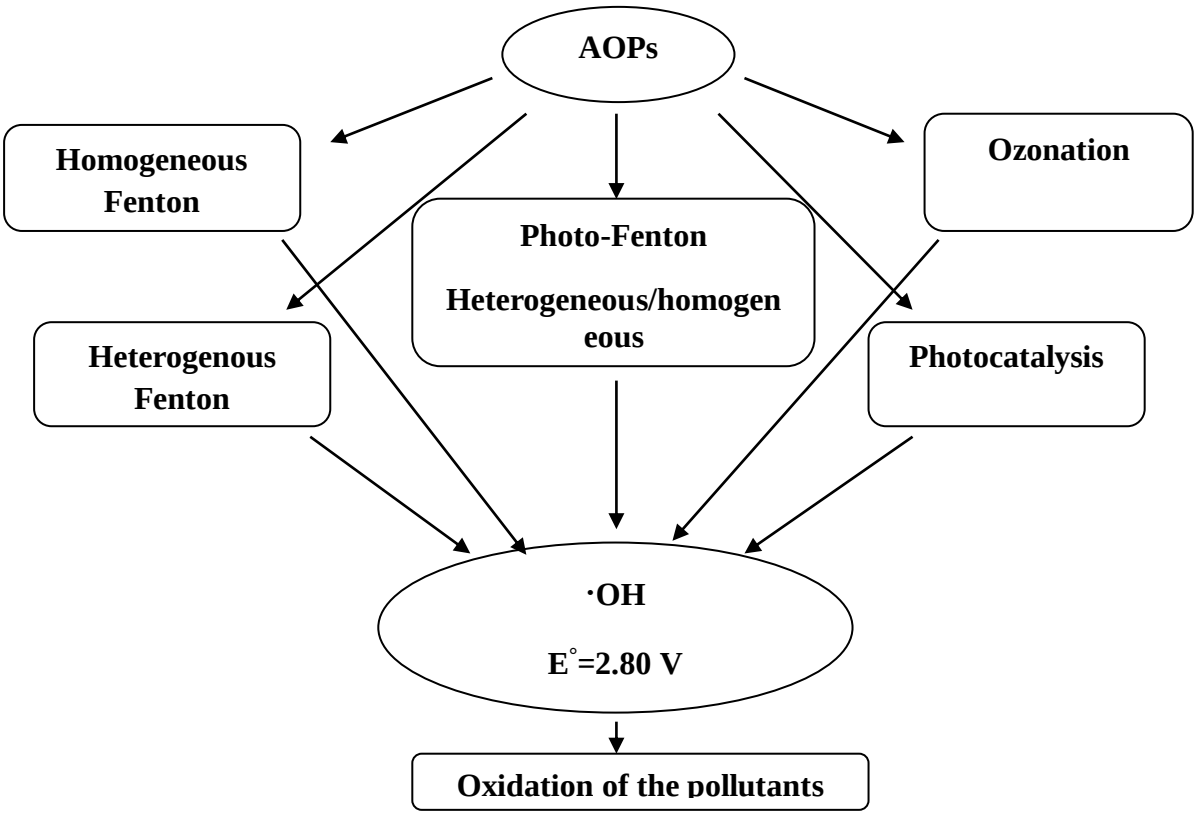

Figure.II.1. AOPs types **[42]**.

Table.II.4. SRP of most common oxidizing agents **[42]**.

Oxidizing agent	F_2	·OH	O	O_3	H_2O_2	·OOH	MnO_4^-	Cl_2	O_2
E°(V)	3.03	2.80	2.42	2.07	1.78	1.70	1.68	1.36	1.23

II.3.2.1. Heterogeneous Fenton reaction

Typically, Fenton processes include heterogeneous and homogeneous Fenton reactions. The heterogeneous Fenton is considered as a reaction between H_2O_2 (hydrogen peroxide) and Fe^{2+} in a solid matrix to generate highly oxidizing compounds. The reaction may occur even at neutral pH, so, acidification and neutralization steps are not necessary, hence preventing the reaction from sludge formation. This reaction has huge advantages compared with homogeneous process. Moreover, applied catalysts can be recovered and reduced. In heterogeneous Fenton reaction the Fe^{2+} in the Fenton reagent is replaced by a solid catalyst, despite homogeneous Fenton reactions are obtained by the combination of other compounds such as (metal ion(s),metal inorganic ligand complexes) and H_2O_2; equations bellow shows Fenton reactions **[42, 44]**:

$$H_2O_2 + Fe^{2+} \rightarrow Fe^{3+} + \cdot OH + OH^- \qquad \text{(eq.1)}$$

H_2O_2 can react with Fe^{3+}, it is known as Fenton like reaction:

$$H_2O_2 + Fe^{3+} \rightarrow FeOOH^{2+} + H^+ \qquad \text{(eq.2)}$$

$$FeOOH^{2+} \rightarrow Fe^{2+} + \cdot OOH \qquad \text{(eq.3)}$$

$$Fe^{3+} + \cdot OOH \rightarrow Fe^{2+} + O_2 + H^+ \qquad \text{(eq.4)}$$

Several parameters can affect the heterogeneous Fenton reaction such as pH, initial dye concentration, H_2O_2 dosage, temperature and so on. Therefore, the study of these parameters effect is very important **[44]**.

II.3.2.1.1. pH effect

The study of pH effect is necessary for Fenton processes because it is an important factor for effective wastewater treatment. In the literature, several studied have been agreed that pH around 3 is the optimum value for the heterogeneous Fenton process. While, other studies revealed that neutral and alkaline conditions offered good results for organic pollutants degradation **[45, 46]**.

II.3.2.1.2. H_2O_2 dosage effect

Hydrogen peroxide is the principle source that produces ·OH under catalysis in Fenton reaction, so, H_2O_2 is an important factor in this process; batch experiments can determine the optimum value of H_2O_2 dosage. Lower H_2O_2 concentrations lead to decreasing in the degradation efficiency, due to the poor producing of hydroxyl radicals by the decomposition

of hydrogen peroxide under catalysis. In contrast, higher H_2O_2 concentrations are not preferable owing to the increase in treatment cost and the scavenger of H_2O_2 on $HO^{\cdot}$, which is increased with the excess of H_2O_2 according to (eq.5):

$$H_2O_2 + HO^{\cdot} \rightarrow H_2O + HO_2^{\cdot} \qquad \text{(eq.5)}$$

The evaluation of H_2O_2 concentration is mainly based on the type and initial concentration of the contaminant **[44]**. To conclude, literature revealed that stepwise addition of hydrogen peroxide is the best way to improve the efficiency of water treatment **[47]**.

II.3.2.1.3. Initial dye concentration effect

Initial dye concentration is one of the operating parameters that can affect degradation efficiency along with initial pH, temperature and hydrogen peroxide concentration .Typically, oxidation rate decreases with the increase of initial concentration of dye due to a limited number of $HO^{\cdot}$ against pollutant molecules. Moreover, the generation of $HO^{\cdot}$ radicals at higher concentrations can be reduced, because dye particles may occupy the active sites on the surface of catalyst **[48]**.

II.3.2.1.4. Temperature effect

According to the Arrhenius' law, higher temperatures may result a faster formation of hydroxyl radicals via the Fenton reaction. Obviously, rise temperature can not only improve the generation of ·OH; but also they could accelerate the molecules movement. Thereby, increase the collision between dye and free radicals and enhance degradation efficiency in short reaction time. Although, in literature various studies revealed that 40 °C or less than that was found as an optimum value; to avoid the simultaneous accelerated decomposition of hydrogen peroxide into water and oxygen, iron leaching and high cost at excessive temperature **[48, 49]**.

II.3.2.2. Heterogeneous photo-Fenton reaction

Fenton reaction can be performed in the presence of light source or without it, when the Fenton reaction coupled with a source of radiation, it will be known as photo-Fenton process which produce $HO^{\cdot}$ according to reactions (eq.6) and (eq.7) .Furthermore, photo-Fenton exhibit better performance than Fenton alone owing to the faster regeneration of iron (II) produced (eq.8) and (eq.9) **[50]**:

$$Fe^{3+} + H_2O + h\upsilon \rightarrow Fe^{2+} + HO^{\cdot} + H^{+} \qquad \text{(eq.6)}$$

$$H_2O_2 + Fe^{3+} + h\upsilon \rightarrow Fe^{2+} + HO_2^{\cdot} + H^{+} \qquad \text{(eq.7)}$$

$$H_2O_2 + Fe^{2+} \rightarrow [Fe(OH)]^{2+} + HO^{\cdot} \qquad \text{(eq.8)}$$

$$[Fe(OH)]^{2+} + h\upsilon \rightarrow Fe^{2+} + HO^{\cdot} \qquad \text{(eq.9)}$$

II.4. Conclusion

During this chapter, we have seen that organic dyes are considered as harmful pollutant and can cause several environmental and health problems. According to the studies consulted in the bibliography, it seems that Fe_3O_4/MWCNTs nanocomposite has proved its efficiency for the removal of those contaminants as an adsorbent or as a catalyst. The various techniques and materials used in the present work will be highlighted in the next chapter beside the experimental methods applied in the preparation of magnetite and the nanocomposite.

References

[1] R. P. Schwarzenbach, T. Egli, T. B. Hofstetter, U. von Gunten, et B. Wehrli, « Global Water Pollution and Human Health », Annu. Rev. Environ. Resour., vol. 35, n° 1, p. 109‑136, nov. 2010, doi: 10.1146/annurev-environ-100809-125342.

[2] Z. Fu et S. Xi, « The effects of heavy metals on human metabolism », Toxicology Mechanisms and Methods, vol. 30, n° 3, p. 167‑176, mars 2020, doi: 10.1080/15376516.2019.1701594.

[3] F. Lu et D. Astruc, « Nanocatalysts and other nanomaterials for water remediation from organic pollutants », Coordination Chemistry Reviews, vol. 408, p. 213180, avr. 2020, doi: 10.1016/j.ccr.2020.213180.

[4] L. Tang, J.J. Wang, L. Wang, C.T. Jia, G.X. Lv, N. Liu, & M.H. Wu, « Facile Synthesis of Silver Bromide-Based Nanomaterials and Their Efficient and Rapid Selective Adsorption Mechanisms Toward Anionic Dyes », ACS Sustainable Chemistry and engineering., vol. 4, n° 9, p. 4617‑4625, sept. 2016, doi: 10.1021/acssuschemeng.6b00743.

[5] A. Bonilla-Petriciolet, D. I. Mendoza-Castillo, et H. E. Reynel-Ávila, Éd., Adsorption Processes for Water Treatment and Purification. Cham: Springer International Publishing, 2017, doi : 10.1007/978-3-319-58136-1

[6] N. Tripathi, « Cationic and anionic dye adsorption by agricultural solid wastes: A comprehensive review by »: IOSR Journal of Applied Chemistr, vol. 5, p. 91‑108, janv. 2013, doi: 10.9790/5736-5391108.

[7] S. Mani et R. N. Bharagava, « Exposure to Crystal Violet, Its Toxic, Genotoxic and Carcinogenic Effects on Environment and Its Degradation and Detoxification for Environmental Safety », Rev Environ Contam Toxicol, vol. 237, p. 71‑104, 2016, doi: 10.1007/978-3-319-23573-8_4.

[8] S. Homaeigohar, « The Nanosized Dye Adsorbents for Water Treatment », Nanomaterials, vol. 10, n° 2, p. 295, févr. 2020, doi: 10.3390/nano10020295.

[9] O. I. M. Ali, E. A. E. Menofy, et A. H. H. T. Kandil, « Synthesis, characterisation and application of ZnO-bentonite nanocomposite for preconcentration and spectrophotometric determination of trace amounts of Bromocresol Purple in water and wastewater samples », International Journal of Environmental Analytical Chemistry, vol. 0, n° 0, p. 1‑18, juill. 2019, doi: 10.1080/03067319.2019.1639689.

[10] L. Aljerf, « High-efficiency extraction of Bromocresol Purple dye and heavy metals as chromium from industrial effluent by adsorption onto a modified surface of zeolite: Kinetics and equilibrium study », Journal of Environmental Management, vol. 225, p. 120‑132, nov. 2018, doi: 10.1016/j.jenvman.2018.07.048.

[11] N. Y. Donkadokula, A. K. Kola, I. Naz, et D. Saroj, « A review on advanced physico-chemical and biological textile dye wastewater treatment techniques », Reviews in environmental science and biotechnology, vol. 19, n° 3, p. 543‑560, sept. 2020, doi: 10.1007/s11157-020-09543-z.

[12] V. Katheresan, J. Kansedo, et S. Y. Lau, « Efficiency of various recent wastewater dye removal methods: A review », Journal of Environmental Chemical Engineering, vol. 6, n° 4, p. 4676‑4697, août 2018, doi: 10.1016/j.jece.2018.06.060.

[13] O. A. Shabaan, H. S. Jahin, et G. G. Mohamed, « Removal of anionic and cationic dyes from wastewater by adsorption using multiwall carbon nanotubes », Arabian Journal of chemistry, vol. 13, n° 3, p. 4797‑4810, mars 2020, doi: 10.1016/j.arabjc.2020.01.010.

[14] Y.-Y. Lau, Y.-S. Wong, T.-T. Teng, N. Morad, M. Rafatullah, et S.-A. Ong, « Degradation of cationic and anionic dyes in coagulation–flocculation process using bi-functionalized silica hybrid with aluminum-ferric as auxiliary agent », RSC Advances., vol. 5, n° 43, p. 34206‑34215, avr. 2015, doi: 10.1039/C5RA01346A.

[15] M. Mehrabi et V. Javanbakht, « Photocatalytic degradation of cationic and anionic dyes by a novel nanophotocatalyst of $TiO_2/ZnTiO_3/\alpha Fe_2O_3$ by ultraViolet light irradiation », Journal of Materials Science: Materials in Electronics, vol. 29, n° 12, p. 9908‑9919, juin 2018, doi: 10.1007/s10854-018-9033-0.

[16] M. Morsi, A. Al-Sarawy, et W. El-Dein, « Electrochemical degradation of some organic dyes by electrochemical oxidation on a Pb/PbO_2 electrode », Desalination and Water Treatment, vol. 26, p. 301‑308, févr. 2011, doi: 10.5004/dwt.2011.1926.

[17] N. P.V., R. Gandhimathi, et R. Srikrishnaperumal, « Degradation of Dyes from Aqueous Solution by Fenton Processes: A Review », Environmental science and pollution research international, vol. 20, janv. 2013, doi: 10.1007/s11
356-012-1385-z.

[18] D. M. Ruthven, Principles of Adsorption and Adsorption Processes. John Wiley & Sons, 1984.

[19] M. Suzuki, Fundamentals of Adsorption. Elsevier, 1993.

[20] J. Rouquerol, F. Rouquerol, P. Llewellyn, G. Maurin, et K. S. W. Sing, Adsorption by Powders and Porous Solids: Principles, Methodology and Applications. Academic Press, 2013.

[21] G. Crini et P.-M. Badot, « Application of chitosan, a natural aminopolysaccharide, for dye removal from aqueous solutions by adsorption processes using batch studies: A review of recent literature », Progress in Polymer Science, vol. 33, nº 4, p. 399‑447, avr. 2008, doi: 10.1016/j.progpolymsci.2007.11.001.

[22] S. J. Allen et B. Koumanova, « Decolourisation of water/wastewater using adsorption », Journal of the University of Chemical Technology and Metallurgy, vol. 40, nº 3, p. 175‑192, 2005.

[23] C. P. Bergmann et F. M. Machado, Éd., Carbon Nanomaterials as Adsorbents for Environmental and Biological Applications. Cham: Springer International Publishing, 2015.

[24] M. T. Yagub, T. K. Sen, S. Afroze, et H. M. Ang, « Dye and its removal from aqueous solution by adsorption: A review », Advances in Colloid and Interface Science, vol. 209, p. 172‑184, juill. 2014, doi: 10.1016/j.cis.2014.04.002.

[25] B. K. Nandi, A. Goswami, et M. K. Purkait, « Removal of cationic dyes from aqueous solutions by kaolin: Kinetic and equilibrium studies », Applied Clay Science, vol. 42, nº 3, p. 583‑590, janv. 2009, doi: 10.1016/j.clay.2008.03.015.

[26] Z. Rehimi, H. Ayadi, et S. Halladja, « Synthesis and characterization of Fe_3O_4–MWCNTs adsorbent: application for Bromocresol Purple dye removal in aqueous medium », vol. 10, no 1, p. 31-37, 2020.

[27] N. Dalali, M. Habibizadeh, K. Rostamizadeh, et S. Nakisa, « Synthesis of magnetite multi-walled carbon nanotubes composite and its application for removal of basic dyes from aqueous solutions: REMOVAL OF BASIC DYES », 2014, doi: 10.1002/apj.1784.

[28] M. Tavakoli, F. Safa, et N. Abedinzadeh, « Binary nanocomposite of Fe_3O_4/MWCNTs for adsorption of Reactive Violet 2: Taguchi design, kinetics and equilibrium isotherms », Fullerenes, Nanotubes and Carbon Nanostructures, vol. 27, nº 4, p. 305‑316, avr. 2019, doi: 10.1080/1536383X.2018.1563543.

[29] W. Liu, C. Yao, M. Wang, J. Ji, L. Ying, et C. Fu, « Kinetics and thermodynamics characteristics of cationic yellow X-GL adsorption on attapulgite/rice hull-based activated carbon nanocomposites », Environmental Progress & Sustainable Energy, vol. 32, nº 3, p. 655‑662, 2013, doi: https://doi.org/10.1002/ep.11680.

[30] B. K. Nandi, A. Goswami, et M. K. Purkait, « Adsorption characteristics of brilliant green dye on kaolin », Journal of Hazardous Materials, vol. 161, nº 1, p. 387‑395, janv. 2009, doi: 10.1016/j.jhazmat.2008.03.110.

[31] Y. Bulut et H. Aydın, « A kinetics and thermodynamics study of methylene blue adsorption on wheat shells », Desalination, vol. 194, nº 1, p. 259‑267, juin 2006, doi: 10.1016/j.desal.2005.10.032.

[32] J. Zhang, Q. Zhou, et L. Ou, « Kinetic, Isotherm, and Thermodynamic Studies of the Adsorption of Methyl Orange from Aqueous Solution by Chitosan/Alumina Composite », Journal of Chemical & Engineering Data, vol. 57, nº 2, p. 412‑419, févr. 2012, doi: 10.1021/je2009945.

[33] M. A. M. Salleh, D. K. Mahmoud, W. A. W. A. Karim, et A. Idris, « Cationic and anionic dye adsorption by agricultural solid wastes: A comprehensive review », Desalination, vol. 280, nº 1, p. 1‑13, oct. 2011, doi: 10.1016/j.desal.2011.07.019.

[34] V. Gómez, M. S. Larrechi, et M. P. Callao, « Kinetic and adsorption study of acid dye removal using activated carbon », Chemosphere, vol. 69, nº 7, p. 1151‑1158, oct. 2007, doi: 10.1016/j.chemosphere.2007.03.076.

[35] H. Yuh-Shan, « Citation review of Lagergren kinetic rate equation on adsorption reactions », Scientometrics, vol. 59, nº 1, p. 171‑177, janv. 2004, doi: 10.1023/b:scie.0000013305.99473.cf.

[36] U. R. Lakshmi, V. C. Srivastava, I. D. Mall, et D. H. Lataye, « Rice husk ash as an effective adsorbent: Evaluation of adsorptive characteristics for Indigo Carmine dye », Journal of Environmental Management, vol. 90, nº 2, p. 710‑720, févr. 2009, doi: 10.1016/j.jenvman.2008.01.002.

[37] Y. S. Ho et G. Mckay, « Kinetic Models for the Sorption of Dye from Aqueous Solution by Wood », Process Safety and Environmental Protection, vol. 76, nº 2, p. 183‑191, mai 1998, doi: 10.1205/095758298529326.

[38] A. W. M. Ip, J. P. Barford, et G. McKay, « A comparative study on the kinetics and mechanisms of removal of Reactive Black 5 by adsorption onto activated carbons and bone char », Chemical Engineering Journal, vol. 157, nº 2, p. 434‑442, mars 2010, doi: 10.1016/j.cej.2009.12.003.

[39] I. Langmuir, « The adsorption of gases on plane surfaces of glass, mica and platinum. », Journal of the American Chemical society., vol. 40, nº 9, p. 1361‑1403, sept. 1918, doi: 10.1021/ja02242a004.

[40] J. de Paula, ATKINS' PHYSICAL CHEMISTRY. W. H. Freeman and Company New York, 2006.

[41] H. Freundlich, « Über die Adsorption in Lösungen », Zeitschrift für Physikalische Chemie, vol. 57U, n° 1, p. 385‑470, 1907, doi: 10.1515/zpch-1907-5723.

[42] M. C. Pereira, L. C. A. Oliveira, et E. Murad, « Iron oxide catalysts: Fenton and Fenton like reactions – a review », Clay miner., vol. 47, n° 3, p. 285‑302, sept. 2012, doi: 10.1180/claymin.2012.047.3.01.

[43] M. Bodzek et K. Konieczny, « Fluorine in the Water Environment - Hazards and Removal Methods », Engineering and Protection of Environment, vol. 21, p. 113‑141, avr. 2018, doi: 10.17512/ios.2018.2.1.

[44] N. Wang, T. Zheng, et P. Wang, « A review on Fenton-like processes for organic wastewater treatment », Journal of Environmental Chemical Engineering, vol. 4, p. 762‑787, mars 2016, doi: 10.1016/j.jece.2015.12.016.

[45] C. Yang, D. Wang, et Q. Tang, « The synthesis of NdFeB magnetic activated carbon and its application in degradation of azo dye methyl orange by Fenton-like process », Journal of the Taiwan Institute of Chemical Engineers, vol. 45, n° 5, p. 2584‑2589, sept. 2014, doi: 10.1016/j.jtice.2014.06.010.

[46] H.-Y. Xu, W.-C. Liu, S.-Y. Qi, Y. Li, Y. Zhao, et J.-W. Li, « Kinetics and optimization on discoloration of dyeing wastewater by schorl-catalyzed fenton-like reaction », Journal of the Serbian Chemical Society, vol. 79, n° 3, p. 361‑377, 2014.

[47] H. Zhang, X. Wu, et X. Li, « Oxidation and coagulation removal of COD from landfill leachate by Fered–Fenton process », Chemical Engineering Journal, vol. 210, p. 188‑194, nov. 2012, doi: 10.1016/j.cej.2012.08.094.

[48] S. Adityosulindro, « Activation of homogeneous and heterogeneous Fenton processes by », p. 251.

[49] X. Lv, Y. Ma, Y. Li, et Q. Yang, « Heterogeneous Fenton-Like Catalytic Degradation of 2,4-Dichlorophenoxyacetic Acid by Nano-Scale Zero-Valent Iron Assembled on Magnetite Nanoparticles », Water, vol. 12, n° 10, p. 2909, oct. 2020, doi: 10.3390/w12102909.

[50] H. Ayoub, « Heterogeneous photo-Fenton process for removal of micropollutants at very low concentration from Meurthe river », p. 237.

Chapter III
Materials and methods

III.1. Introduction

This work includes the oxidation of MWCNTs method and the functionalization of their surface with magnetite. The prepared nanocomposite was characterized and investigated as an adsorbent for the removal of Bromocresol Purple (BCP) in aqueous medium. Furthermore, the study of Fe_3O_4/MWCNTs efficiency as a catalyst was carried out in the degradation of Crystal Violet (CV) molecules in aqueous solution, through Fenton and photo-Fenton processes. In this section, reagents, experimental materials, preparation and analysis methods are discussed.

III.2. Chemical products

Experimental study requires many types of reagents to accomplish the work, so, the essential products utilized in the synthesis methods or other experiments have been highlighted in table.III.1. Various reagents were used without further purification only the MWCNTs which were treated before the functionalization.

Table III.1. Manufacturer and quality of reagents used.

Reagent	Molecular formula	Purity	Manufacturer
Multi-walled carbon nanotubes	MWCNTs	> 90%	Nanocyl 7000
Nitric acid	HNO_3	53%	Montplet & Esteban SA(Panreac)
Sodium hydroxide	NaOH	98%	Prolabo
Hydrochloric acid	HCl	36.5-38%	Honeywell Fluka
Ammonium hydroxide	NH_4OH	25%	Ho
Hydrogen peroxide	H_2O_2	30%	Biochem
Iron(II) sulfate sesquihydrate	$FeSO_41.5H_2O$	-	Biochem
Ferric trichloride hexahydrate	$FeCl_3.6H_2O$	-	Biochem
Bromocresol Purple	$C_{21}H_{16}Br_2O_5S$	-	Biochem
Crystal Violet	$C_{25}H_{30}ClN_3$	-	Sigma-Aldrich

III.3. Physical and chemical characteristics of BCP and CV dyes

Bromocresol Purple is a dye of the triphenylmethane family; it is a substrate of solid form and complex structure. BCP dye can possess two different forms under equilibrium state **[1]**; the dominant form in this study is showed in figure.III.1 "b" at pH about 6. Wherein, Crystal Violet or Methyl Violet 10B is another synthetic dye, known as a triarylmethane **[2]**. The choice of the two dyes is based on the following parameters: high solubility in water, simple analysis by UV-visible spectrophotometry and low (or no) volatility **[1]**. Choice of two synthetic dyes with different structure: cationic for Crystal Violet and anionic for Bromocresol Purple. Table.III.2 summarizes some physical and chemical characteristics of the two substrates.

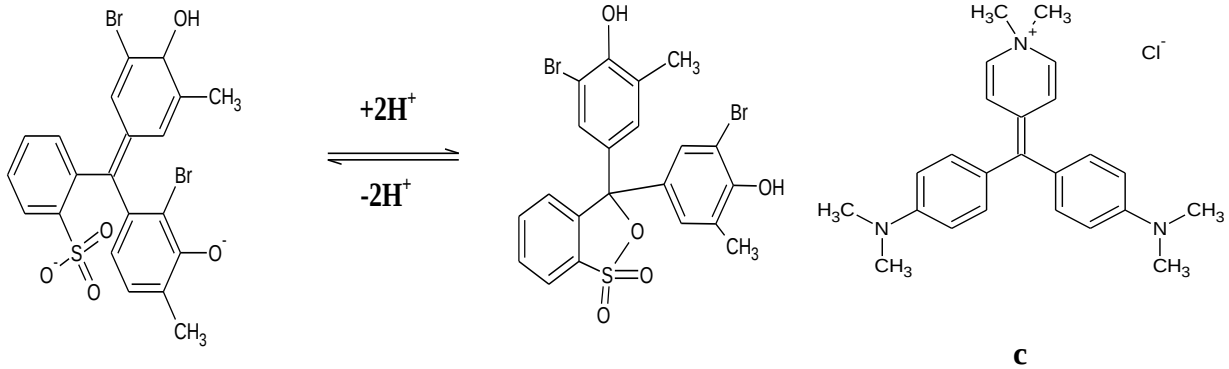

a **b** **c**

Figure.III.1. (a) and (b) the two forms of BCP molecule structures **[3]**, (c) CV molecule structure **[2]**.

Table.III.2. Physical-chemical characteristics of BCP and CV dyes **[2-4]**.

Dye	BCP	CV
Chemical name	5′,5″-dibromo-*o*-cresolsulfophthalein	Chlorure de 4-[4,4' bis(diméthylamino) benzhydrylidène]cyclohexa-2,5-dien-1-llidène]diméthylammonium
Molecular weight (g/mol)	540.24	407.98
λ_{max}(nm)	432	590
Solubility in water at 25 °C (g.L^{-1})	20	16
pK_a	6.3	9.4
Appearance	Purple powder	Light green to dark (green-brown)

III.4. Synthesis of Fe_3O_4/MWCNTs nanocomposites

The preparation of Fe_3O_4/MWCNTs nanocomposites is divided into two main steps; the first one is the oxidation of pure multi-walled carbon nanotubes. The second one is the functionalization of oxidized-MWCNTs by magnetite.

III.4.1. Activation of MWCNTs

The activation of MWCNTs particles was the initial step, it aims to reduce the impurities, introduce functional groups as well as defects, cut and open the extremities of the nanotubes (figure.III.2) **[5]**. Furthermore, this method can increase pore volume and the surface area, which enhance the adsorption of species onto CNTs **[6]**. In this work, the activation process was carried out in order to increase the dispersion of nanoparticles in aqueous mediums, and improve the functionalization of carbon nanotubes with magnetite, by increasing the interfacial adhesion to obtain MWCNTs-based nanocomposites **[7]**. Chemical oxidation by nitric acid (HNO_3) is one of the most common methods used in the activation of CNTs **[8, 9]**. In 250 mL flask, 1g of MWCNTs was introduced, and then 200 mL of nitric acid (HNO_3, 3M) was added to the solid, for a good dispersion, the flask was placed in an ultrasonic bath (BRANSONIC 220/F, 48 KHz) for 30 min. Then the mixture was placed under reflux at temperature equal to 80 °C with rigorous stirring during 4 hours. After the cooling, the mixture was washed with distilled water several times until neutral pH. The obtained solid was dried in oven at 80°C for 4 hours. Finally, the oxidized- MWCNTs was calcined in furnace at 450°C for 4 hours **[7]**.

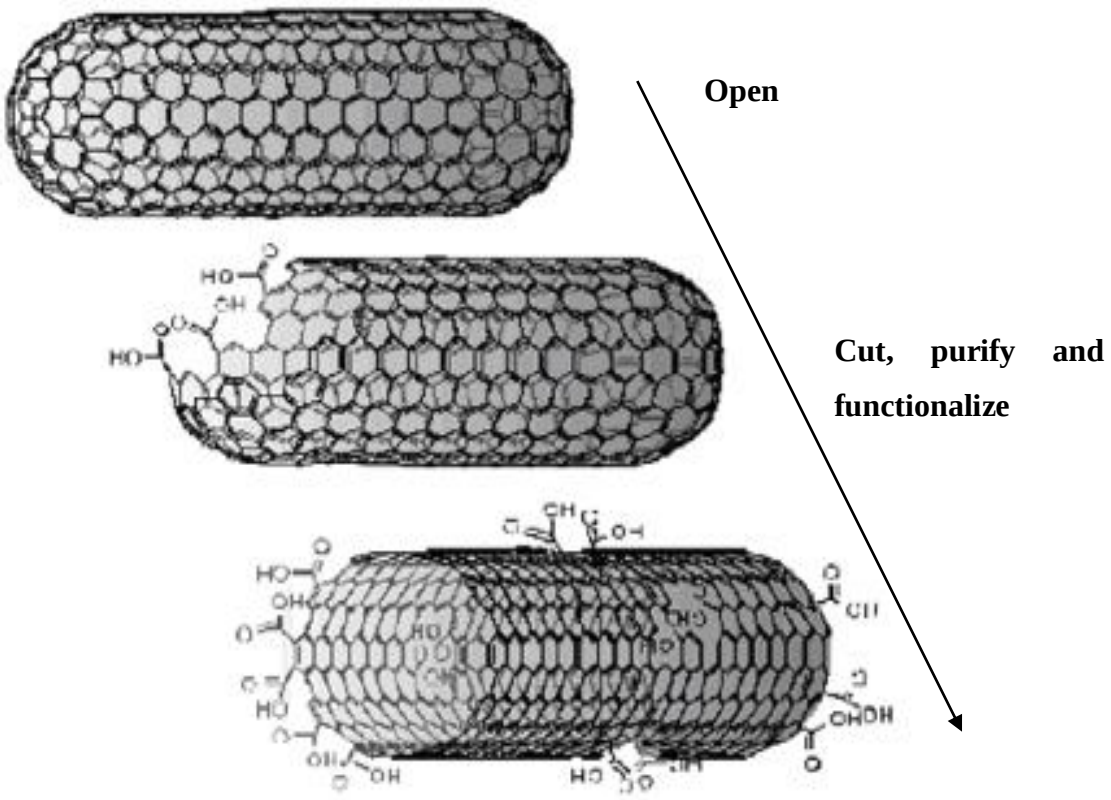

Figure. III.2. Representation of nitric acid oxidation of CNTs **[10]**.

III.4.2. Functionalization of MWCNTs by Fe_3O_4 via coprecipitation method

In this experiment Fe_3O_4/MWCNTs nanocomposites were synthesized through coprecipitation process, based on the method reported by Dalali et al, 2014 with slight modification according to the following reaction **[11]**:

$$MWCNTs+2Fe^{3+}+Fe^{2+}+8OH^{-}\rightarrow Fe_3O_4/MWCNTs+4H_2O \qquad \text{(eq.1)}$$

First of all, iron salts (0.350 g of $FeCl_3.6H_2O$ and 0.112 g of $FeSO_41.5H_2O$) were well dissolved in distilled water. In flask, 0.150 g of MWCNTs were mixed with 50 mL of dissolved $FeCl_3.6H_2O$ under stirring, 50 mL of dissolved $FeSO_41.5H_2O$ was added to the mixture under N_2 flow to protect the reaction from undesired oxidation **[12]**. When the temperature reached 80°C, dropwise of ammonium hydroxide (NH_4OH) were added to initiate the coprecipitation of Fe_3O_4/MWCNTs in alkaline medium. The reaction was aged for another hour. After that, the flask was cooled at room temperature, and then the solid was separated using external magnetic field and washed several times with distilled water. Finally, the resulted nanocomposite was dried in oven for 4 hours at 80 °C. Figure.III.3 shows the illustration of Fe_3O_4/MWCNTs preparation steps. The preparation of different samples was

carried out by following the same steps but with changing the amounts of reagents appropriate for each weight ratio.

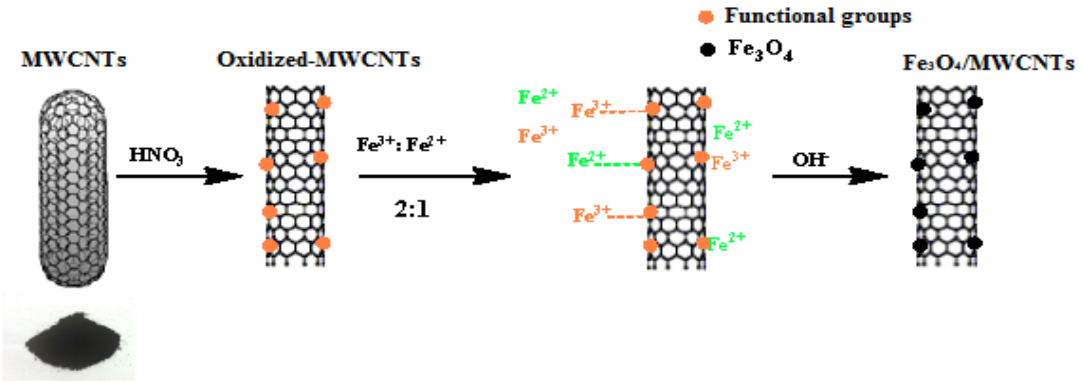

Figure.III.3. Illustration of Fe_3O_4/MWCNTs preparation steps.

III.5. Synthesis of Fe_3O_4 iron oxide

Magnetite nanoparticles were synthesized via coprecipitation method according to the way previously reported by Hariani et al, 2013 with slight modification. In the flask, 0.350 g of $FeCl_3.6H_2O$ and 0.112 g of $FeSO_4 1.5H_2O$ were dissolved into 100 mL of distilled water under vigorous stirring and N_2 flow at 80°C. The reaction was initiated by adding dropwise of NH_4OH to obtain an alkaline medium. The obtained precipitates were separated from the solution using external magnetic field. Finally, prepared magnetite was washed until a neutral pH with distilled water and dried at 80°C for 4 hours. The chemical reaction of the precipitation of ferric and ferrous salts is expressed by the equation bellow **[13]**:

$$2Fe^{3+} + Fe^{2+} + 8OH^- \rightarrow Fe_3O_4 + 4H_2O \qquad \text{(eq.2)}$$

III.6. Experimental methods of analysis and characterization

Various techniques are applied in the aim to understand the materials or either verifying a theory. The information provided by the analysis path the way to researchers and manufacturers to know the chemical composition of the material, impurities (at trace level), physical structure and so on **[14]**. This section will be focus on common applied and available techniques to characterize Fe_3O_4/MWCNTs nanocomposite.

III.6.1. X-ray Diffraction (XRD)

The X-ray diffraction (XRD) is a common analytic technique mainly utilized for the phase identification of crystalline samples. Furthermore, it can offer information about the unit cell dimensions. The XRD principle is based on the constructive interference between the crystalline matter and monochromatic X-rays **[15]**. Inside cathode ray tube, X-ray is produced by heating the filament in order to generate electrons, which are accelerated by applying an

electric potential to bombard the target material. We get the X-ray characteristic spectra, when the emitted electrons have the required energy to eject electrons from the inner shell of the target material. K_α and K_β are the most common components of The X-ray spectra. While, K_α is consisted of $K_{\alpha1}$ and $K_{\alpha2}$, the difference between them lies on the wavelength and intensity ($K_{\alpha1}$ has relatively shorter wavelength and double intensity). Target material (Mo, Cu, Cr, Fe) are characterized by specific wavelengths. The diffraction necessitates only monochromatic X-rays, which can result by filtering either by foils or crystal monochrometers. Copper is mostly used for the single-crystal diffraction, in which the radiation of the target material (CuK_α) is equal to 1.5418 A°. When the Bragg's low conditions verified, it means that the interaction between sample and incident rays produces diffracted ray and constructive interference **[16]**.

$$\boldsymbol{\lambda n = 2dsin\theta} \qquad \text{(eq.3)}$$

λ: the wave length of the incident X-rays;

n: the order of reflection;

d: inter lattice spacing ;

θ: incident angle.

All the possible diffraction directions corresponding to the lattice can be achieved by sample scanning in the range of 2θ angles. Figure.III.4 shows X-ray diffraction principle.

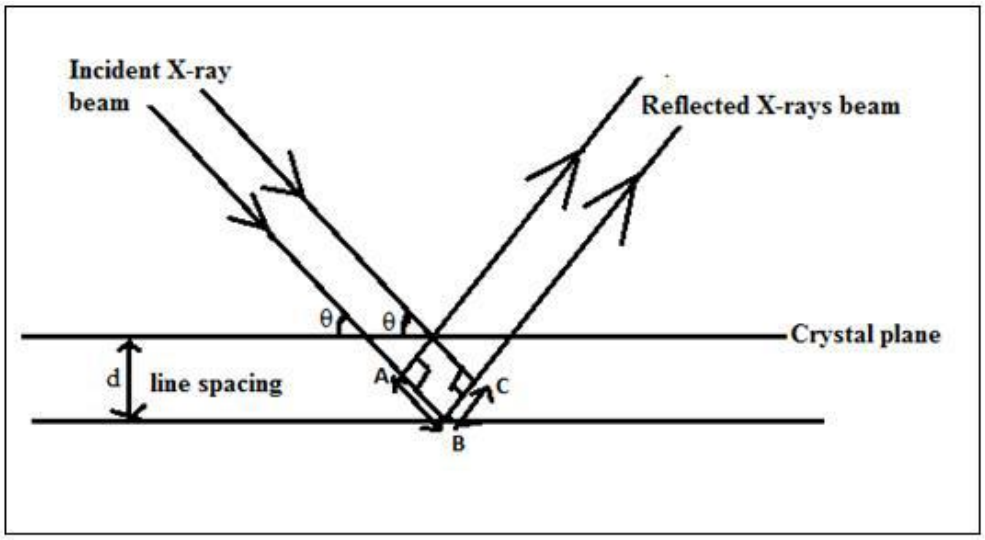

Figure.III.4.X-ray diffraction **[16]**.

Since each mineral has a specific collection of d-spacings, converting the diffraction peaks to d-spacings enables the identification of the mineral by comparing d-spacings and standard reference patterns. Joint Committee on Powder Diffraction Standards (JCPDS) contains the standard diffraction files, which allows the identification of the desirable crystal

structure by comparison of the obtained pattern with the known references embedded in JCPDS files **[15, 16]**. In order to identify the crystalline phase of the prepared samples **[17]**, it is necessary to carry out an X-ray diffraction characterization of the following specimens: (commercial MWCNTs, Fe_3O_4 and Fe_3O_4/MWCNTs). To obtain a representative sample for XRD analysis, the particle size of specimens should be in the range of 2 micron to a 100 micron as a maximum value. Therefore, grounding step using mortar is necessary to yield reduced size in the order. After that, the powder and a binder were mixed together then pressed into steel ring to obtain mechanically stable specimen **[1]**. The spectra were recorded using an X'Pert PRO difractometer; the radiation emitted corresponds to the K_α line of copper (λ_{Cu}=1.54056A°). The X'PERT software was used for recording and analyzing diffraction patterns with one scan, 2θ ranges from 20° to 80°.

III.6.2. Infrared spectroscopy (FTIR)

The analytical technique called Fourier transform infrared spectroscopy (FTIR) is mainly used to identify organic and some inorganic compounds by applying infrared radiation **[18]**. This technique determines the absorption of IR radiation by the material as a function of wavelength. In addition to the identification of unknown materials, the FTIR spectroscopy can be used in detecting impurities in the sample, identifying oxidation, decomposition and finding additives. Figure.III.5 depicts the FTIR diagram; the radiations emitted from the source achieve the detector via an interferometer, the resulted signal amplified and transformed to a digital signal using an amplifier and convertor. At the end, the signal is transferred to a computer in which the Fourier transform is run out. IR radiation with wavelength varies between 10 000 and 100 cm^{-1} is transferred through the sample, part of these radiations are absorbed. These absorbed radiations are converted to rotational or vibrational energy. The resulted signals at the detector represent the spectrum with wavelength in the interval 4000 to 400 cm^{-1}, which correspond to the molecular fingerprint of the samples. Each molecule has its specific fingerprint that makes the FTIR technique a useful analysis in chemical identification **[19]**.

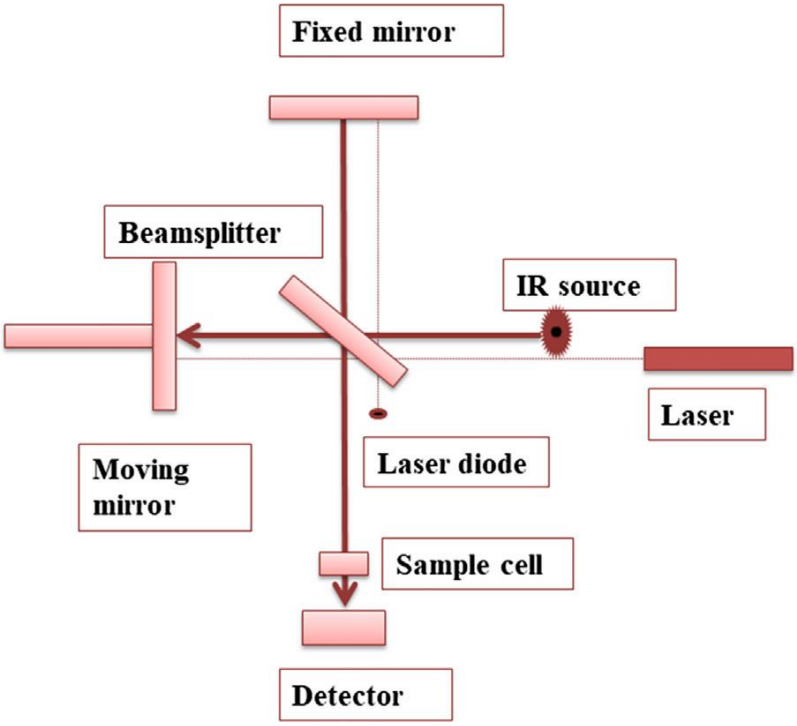

Figure.III.5. FTIR Spectrometer diagram **[19]**.

The Fourier transform infrared spectroscopy (FTIR) was used to characterize the functional groups of the prepared samples (Fe_3O_4, oxidized-MWCNTs and Fe_3O_4/MWCNTs) **[14]**. Small amount of powder specimens was enough to cover the spatula tip, and then it was mixed with KBr powder. Using a mortar, this mixture was ground to obtain fine powder (crystallites). Quick Hand was utilized to press the fine powder for about 2 minutes to get a thin pellet **[1]**, which placed into sample holder for analysis using FTIR designed for analysis in the middle IR (4000-400 cm^{-1}) and near IR (12000-4000 cm^{-1}). Obtained data were analyzed with OPUS 7.0 and ORIGIN Pro 8.5 software.

III.6.3. Scanning electron microscopy (SEM)

The scanning electron microscopy is one of the electron microscopes used to produce images of surface sample by deep scanning using a focalized electron beam with high energy **[20]**. First of all, the SEM analysis begins by the surface sputtering using fine layer of metal gold if the sample is insulator; which makes it electrically conductive **[14]**, to prevent charge accumulation. The interactions between the electrons beam and the surface electrons yield characteristic X-ray, secondary and scattered electrons. The characteristic X-rays are detected and provided information about composition and surface topology of the analyzed material. SEM could produce extremely high resolution images of the nonmaterial surface (at nanometer scale). The electron beam is extremely narrow which generate micrographs with

wide depth of field, then result a characteristic three-dimensional (3D) morphology for well understanding the sample surface structure **[16]**.

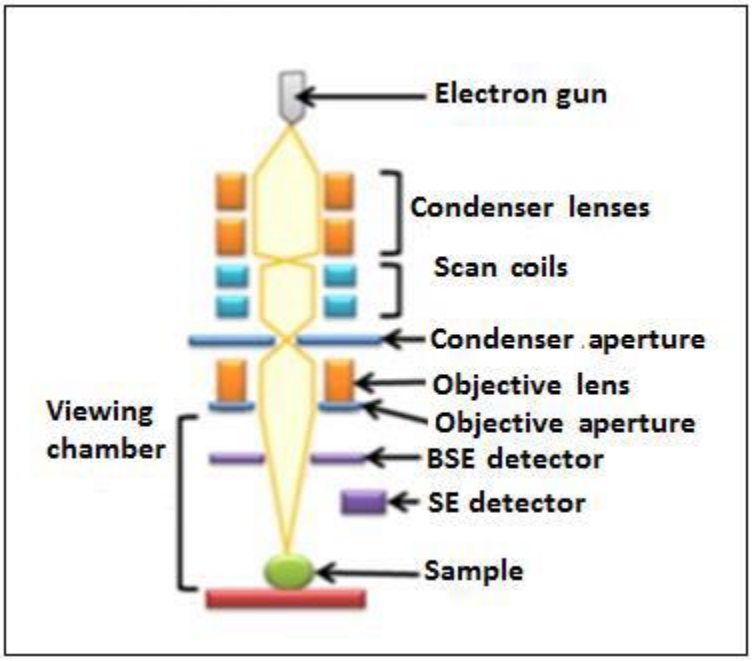

Figure. III.6. Diagram of SEM **[16]**.

The morphologies of samples were characterized using scanning electronic microscopy **[21]**. In this technique the sizes can vary from a few centimeters, and the surfaces should be polished to obtain a flat face **[1]**, and then placed in SEM (model DSM 962; Carl ZEISS Auriga microscope, Jena, Germany) operating at 25 kV.

III.6.4. Brunauer, Emmett, and Teller (BET) analysis

BET analysis is the commonly method applied in order to obtain the specific surface area (SSA), which is the most important parameter in characterizing porous materials by using nitrogen adsorption isotherms. The BET method suggests that adsorption carried out by multilayer formation, and at saturation pressure the adsorbed layers number is infinite **[22]**.

The SSA is determined by the measure of nitrogen volume necessary to create a monolayer of N_2 onto the sample surface; these measurements are carried out on micrometer-type equipments at 77 K (the temperature in which nitrogen is in its liquid state). Before running each measurement, samples should be degassed to desorb the molecules from the surface of the specimen. SSA can be defined as “the total surface area per unit mass “of the material, taking into consideration the entire surface of each particle (molecules / atoms) and even the pores. Determination of the air mass is mainly depending on the gases adsorption at lower temperatures. The adsorption phenomenon is occurred by Van der Waals forces at the solid surface. The SSA determination is based on the analytical treatment of the

experimentally calculated adsorption isotherm, and then estimating the gas quantity adsorbed in entire monolayer, which allows the calculation of this layer area. The (eq.4) indicates the BET formula, which expresses the physical adsorption of a gas onto solid:

$$\frac{P}{V(P_0-P)} = \frac{1}{V_M C} + \frac{(C-1)}{V_M C}.\frac{P}{P_0} \qquad \text{(eq.4)}$$

P: equilibrium pressure (kPa);

P_0: saturation vapor pressure of the adsorbate at the test temperature (kPa);

V: volume of vapor adsorbed per gram of solid at pressure P (L);

V_M: volume of vapor required to completely cover the solid surface of a molecular monolayer of adsorbate (L);

C: characteristic constant of the gas-solid system studied.

V_M: measurements allow the calculation of SSA by using (eq.5):

$$S_{BET} = \frac{V_M m N_A \sigma}{22414} \qquad \text{(eq.5)}$$

S_{BET}: total surface area of the sample ($m^2.g^{-1}$);

m: sample mass (g);

N_a : Avogadro number ($6.0224.10^{23}$ mol^{-1});

σ: surface area occupied by an adsorbate molecule (m^2);

22414: volume occupied by one mole of gas ($L.mol^{-1}$).

The sample is introduced to liquid nitrogen in a measuring cell. Dead volume is the name of port not occupied by the sample itself, to determine this volume the helium is required. Nitrogen is used as adsorbate under atmospheric pressure and boiling temperature.

This technique is based on volumetric measurements to estimate the quantities of gas adsorbed versus equilibrium pressure. Particularly, the isotherm is calculated by successively adding known amounts of adsorption gas to the sample holder. The adsorption of gas onto the sample occurs and the pressure declines until the remaining gas and adsorbate reach the equilibrium.

Boyle Mariotte's law allows the determination of the quantity of gas adsorbed at each equilibrium pressure; by calculate the difference between the quantity of gas initially added and the quantity of the remained gas. These measurements allow the establishing of adsorption isotherm, and then calculating the SSA of the sample **[23]**. Textural characterization was investigated using the Brunauer-Emmett-Teller (BET) technique (micromeritics ASAP-2020) through the determining of N_2 physisorption curves. Before analyzing, specimens were out gassed at an analysis batch temperature equal to (-195.968 °C) for nearly 8 hours. In order to measure the surface area of the nanocomposites

(Fe_3O_4/MWCNTs) comparing with magnetite surface area**.** While, the size and volumes of nanoparticles pores were calculated by Barret–Joyner–Halenda (BJH) model **[24]**.

III.6.5. UV-visible spectrophotometry analysis for organic dyes

UV-visible spectrophotometry reviewed as non-destructive physical method based on the interaction between matter and radiation. The electromagnetic radiation is identified by its wavelength (nm); this technique is mainly used to characterize molecules, determine the concentrations of chemical species in solution (dyes), and by extension to carry out kinetic monitoring. When polychromatic radiation penetrates a solution, it can attenuate the intensity of radiation at certain wavelengths. So, radiation is absorbed by the solution due to the electronic transition between molecular orbitals of the present species in the solution. Figure.III.7 shows the absorbance and transmittance of electromagnetic radiation **[25]**.

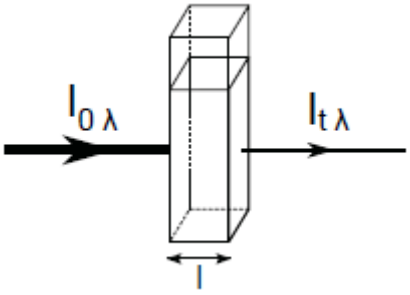

Figure.III.7. Representation of a cell traversed by an incident beam of intensity $I_{0\lambda}$, and beam of intensity $I_{t\lambda}$ is transmitted **[25]**.

Beam of monochromatic light with characterized wavelength λ and incident intensity $I_{0\lambda}$ passes through a length ℓ of clear solution placed in a cell. Part of the incident radiation is absorbed by the solution, the other part is transmitted and its intensity is noted $I_{t\lambda}$ with $I_{t\lambda} < I_{0\lambda}$.

In order to measure the intensity of the radiation absorbed at a given λ, two quantities should determined: the transmittance, noted T_λ and the absorbance, noted A_λ using equations bellow:

$$T_\lambda = \frac{I_{t\lambda}}{I_{0\lambda}} \qquad \text{(eq.6)}$$

$$A_\lambda = log\left(\frac{I_{0\lambda}}{I_{t\lambda}}\right) = log(\frac{1}{T_\lambda}) \qquad \text{(eq.7)}$$

T_λ: transmittance, often expressed in %;

A_λ: absorbance, unitless.

If T_λ = 100 %, the medium is perfectly limpid (transparent) and $A_\lambda = 0$;

If T_λ = 0 %, the medium is perfectly opaque and $A_\lambda \rightarrow +\infty$.

The absorbance (or transmittance) can be measured by a single-beam spectrophotometer (figure.III.8), using a polychromatic light source, a dispersive system (prism, grating) and a

diaphragm which allows the selection of the desired wavelength. After the absorption of the incident radiation part by the solution, a photodetector collects the transmitted intensity ($I_{t\lambda}$). Then absorbance (or transmittance) of the solution is directly determined.

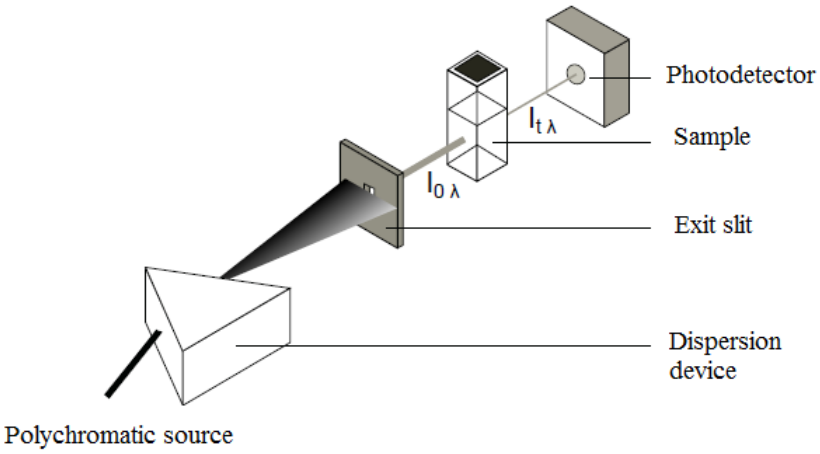

Figure.III.8. Operating principle of a single-beam spectrophotometer **[25, 26]**.

The plot of absorbance as a function of wavelength $A_\lambda = f(\lambda)$ is known as the absorption spectrum is used to determine the wavelength at the maximum absorbance λ_{max}. The Beer-Lambert law gives a correlation between concentration of species in solution and their absorbance A_λ at λ_{max} according to (eq.8):

$$A_\lambda = \ell\, \varepsilon_\lambda C \qquad \text{(eq.8)}$$

Where:

ℓ: length of cell (cm), 1 cm cuvettes are often used;

ε_λ: the molar absorption coefficient (usually expressed in $L.mol^{-1}$.It depends on chemical species, solvent, wavelength and temperature;

C: species concentration in the solution ($mol.L^{-1}$).

When different chemical species (i) with concentration C_i and molar absorption coefficients $\varepsilon_{i\lambda}$ at λ, the solution total absorbance can be given by the (eq.9):

$$A_\lambda = \sum_i \ell\, \varepsilon_{i\lambda} C_i \qquad \text{(eq.9)}$$

The Beer-Lambert law is limited, because it is applied only for diluted solutions. Moreover, it is preferable to use the wavelength (λ_{max}) in order to minimize the errors of absorbance ΔA_λ, and to increase sensitivity of the measurements **[27]**. Distilled water was used as a solvent background for BCP and CV dye solutions. Approximately 2.5 mL of sample was introduced in standard quartz cuvette, which placed into UV-visible spectrophotometer for analysis.

III.7. Efficiency of Fe_3O_4/MWCNTs nanocomposite on the removal of BCP by adsorption process

III.7.1. Determination of point of zero charge

This study is necessary since the prepared nanocomposites contain different functional groups. Therefore, point of zero charge (pH_{PZC}) was determined in order to investigate the effect of pH at which those groups have no influence on adsorption process. Herein, solid addition technique was applied to determine the value of pH_{PZC} **[1]**. The adjustment of the pH of solutions was carried out using 0.1 $mol.L^{-1}$ of HCl and 0.1 $mol.L^{-1}$ of NaOH by pH meter (Type: ST320; OHAUS corporation), the pH ranges between 2 and 12. About 0.01 $mol.L^{-1}$ of NaCl was added to the solution to obtain a constant ionic strength for the determination of pH_{PZC} **[28]**. Then, small amount (0.03 g) of Fe_3O_4/MWCNTs was introduced to six flasks (10 mL) on a shaker (Johanna Otto GmbH) at180 rpm for 48 hours. The value of pH_{PZC} was obtained after the determination of final pH values and plotted them against initial pH values **[29]**.

III.7.2. Preparation of standards and simple solutions

Stock solution of Bromocresol Purple (1000 $mg.L^{-}1$; 1L) was prepared by dissolving 1.0 g of the BCP dye in 1L of distilled water in volumetric flask under magnetic stirring for 24 hours. To get the calibration curve of BCP, standard solutions were prepared at varied concentrations between 1 and 10 $mg.L^{-1}$. The UV-visible spectroscopy technique was used to determine both of wavelength λ_{max} (which corresponds to a maximum absorbance) and absorbance values of the prepared standards.

III.7.3. Optimization of adsorption parameters

III.7.3.1. Effect of contact time on BCP adsorption

In conical flasks contain 200 ml of BCP (10 $mg.L^{-1}$) solutions, 20 mg of adsorbent were added at room temperature (20°C) and free pH. The mixtures were agitated at different intervals of time ranged from 5 to 120 min. After the magnetic separation, residual concentrations were measured using UV-visible spectrophotometer (1605 SHIMADZU).

III.7.3.2. Effect of pH on BCP adsorption

The pH of BCP solution (200 mL; 10 $mg.L^{-1}$) was adjusted using 1 $mol.L^{-1}$ of HCl and 1 $mol.L^{-1}$ of NaOH. An amount equal to 20 mg of nanocomposite was added to dye solution at different pH values ranging from 5 to 11, under stirring and at room temperature (20°C).

III.7.3.3. Effect of temperature on BCP adsorption

The effect of temperature on the adsorption phenomenon was studied by varying the temperature from 20 to 50 °C. Batch experiments were carried out by stirring 20 mg of composites in the BCP solution (200 mL; 10 $mg.L^{-1}$) at free pH around 6 for 80 min.

III.7.3.4. Effect of initial dye concentrations and isotherms model for BCP adsorption

The isotherms model for BCP dye adsorption were obtained by varying the initial concentrations of BCP (from 5 to 50 $mg.L^{-1}$) at room temperature (20 °C) and free pH about 6. Approximately 20 mg of adsorbent was added in the flasks (200 mL) of the prepared solutions at different concentrations. Magnetic separation was applied, and then the residual concentrations of BCP were obtained via UV-visible spectrophotometer. The results obtained were fitted to the Langmuir, Freundlich and Dubinin–Radushkevich models. Figure.III.9 shows the illustration of BCP adsorption method.

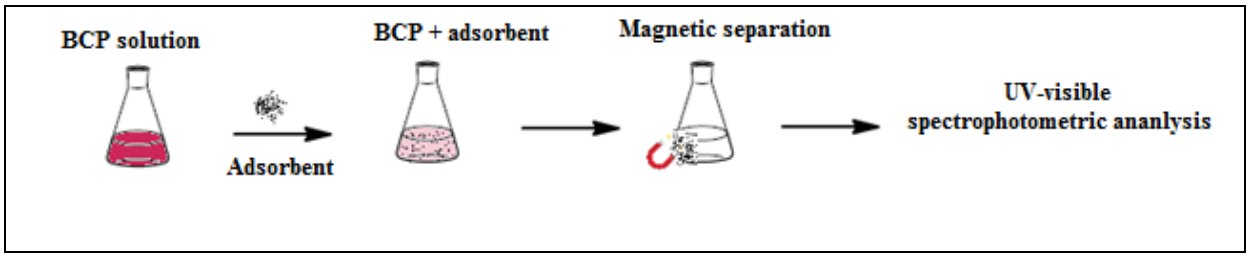

Figure. III.9. Illustration of BCP adsorption onto Fe_3O_4/MWCNTs nanocomposites.

III.8. Efficiency of Fe_3O_4/MWCNTs nanocomposite in the removal of CV dye via heterogeneous Fenton process

III.8.1. Preparation of standards and sample solutions

Stock solution of Crystal Violet (100 $mg.L^{-1}$; 1L) was prepared by dissolving 0.1 g of the CV dye in 1L of distilled water in volumetric flask under magnetic stirring. To obtain the calibration curve of CV, standard solutions were prepared at varied concentrations range between 0.8 and 8 $mg.L^{-1}$, from the stock solution. The UV-visible spectroscopy technique (CARY WinUV) was used to determine both of wavelength λ_{max} and absorbance values corresponding to the concentrations of the prepared standards.

III.8.2. Optimization of degradation parameters

III.8.2.1. Weight ratio effect on the degradation of CV dye

Two weigh ratios of (Fe_3O_4/MWCNTs: 1/1; 1/3) nanocomposites were synthesized in order to optimize the catalyst efficiency in the removal of CV contaminant using heterogeneous Fenton process. Batch experiments were carried out in the darkness by introducing successively into a 250 mL flask 200 mL of CV dye (6$mg.L^{-1}$), 20mg of catalyst and 1.53 mL of hydrogen peroxide H_2O_2 (0.2 $mol.L^{-1}$) with agitation , at room temperature

(20 °C) and pH adjusted between 2 and 2.5 using HCl acid (1M). After 310 min, the catalysts were separated from the solution using external magnetic field (figure.III.10). The residual concentrations of CV dye were estimated using UV-visible spectrophotometer.

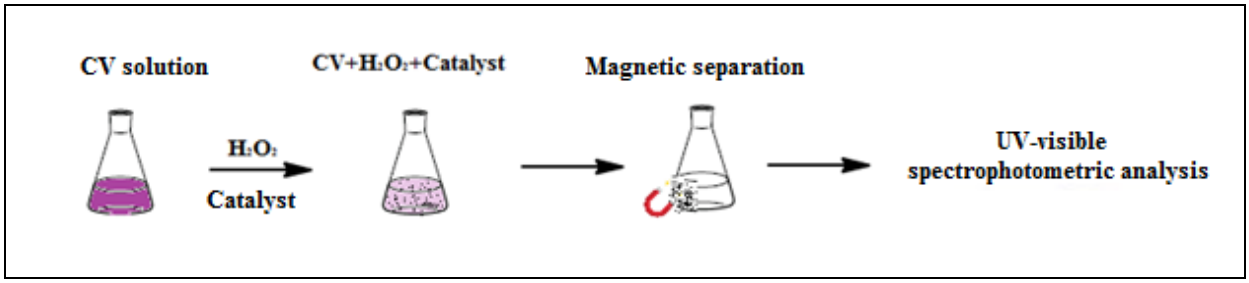

Figure.III.10. Illustration of CV degradation using Fe_3O_4/MWCNTs catalyst via heterogeneous Fenton process.

III.8.2.2. Effect of hydrogen peroxide dose on the degradation of CV dye

In order to determine the optimal H_2O_2 concentration, the degradation of CV (200 mL; 6mg.L^{-1}) at different H_2O_2 concentrations (0.1; 0.15; 0.2; 0.25 mol.L^{-1}) was studied. The amount of catalyst was about 20 mg; the batch experiments were occurred at room temperature (20°C) and pH around 2.3, under agitation in darkness for approximately 300 min. Magnetic separation was applied to isolate the catalyst from solution, and then analyze the residual concentrations of CV dye over time.

III.8.2.3. Effect of temperature on the degradation of CV dye

In order to determine the optimum temperature, an amount of catalyst around 20 mg was added to CV solution (200 mL; 6 mg.L^{-1}) at pH around 2.3, and then 1.5 mL of H_2O_2 (0.15 mol.L^{-1}) was introduced to initiate the reaction under agitation in darkness for approximately 250 min. Batch experiments were carried out at different temperatures (25; 35; 45; and 55 °C), using water bath to maintain the reaction at the desired temperature.

III.8.3. Reuse of the catalyst Fe_3O_4/MWCNTs

To evaluate the capacity and stability of the nanocomposites in heterogeneous Fenton reaction, five tests were performed at 45 °C and under agitation in darkness for 210 min. 20 mg of the catalyst and 1.5 mL of H_2O_2 (0.15 mol.L^{-1}) were added to CV solution (200 mL; 6 mg.L^{-1}); the pH was adjusted to 2.3. Five successive cycles were carried out, it should be noted that before running out each cycle the catalyst was separated by external magnetic field, washed several times with distilled water until pH reached around 6, and then dried in oven at 80 °C for 4 hours.

III.9. Efficiency of Fe_3O_4/MWCNTs catalyst in the removal of CV under polychromatic light

III.9.1. Preparation of Standards and Sample Solutions

As previous, the stock solution of Crystal Violet (200 $mg.L^{-1}$; 500 mL) was prepared by dissolving 100 mg of the CV dye in 500 mL of distilled water in volumetric flask; under magnetic stirring. To obtain the calibration curve of CV, standard solutions were prepared at varied concentrations range between 0.5 and 5 $mg.L^{-1}$. The UV-visible spectroscopy technique was used to analyze dye solution.

III.9.2. Removal of CV dye under polychromatic light

Batch experiments were carried out under polychromatic light, in cylindrical device equipped with one TLAD 15W/05 fluorescent tube emitting within the wavelength range [300–450 nm] with a maximum of emission at 365 nm and in a Pyrex glass reactor. It was equipped also with reflecting inner walls and the reactor was placed in the centre of the device.

III.9.2.1. Photolysis of CV

In this system, 100 mL of CV solution (4 $mg.L^{-1}$) was exposed to ultraviolet radiation for 180 min at room temperature (24 °C) under agitation; the initial pH of dye was adjusted to 2.5 using HCl (1M). The residual concentration was estimated by UV-Visible spectrophotometer.

III.9.2.2. Degradation of CV in the presence of H_2O_2 and light irradiation

In this system, 1.5 mL of H_2O_2 (0.15 $mol.L^{-1}$) was added to 100 mL of CV solution (4 $mg.L^{-1}$). Then, the mixture was exposed to polychromatic light irradiation for 180 min at room temperature (24 °C) and pH around 2.5, under agitation; the residual concentration was estimated by UV-visible spectrophotometer.

III.9.2.3. Degradation of CV in the presence of Fe_3O_4/MWCNTs and light irradiation

In this system, 10 mg of catalyst were introduced in flask contain 100 mL of CV solution (4 $mg.L^{-1}$). This mixture was exposed to polychromatic light irradiation for 180 min at room temperature (24 °C) and pH around 2.5, under agitation.

III.9.2.4. Photo-Fenton degradation of CV using Fe_3O_4

In this system, an amount of 10 mg of Fe_3O_4 and 1.5 mL of H_2O_2 (0.15 $mol.L^{-1}$) were introduced in flask contain 100 mL of CV solution (4 $mg.L^{-1}$). This mixture was exposed to polychromatic light irradiation for 180 min at room temperature and pH around 2.5, under agitation.

III.9.2.5. Photo-Fenton degradation of CV using Fe_3O_4/MWCNTs

In this system, an amount of 10 mg of catalyst and 1.5 mL of H_2O_2 (0.15 $mol.L^{-1}$) were introduced in flask contain 100 mL of CV solution (4 $mg.L^{-1}$). This mixture was exposed to polychromatic light irradiation for 180 min at room temperature (24°C) and pH about 2.5. Figure.III.11 shows the degradation method of CV using Fe_3O_4/MWCNTs catalyst via heterogeneous photo-Fenton process.

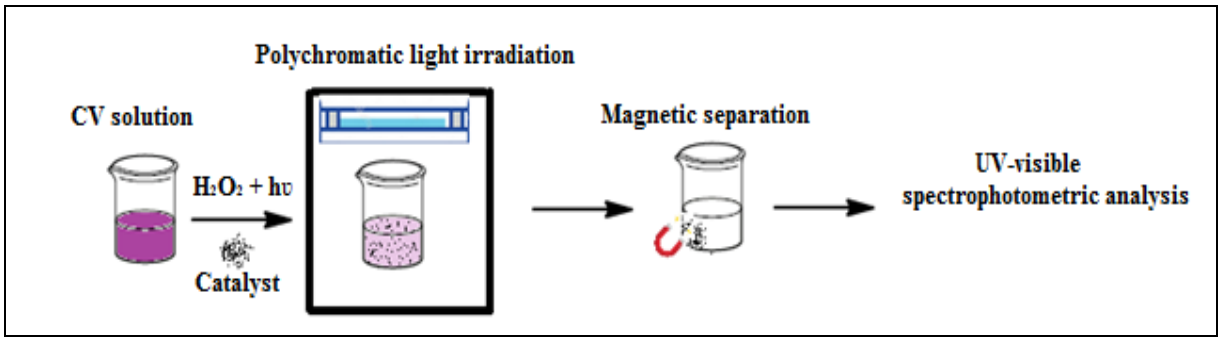

Figure.III.11. Illustration of CV degradation using Fe_3O_4 /MWCNTs catalyst via heterogeneous photo-Fenton process.

III.10. Conclusion

In this chapter, we have tried to outline the characteristics of the products and devices used, as well as the methods of preparation and characterization of nanomaterials. Finally, we ended by describing the experimental protocols followed during the adsorption and heterogeneous Fenton tests. The characterization of the prepared materials Fe_3O_4 and the nanocomposite Fe_3O_4/MWCNTs: 1/1; 1/3 will be showed in the next chapter, along with the results obtained by the application of material for the removal of Bromocresol Purple and Crystal Violet dyes from aqueous solutions.

References

[1] S. K. Silvanus, « Fabrication and characterization of magnetoresponsive carbon nanotube-infused polysulfone (cnt-ipsf) nanocomposites for water purification », p. 170.

[2] T. H. Nazifa, N. Habba, Salmiati, A. Aris, et T. Hadibarata, « Adsorption of Procion Red MX-5B and Crystal Violet Dyes from Aqueous Solution onto Corncob Activated Carbon: Adsorption of Procion Red MX-5B and Crystal Violet Dyes », Journal of the Chinese Chemical Society, vol. 65, nº 2, p. 259‑270, févr. 2018, doi: 10.1002/jccs.201700242.

[3] I. Bousnoubra, K. Djebbar, A. Abdessemed, et T. Sehili, « Decolorization of methyl green and Bromocresol Purple in mono and binary systems by photochemical processes: direct UV photolysis, Acetone/UV and H_2O_2/UV. A comparative study », Desalination and Water Treatment, p. 1‑16, avr. 2016, doi: 10.1080/19443994.2016.1174741.

[4] R. Qiu, Y. Qiu, S. Yin, X. Song, Z. Meng, X. Xu, & W.Y. Wong , « Facile separation catalyst system: direct diastereoselective synthesis of (E)-α,β-unsaturated ketones catalyzed by an air-stable Lewis acidic/basic bifunctional organobismuth complex in ionic liquids », Green chemistry., vol. 12, nº 10, p. 1767, 2010, doi: 10.1039/c004940a.

[4] G.Crini, P.M. Badot,(Eds.). « Sorption processes and pollution: conventional and non-conventional sorbents for pollutant removal from wastewaters». Presses Univ. Franche-Comté , 2010.

[5] Y. Wang, L. Gao, J. Sun, Y. Liu, S. Zheng, H. Kajiura, & K. Noda, « An integrated route for purification, cutting and dispersion of single-walled carbon nanotubes », Chemical Physics Letters, vol. 432, nº 1, p. 205‑208, déc. 2006, doi: 10.1016/j.cplett.2006.10.054.

[6] J. Lyu, V. Kudiiarov, et A. Lider, « An Overview of the Recent Progress in Modifications of Carbon Nanotubes for Hydrogen Adsorption », Nanomaterials, vol. 10, nº 2, p. 255, févr. 2020, doi: 10.3390/nano10020255.

[7] V. Datsyuk, M.Kalyva, K. Papagelis, J. Parthenios, D. Tasis, A. Siokou, & C.Galiotis, « Chemical oxidation of multiwalled carbon nanotubes », Carbon, vol. 46, nº 6, p. 833‑840, mai 2008, doi: 10.1016/j.carbon.2008.02.012.

[8] R. M. Lago, S. C. Tsang, K. L. Lu, Y. K. Chen, et M. L. H. Green, « Filling carbon nanotubes with small palladium metal crystallites: the effect of surface acid groups », Journal of the Chemical Society, Chemical Communications, nº 13, p. 1355, 1995, doi : https://doi.org/10.1039/C39950001355.

[9] N. Sezer et M. Koç, « Oxidative acid treatment of carbon nanotubes », Surfaces and Interfaces, vol. 14, p. 1‑8, mars 2019, doi: 10.1016/j.surfin.2018.11.001.

[10] T. T. Nguyen, « Utilisation de nanotubes de carbone pour la préparation de catalyseurs confinés », p. 63.

[11] N. Dalali, M. Habibizadeh, K. Rostamizadeh, et S. Nakisa, « Synthesis of magnetite multi-walled carbon nanotubes composite and its application for removal of basic dyes from aqueous solutions: REMOVAL OF BASIC DYES », Yan, p. n/a-n/a, janv. 2014, doi: 10.1002/apj.1784.

[12] S. Laurent, D. Forge, M. Port, A. Roch, C. Robic, L. Vander, L. Elst, & R.N. Muller, « Magnetic Iron Oxide Nanoparticles: Synthesis, Stabilization, Vectorization, Physicochemical Characterizations, and Biological Applications », Chemical. Reviews., vol. 108, nº 6, p. 2064‑2110, juin 2008, doi: 10.1021/cr068445e.

[13] P. L. Hariani, M. Faizal, R. Ridwan, M. Marsi, et D. Setiabudidaya, « Synthesis and Properties of Fe_3O_4 Nanoparticles by Co-precipitation Method to Removal Procion Dye », International Journal of Environmental Science and Development, p. 336‑340, 2013, doi: 10.7763/IJESD.2013.V4.366.

[14] S. Ebnesajjad, « 4 - Surface and Material Characterization Techniques », in Handbook of Adhesives and Surface Preparation, S. Ebnesajjad, Éd. Oxford: William Andrew Publishing, 2011, p. 31‑48.

[15] C. Suryanarayana et M. G. Norton, X-Ray Diffraction: A Practical Approach. Springer Science & Business Media, 2013.

[16] S. K. Silvanus, « Fabrication And Characterization Of Magnetoresponsive Carbon Nanotube-Infused Polysulfone (Cnt-Ipsf) Nanocomposites For Water Purification », p. 170.

[17] R. Rahmawati, A. Taufiq, Sunaryono, B. Yuliarto, Suyatman, Nugraha, & D. Kurniadi, « The synthesis of Fe_3O_4/MWCNT nanocomposites from local iron sands for electrochemical sensors », Selangor, Malaysia, 2018, p. 020016, doi: 10.1063/1.5034547.

[18] S. Sravan Kumar, P. Manoj, et P. Giridhar, « Fourier transform infrared spectroscopy (FTIR) analysis, chlorophyll content and antioxidant properties of native and defatted foliage of green leafy vegetables », Journal of Food Science and Technology, vol. 52, nº 12, p. 8131‑8139, déc. 2015, doi: 10.1007/s13197-015-1959-0.

[19] D. Titus, E. James Jebaseelan Samuel, et S. M. Roopan, « Chapter 12 - Nanoparticle characterization techniques », in Green Synthesis, Characterization and Applications of Nanoparticles, A. K. Shukla et S. Iravani, Éd. Elsevier, 2019, p. 303‑319.

[20] J. Goldstein, A. Buckley, JI. Goldstein, DE. Newbury, P. Echlin, DC Joy, AD RomigJr, CE Lyman, C. Fiori & E. Lifshin., Scanning Electron Microscopy and X-Ray Microanalysis: A Text for Biologists, Materials Scientists, and Geologists, 2e éd. Springer US, 1992.

[21] X. He, X. Xu, G. Bo, et Y. Yan, « Studies on the effects of different multiwalled carbon nanotube functionalization techniques on the properties of bio-based hybrid non-isocyanate polyurethane », RSC Advances., vol. 10, no 4, p. 2180‑2190, 2020, doi: 10.1039/C9RA08695A.

[22] K. S. Walton et R. Q. Snurr, « Applicability of the BET Method for Determining Surface Areas of Microporous Metal−Organic Frameworks », Journal of the American Chemical Society., vol. 129, no 27, p. 8552‑8556, juill. 2007, doi: 10.1021/ja071174k.

[23] A. Temmar, « Synthèse d'un support polypyrrole intercalé dans la bentonite. Applications a lélimination des métaux lourds (Cr^{6+}, Pb^{2+}, Zn^{2+}, Cd^{2+}) », Université M'Hamed Bougara : Faculté des sciences de l'ingénieur, 2016.

[24] C. M. Carbonaro et al., « How porosity affects the emission of fluorescent carbon dot-silica porous composites », Microporous and Mesoporous Materials, vol. 305, p. 110302, oct. 2020, doi: 10.1016/j.micromeso.2020.110302.

[25] A.-S. Bernard, S. Clède, M. Emond, H. Monin-Soyer, et J. Quérard, Techniques expérimentales en chimie-Classes prépas et concours: Travaux pratiques. Dunod, 2018.

[26] S. M. Nilapwar, M. Nardelli, H. V. Westerhoff, et M. Verma, « Chapter four - Absorption Spectroscopy », in Methods in Enzymology, vol. 500, D. Jameson, M. Verma, et H. V. Westerhoff, Éd. Academic Press, 2011, p. 59‑75.

[27] J. H. Hardesty et B. Attili, « Spectrophotometry and the Beer-Lambert Law: An Important Analytical Technique in Chemistry », Collin College, Department of Chemistry, 2010.

[28] N. Fiol et I. Villaescusa, « Determination of sorbent point zero charge: usefulness in sorption studies », Environ Chemical Letters, vol. 7, no 1, p. 79‑84, févr. 2009, doi: 10.1007/s10311-008-0139-0.

[29] Y. Amano, Y. Misugi, et M. Machida, « Adsorptive Behavior of Phosphate onto Activated Carbons Varying Surface Physicochemical Properties », Separation Science and Technology, vol. 47, no 16, p. 2348-2357, 2012, doi: https://www.tandfonline.com/doi/abs/10.1080/01496395.2012.669445.

Chapter IV
Results and discussion

IV.1. Introduction

This chapter reports results and discussions on the characterization of Fe_3O_4/MWCNTs and their application for the removal of organic dyes. The adsorption capacity of prepared Fe_3O_4/MWCNTs was evaluated, and the optimal parameters of BCP adsorption were determined such as contact time, pH and temperature. Kinetic and thermodynamic studies were performed besides the modeling of experimental isotherms.

Furthermore, the nanocomposite efficiency in the degradation of Crystal Violet dye via heterogeneous Fenton reaction was investigated. The effect of various parameters was studied such as weight ratio of nanocomposite, temperature, hydrogen peroxide and initial dye concentrations. The stability of the catalyst was investigated via the reuse of this material five times. This work was ended by the investigation of catalyst efficiency in the removal of CV dye in the presence of polychromatic light irradiations. The results of batch experiments were discussed and kinetic studies were performed.

IV.2. Analysis and characterization of nanoparticles

IV.2.1. XRD characterization

Figure.IV.1 represents the X-ray diffraction patterns of pure MWCNTs, magnetite, Fe_3O_4/MWCNTs: 1/1 and Fe_3O_4/MWCNTs: 1/3 nanocomposites. Characteristic peak of CNTs was observed at 2θ=26° in both nanocomposites patterns **[1]**, which confirms the functionalization of MWCNTs surface without destroying their structure neither by acid oxidation nor by the chemical coprecipitation of iron oxide. Furthermore, diffraction peaks referred to magnetite were observed in the prepared magnetite and nanocomposites patterns (2θ = 30, 35, 43, 53, 57 and 62°) based on (JCPDS) 19-0629 **[2, 3]**. The main peak of MWCNTs in the XRD patterns is broadened, which indicates the small crystallite size of nanoparticles **[2]**. The formula of Debyee Scherrer was used to calculate the mean size of pure MWCNTs, synthesized magnetite and nanocomposites **[4]**:

$$\boldsymbol{L = \frac{0.9\lambda}{\beta cos\theta}} \qquad \text{(eq.1)}$$

β (rad): the full width at half maximum (FWHM) of the diffraction of the intense peak;

θ (rad): the Bragg's diffraction angle;

λ: wavelength of the copper radiation (1.54060 °A).

Table.IV.1 shows slight increase of the average crystallite size with the increasing of magnetite weight ratio.

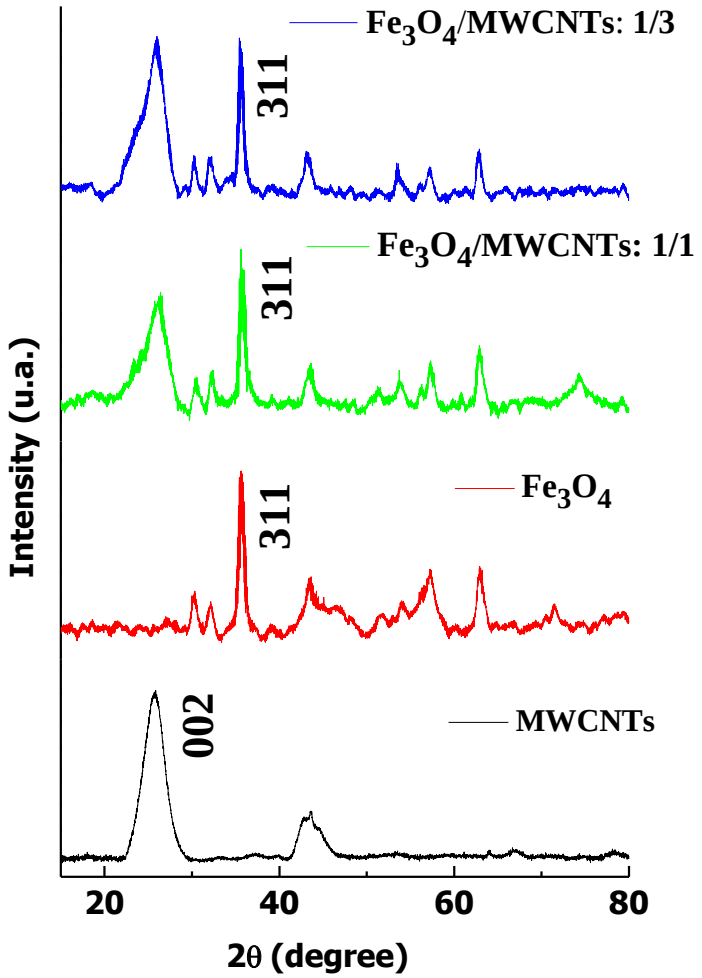

Figure.IV.1. XRD patterns of pure MWCNTs, Fe_3O_4/MWCNTs nanocomposites and magnetite.

Table.IV.1. The average size of nanoparticles.

Sample	β (rad)	λ (nm)	θ (rad)	k	Average size (±1nm)
MWCNTs (002)	0.0071436	0.15406	0.19595382	0.9	19.79
Fe_3O_4 (311)	0.0071436	0.15406	0.31167479	0.9	20.39
Fe_3O_4/ MWCNTs:1/1	0.0071436	0.15406	0.31260505	0.9	32.63
Fe_3O_4/ MWCNTs:1/3	0.0053582	0.15406	0.31103774	0.9	27.18

IV.2.2. FTIR characterization

Figure.IV.2 represents the FTIR spectra of nanocomposite (c) compared with the prepared magnetite (b) and oxidized-MWCNTs (a). The broad peak at 3450 cm^{-1} in all the samples spectra, is attributed to the stretching vibration of –OH bonds, the peak at 2925 cm^{-1}

is attributed to C–H vibration, and the peaks at 1640 and 1081cm^{-1}are attributed to C= O and C–O bonds, respectively **[5]**. The characteristic peak of Fe–O bond is at 575.95cm^{-1} in both spectra of magnetite and nanocomposites **[6]**.

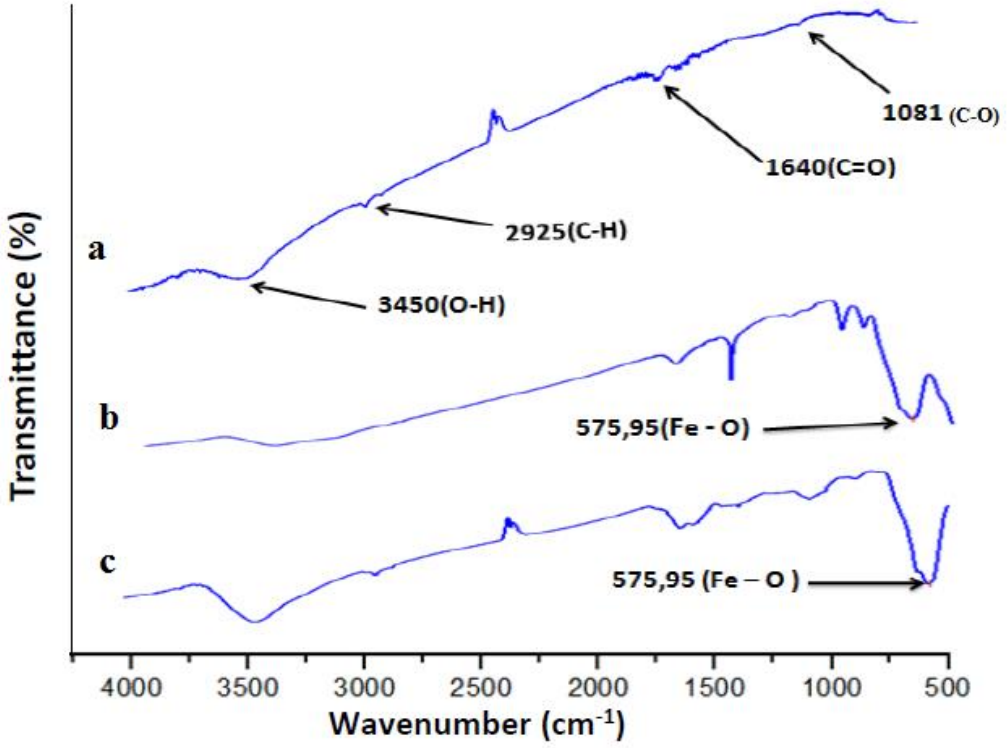

Figure.IV.2. FTIR spectra of (a) oxidized-MWCNTs, (b) Fe_3O_4 and (c) Fe_3O_4/MWCNTs.

IV.2.3. Morphology of the samples

Figure.IV.3 shows the morphologies of the pure MWCNTs, synthesized magnetite and Fe_3O_4/MWCNTs nanocomposites in A, B and C images, respectively. MWCNTs morphology was observed as a homogeneous surface of curly hair-like structure. In addition, the nanotubes alignment is not straight; it is completely wavy **[7]**. The magnetite nanoparticles are characterized by their spherical shape and homogeneous size distribution **[8]**, which almost coated the MWCNTs as seen on image C, the nanocomposites surface was relatively uniform.

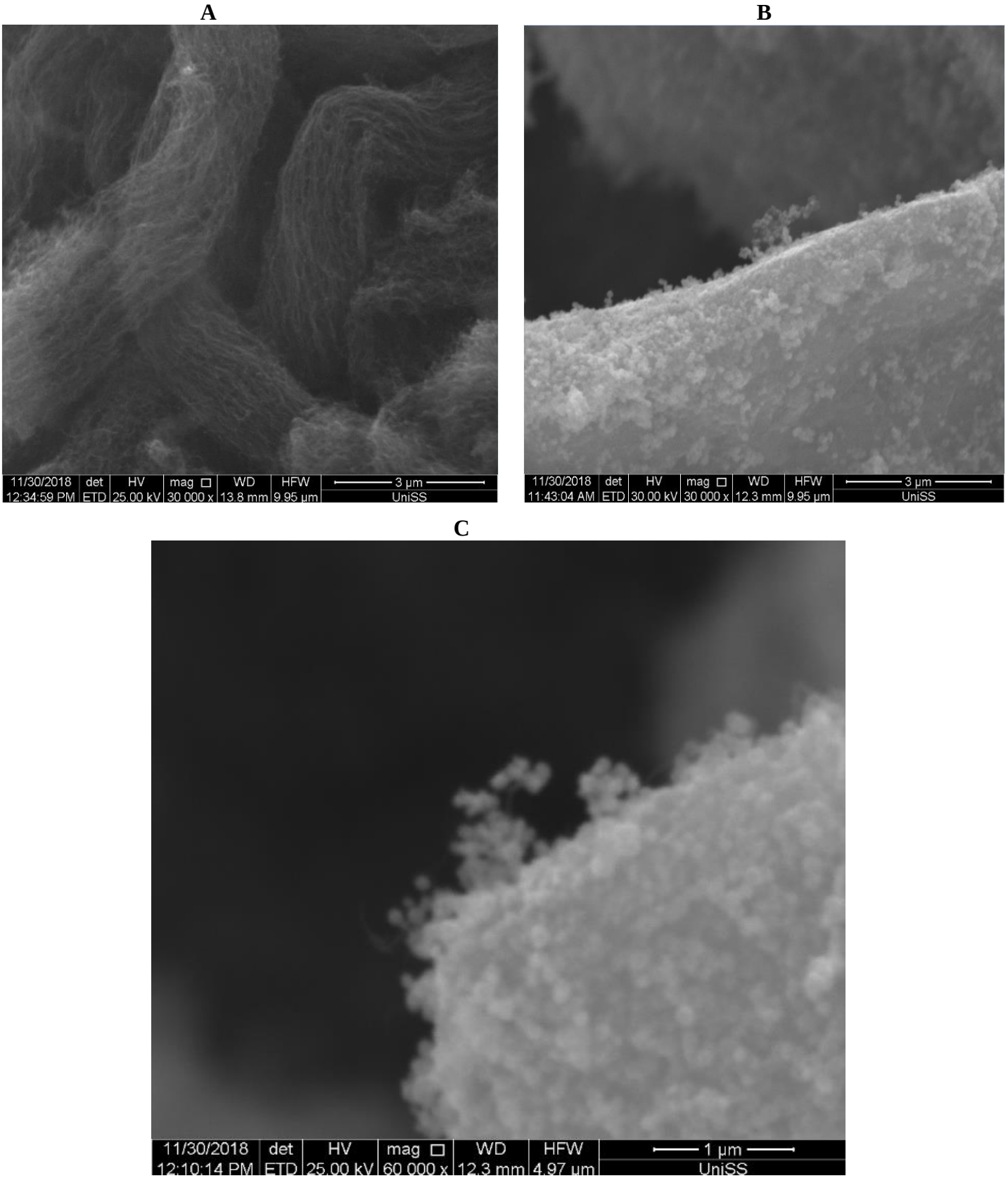

Figure.IV.3. SEM images of A. pure MWCNTs, B. magnetite and C. Fe_3O_4/MWCNTs nanocomposite.

IV.2.4. BET characterization

Table.IV.2 shows that the specific surface areas (SSA) of nanocomposites are increased with the increase of MWCNTs loading and vice versa. This is due to the tendency of magnetite to agglomerate which may be attributed to strong interactions (magneto-dipole) between nanoparticles **[9]**.

Table.IV.2. SSA of samples.

Sample	**SSA ($m^2.g^{-1}$)**
Fe_3O_4	78.77
Fe_3O_4/MWCNTs: 1/1	187.09
Fe_3O_4/MWCNTs: 1/3	269.38

IV.3. Efficiency of Fe_3O_4/MWCNTs nanocomposite on the removal of BCP by adsorption process

IV.3.1. Analysis of BCP dye using UV-visible spectrophotometer

Evolution of the concentration during the adsorption process was determined by a calibration curve, obtained from standards with different concentrations (Table.IV.3). A series of samples was prepared to establish the calibration curve from the stock solution. The analysis by UV-visible absorption at λ_{max} =431 nm was carried out using a diluted solutions in order to verify the Beer - Lambert law.

Table.IV.3. Concentration values and their corresponding absorbance of the calibration curve.

C ($mg.L^{-1}$)	0	1	2	4	6	8	10
A	0	0.0140	0.0230	0.0500	0.0880	0.1130	0.1370

The curve below (figure IV.4) is linear in the range of the selected concentrations; so Beer - Lambert's law is verified.

R^2: Correlation coefficient.

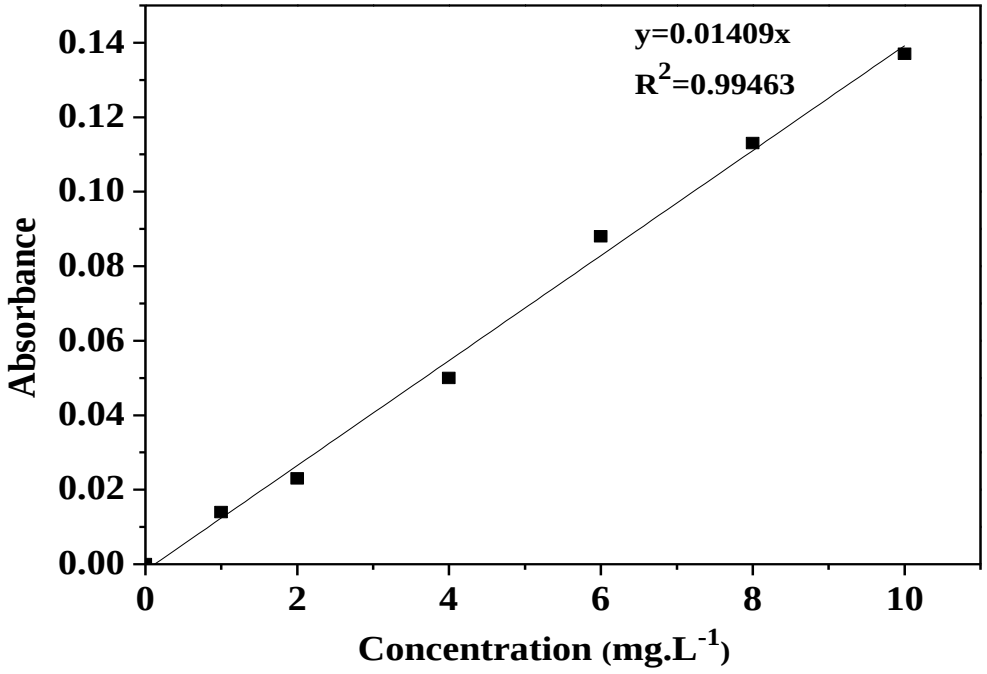

Figure.IV.4. Calibration curve for BCP standards.

IV.3.2. Optimization parameters

IV.3.2.1. The point zero charge of Fe_3O_4/MWCNTs nanocomposite and pH effect

IV.3.2.1.1. The point zero charge of Fe_3O_4/MWCNTs nanocomposite

It is very important to know the point zero charge (pH_{PZC}) in adsorption studies, owing to the useful information provided about the type of interactions that can occur between adsorbent and adsorbate (attraction/ repulsion). Briefly, the pH_{PZC} can denote the point at which the potential of hydrogen pH of the adsorbent surface charge is equal to zero (the total of negative and positive charges of the surface sites takes a zero) **[10]**. The Fe_3O_4/MWCNTs surface has a net neutral charge at pH about 6.6 as shown in figure.IV.5. Before this point the adsorbent is positively charged because the CNTs surface after chemical treatment with nitric acid has some oxygen groups and hydroxyl groups (COOH; OH). At pH lower than 6.6, the positive charge dominates due to the protonation of electron π-rich regions onto the MWCNTs surface. When the pH value increases, the ionization of carboxylic groups occurs and then the negative charge dominates **[5]**.

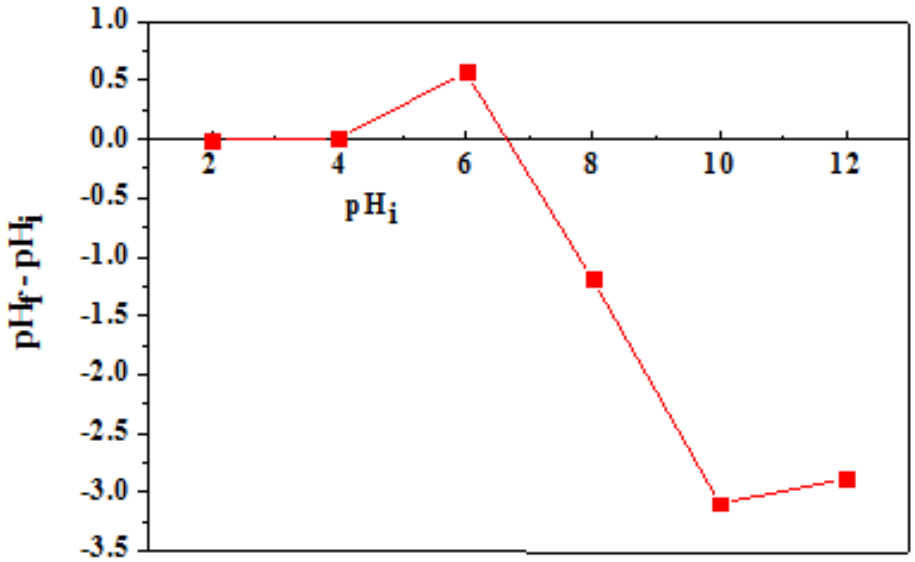

Figure.IV.5. Plot shown the pH_{PZC} of Fe_3O_4/MWCNTs nanocomposite.

IV.3.2.1.2. Effect of pH

The pH study is one of the most important steps in adsorption process, because both of adsorbent and adsorbate charges can be affected by the pH variation and then control the adsorption mechanism **[11]**. The zeta potential of Fe_3O_4/MWCNTs results indicated that the adsorption of BCP onto the nanocomposite is favorable at all the pH range. It is well known that BCP dye has pKa around 6.3 with two different structures **[12]**. Slight increase in the adsorption capacity is noticed by the increase of pH values until pH = 8.3 which can be considered as an optimum value. At pH around 11, there is a neglected loss in the adsorption capacity. All the other experiments were carried out at pH around 6 because the attraction between the adsorbent surface and dye molecules is favorable over a large pH range. As a result, we adopted that the influence of pH factor is almost neglected in this adsorption as shown in figure.IV.6. Note that same result was reported by El-Dares et al **[13]**.

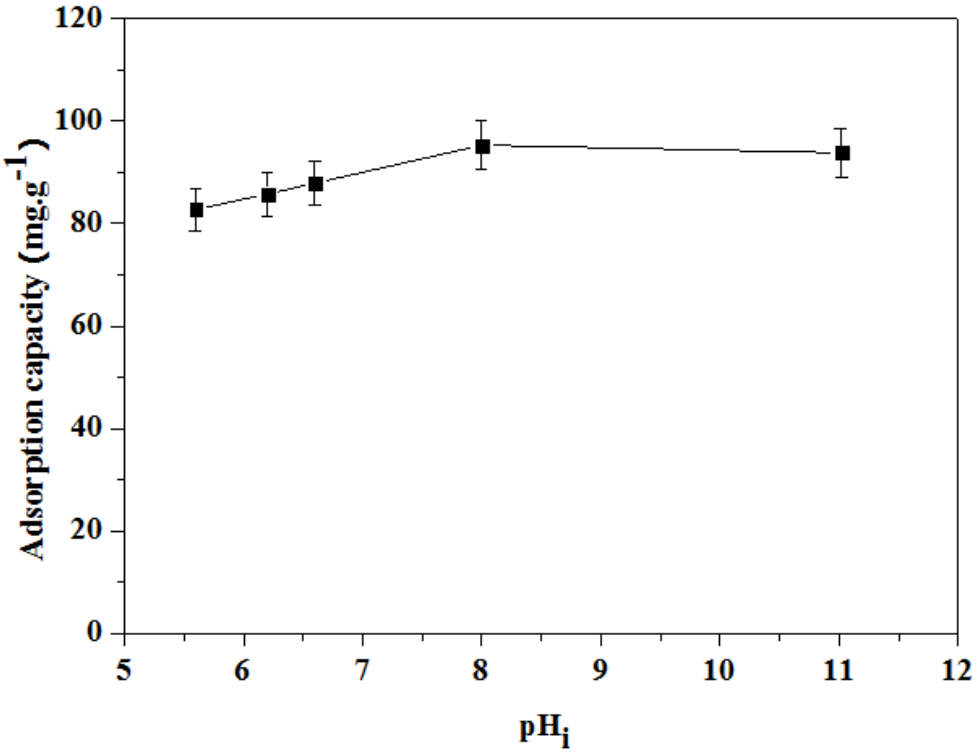

Figure.IV.6. Effect of pH on the BCP adsorption onto nanocomposite (pH= 5.5-11; m=20 mg of Fe_3O_4/MWCNTs; 200 mL; 10 mg.L^{-1} of BCP and 293 K).

IV.3.2.2. Effect of contact time and kinetic study

IV.3.2.2.1. Effect of contact time

Contact time is an important factor in the adsorption study, figure.IV.7.shows the plot of adsorption capacity Q_t (mg.g^{-1}) as function of time t (minutes), in the range of 0 to 20 min the evolution of adsorption was rapid; from 20 until 60 min adsorption was slower; in the interval of 60 to 120 min the plateau was appeared which indicated that equilibrium time was achieved. The equilibrium time and maximum adsorption capacity were determined to be about 90 min and 90.28 mg.g^{-1}, respectively.

IV.3.2.2.2. Kinetic models

Interesting data about adsorption mechanism are provided by applying the kinetic models **[14]**. In this study, we used the major models to fit adsorption experiments which are: pseudo-first order (PFO) and pseudo-second order (PSO) **[16]**, in the aim to describe the mode of the dye molecules transport from the solution into the solid **[17]**. The following nonlinear equations were plotted for PFO and PSO, respectively (figure.IV.7) **[14]**:

$$\frac{dq}{dt} = k_1(Q_e - Q_t) \qquad \text{(eq.2)}$$

$$\frac{dq}{dt} = k_2(Q_e - Q_t)^2 \qquad \text{(eq.3)}$$

k_1: the rate constant for PFO (min^{-1});

k_2: the rate constant for PSO (min^{-1}).

Q_t: adsorbed amount at time t ($mg.g^{-1}$);

Q_e: amount adsorbed at equilibrium ($mg.g^{-1}$);

t: time (min).

Another model called intraparticle diffusion was used in order to determine the rate of diffusion in pores. The (eq.4) represents the nonlinear equation corresponding to this model **[18]**:

$$Q_t = k_d t^{\frac{1}{2}} + C_d \qquad \text{(eq.4)}$$

k_d ($mg.g^{-1}.min^{-1/2}$) : is the intraparticle diffusion rate constant;

C_d ($mg.g^{-1}$): is the intercept.

Table.IV.4 summarizes the obtained results of kinetic study; according to the adsorption capacity Q_e and correlation coefficient R^2, we can conclude that the PSO fitted well the adsorption of BCP dye onto Fe_3O_4/MWCNTs. Figure.IV.8 indicates that the plot was not linear over the range of time, which means that there are more than one process that affected the adsorption. As shown in the curve pattern there are two steps: (*i*) the first one consists of an external surface adsorption at the initial stage; which is characterized by rapid evolution of adsorption (because the dye particles were adsorbed onto the external adsorbent surface), (*ii*) the second one is characterized by slow diffusion of the dye molecules into the nanocomposite pores after the saturation of external surface. As a result, the line deviation indicates that intra-particle diffusion was not the only rate limiting stage for the BCP adsorption process **[19]**.

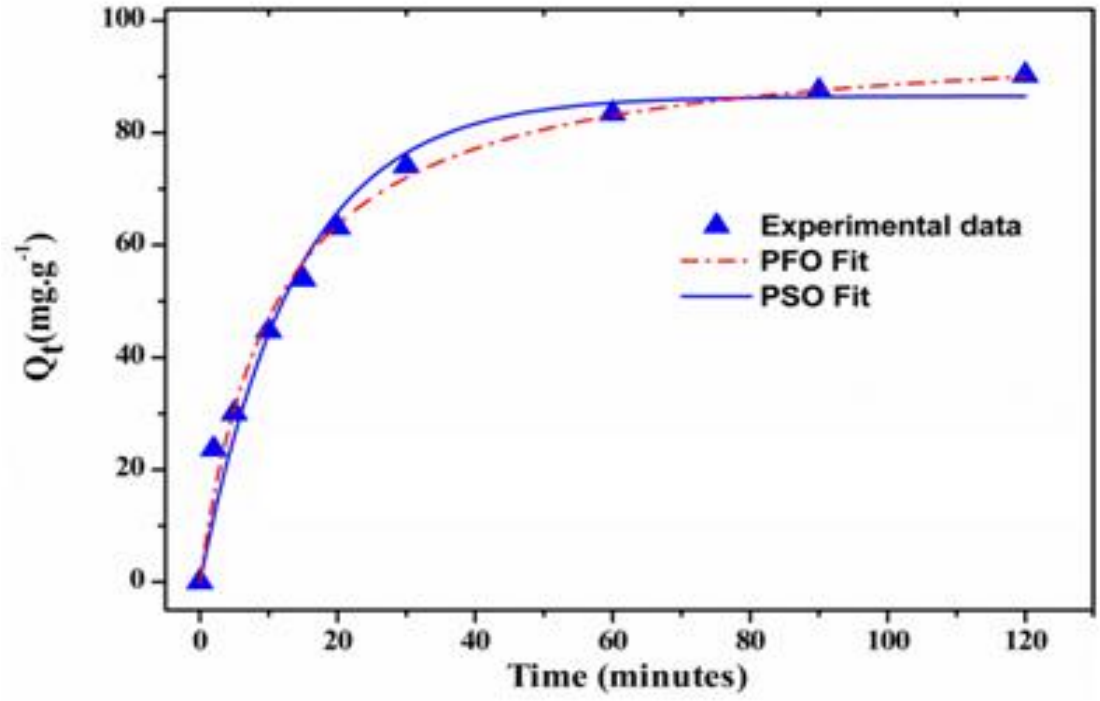

Figure.IV.7. Adsorption kinetics of BCP using Fe_3O_4/MWCNTs and fitting curves of kinetic models (pH=6; m=20 mg of Fe_3O_4/MWCNTs; 200 mL; 10 mg.L^{-1} of BCP and ± 293 K).

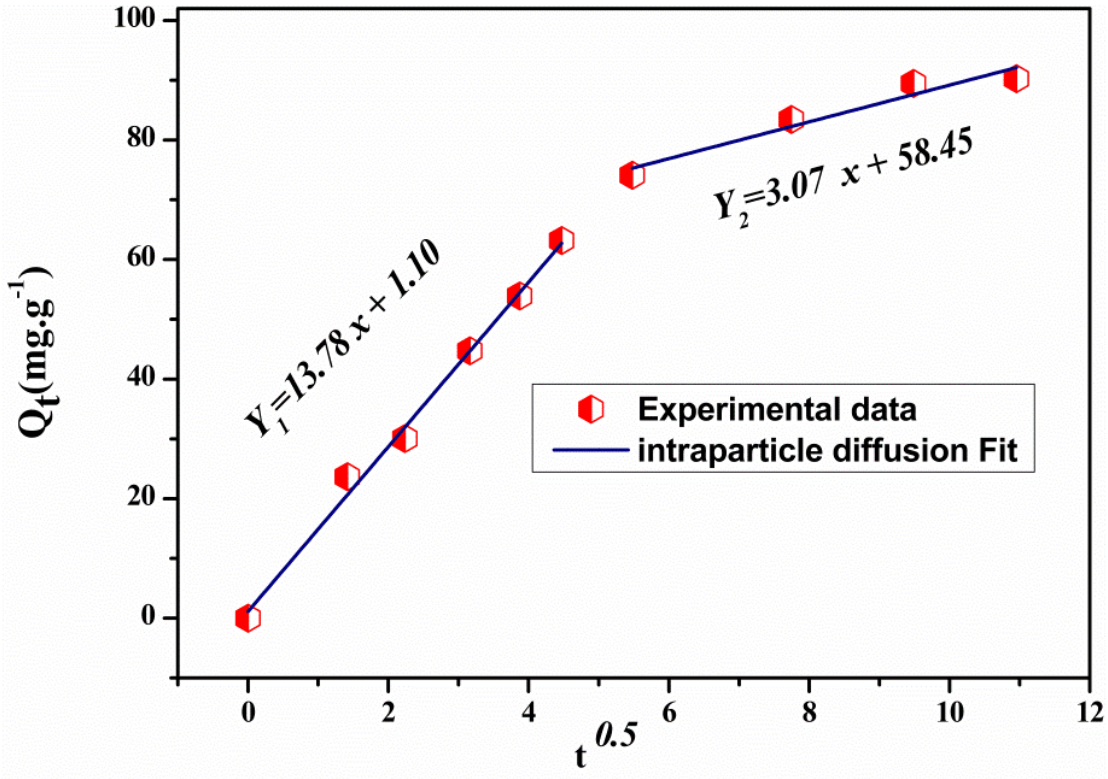

Figure.IV.8. Intra-particle diffusion plot for BCP dye adsorption onto Fe_3O_4/MWCNTs adsorbent (pH=6.0; m=20 mg of Fe_3O_4/MWCNTs; 200 mL; 10 mg.L^{-1} of BCP and ± 293 K).

Table.VI.4. Kinetic parameters of PFO, PSO and intraparticle diffusion models.

Kinetic model	**$q_{e(exp)}$(mg.g^{-1})**	**$q_{e(cal)}$ (mg.g^{-1})**	**k_1(L.min^{-1})**	**R^2**
PFO model	90.28	86.53	0.071	0.972
PSO model	**$q_{e(exp)}$ (mg.g^{-1})**	**$q_{e(cal)}$ (mg.g^{-1})**	**k_2(g^{-1}.min^{-1}) mg**	**R^2**
	90.28	91.12	0.009	0.988
Intraparticle diffusion model	**First step**	**k_{ip1} (mg.g^{-1}.min$^{-1/2}$)**	**C_1(mg.g^{-1})**	**R_1^2**
		13.78	1.10	0.993
	Second step	**k_{ip2} (mg.g^{-1}.min$^{-1/2}$)**	**C_2(mg.g^{-1})**	**R_2^2**
		3.07	58.45	0.913

IV.3.2.3. Effect of initial BCP concentrations and isotherm models

IV.3.2.3.1. Effect of initial BCP concentrations

Experimental data plotted in figure.IV.9 show that the adsorption capacity of PCB onto nanocomposite significantly increased with the increasing of initial dye concentrations from 5 to50 mg.L^{-1}.

IV.3.2.3.2. Adsorption isotherm models

In order to explain the sorption process, isotherm models of BCP dye adsorption were applied by plotting q_e as function of C_e at equilibrium. According to the Brunauer classification, the isotherm of BCP adsorption onto Fe_3O_4/MWCNTs correlates with isotherm (type I) **[20]**. Among the major theoretical isotherms, Langmuir, Freundlich and Dubinin–Radushkevich models were used. The Langmuir model indicates that the adsorption occurred on a homogeneous phase, (eq.5) presents the Langmuir nonlinear equation **[1, 14, 21]**:

$$q_0 = \frac{Q^0_{max} K_L C_e}{1 + k_L C_e} \qquad \text{(eq.5)}$$

where:

$Q^o_{max}(\text{mg.g}^{-1})$: The maximum mono layer adsorption capacity;

$k_L(\text{L.mg}^{-1})$: Langmuir constant.

Another factor can be determined by applying Langmuir model, it is known as the dimensionless parameter (R_L), which is given as **[22]**:

$$R_L = \frac{1}{1 + k.C_0} \qquad \text{(eq.6)}$$

The R_L value suggests that the adsorption is irreversible if (R_L = 0), unfavorable if (R_L>1), linear if (R_L=1), and favorable if (0<R_L<1) **[23]**.

Freundlich isotherm suggests that the multilayer adsorption occurred on a heterogeneous surface of the adsorbent. The nonlinear equation of Freundlich model presented as follows **[24]**:

$$q_e = k_F C_e^{\frac{1}{n}} \quad \text{(eq.7)}$$

Where:

K_F: Freundlich constant associated to adsorption capacity;

$\frac{1}{n}$: Heterogeneity factor.

Dubinin-Radushkevich (D-R) isotherm model is used to estimate the free adsorption energy, which indicates the type of interactions between the adsorbent and adsorbate. The nonlinear form of D-R equation is represented by **[25]**:

$$q_e = q_{DR} e^{-k_{DR}\varepsilon^2} \quad \text{(eq.8)}$$

Where:

q_{DR}(mg.g^{-1}): Maximum adsorption capacity;

k_{DR}(mol^2.Kj^{-2}): Constant related to the sorption energy;

ε: Polanyi potential given by:

$$\varepsilon = RTln(1 + \frac{1}{C_e}) \quad \text{(eq.9)}$$

R: Gas constant (8.314 J.mol^{-1}.K^{-1}).

The energy of mean sorption (E) can be determined by applying the (eq.10); the energy value can indicate the nature of adsorption as follows:

If: E< 8 kJ.mol^{-1} it is a physorption type;

If: 8< E < 16 kJ.mol^{-1} the nature of adsorption process is ion exchange **[26]**.

$$E = \frac{1}{\sqrt{2k_{DR}}} \quad \text{(eq.10)}$$

The nonlinear regression of the aforementioned isotherms models was presented in Figure.IV.9. Langmuir isotherm fitted well the equilibrium data according to the value of correlation (R^2 = 0.99) (Table.IV.5).The obtained maximum adsorption capacity (Q^o_{max}) evaluated by the Langmuir and D-R models are comparable: 296.52 and 239.47 mg.g^{-1}, respectively. Furthermore, the favorability of BCP dye adsorption onto Fe_3O_4/MWCNTs was confirmed by R_L value which comprises between 0 and 1 in addition to the intensity of adsorption n (exponent of Freundlich), which comprises between 0 and 10) **[27]**. The nature of adsorption was determined theoretically by the energy value (E=2.06 kJ.mol^{-1}), which suggests the physical nature of BCP adsorption onto Fe_3O_4/MWCNTs.

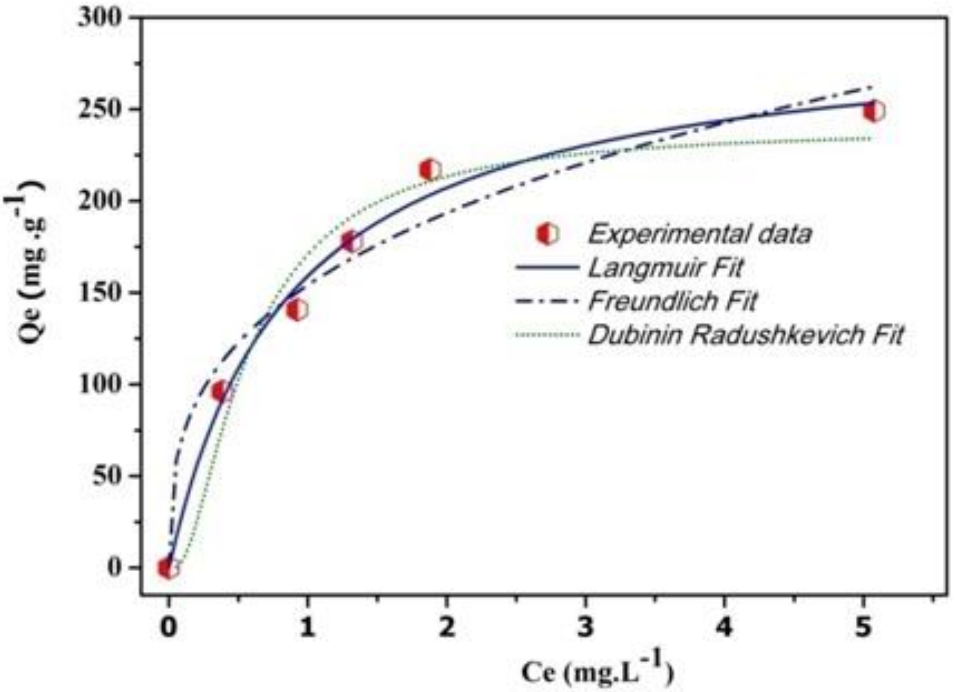

Figure.IV.9. Isotherms model of BCP adsorption onto Fe_3O_4/MWCNTs nanocomposite (pH=6; m=20 mg of Fe_3O_4/MWCNTs; 200 mL; 5-50 $mg.L^{-1}$ of BCP and 293 K).

Table.IV.5. Isotherm constant parameters for the adsorption of BCP onto Fe_3O_4/MWCNTs nanocomposite.

Models	**Parameter**			
Langmuir	Q^0_{max} ($mg.g^{-1}$)	k_L($L.mg^{-1}$)	R^2	R_L
	296.52	1.16	0.99	0.08
Freundlich	k_F($mg.g^{-1}$)	n	R^2	
	154.22	0.33	0.96	
Dubinin–	Q_{max}($mg.g^{-1}$)	k_{DR}($mol^2.K^{-1}J^{-2}$)	R^2	E($kJ.mol^{-1}$)
Radushkevich	239.47	$1.18.10^{-7}$	0.96	2.06

IV.3.2.4. Effect of temperature and thermodynamic study

III.3.2.4.1. Effect of temperature

Temperature is considered as an interesting factor in dye adsorption onto carbon nanotubes **[28]**, figure.IV.10 shows that the adsorption capacity at equilibrium time slightly decreased (from 95.34 to 92.25 $mg.g^{-1}$), when the temperature increased from 293 to 323 K. This suggests that the adsorption of BCP onto Fe_3O_4/MWCNTs nanocomposites is exothermic **[29]**.

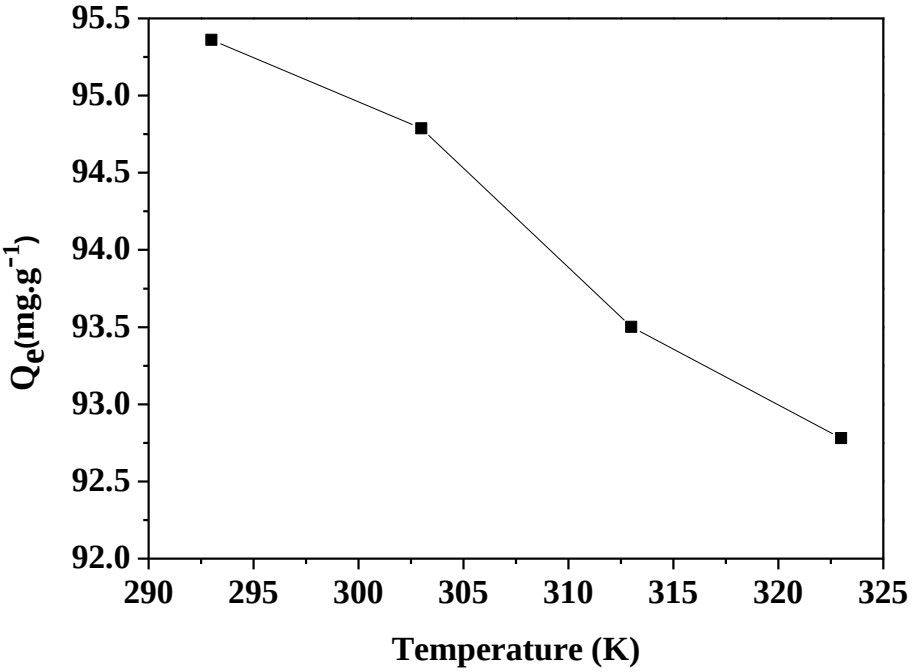

Figure.IV.10. Effect of temperature on the adsorption of BCP dye onto Fe_3O_4/MWCNTs nanocomposites (pH=6; m=20 mg of Fe_3O_4/MWCNTs; 200 mL; 10 mg.L^{-1} of BCP).

III.3.2.4.2. Thermodynamic study

Owing to the importance of thermodynamic study, estimation of various energies was carried out: standard Gibbs free energy change (ΔG^0), standard enthalpy change (ΔH^0), and standard entropy change (ΔS^0). These parameters are in correlation by the (eq.12) as follows **[14]**:

$$\Delta \boldsymbol{G^0} = -\boldsymbol{RTLnK_e} \quad \text{.....(eq.11)}$$

$$\boldsymbol{\Delta G^0} = \boldsymbol{\Delta H^0} - \boldsymbol{T\Delta S^0} \quad \text{.....(eq.12)}$$

$$\boldsymbol{K_e} = \frac{\boldsymbol{Q_e}}{\boldsymbol{C_e}} \quad \text{.....(eq.13)}$$

The aforementioned energies were determined by applying Van'tHoff equation (eq.14) and plotted in figure.IV.11 **[30]**:

$$LnK_e = -\frac{\Delta \boldsymbol{H^0}}{\boldsymbol{RT}} + \frac{\Delta \boldsymbol{S^0}}{\boldsymbol{R}} \qquad \text{(eq.14)}$$

R: Gas constant (8.314 J.mol^{-1}.K^{-1});

Q_e: Adsorption capacity at the thermodynamic equilibrium (mg.g^{-1});

C_e: Concentration at the equilibrium (mg.L^{-1});

T: Temperature (K);

K_e: Equilibrium thermodynamic constant.

According to data obtained in (Table.IV.6), the adsorption of BCP dye onto Fe_3O_4/MWCNTs exhibited an exothermic nature because ΔH^0 is around -15.45 kJ.mol^{-1} which is a negative value of standard enthalpy change; furthermore this value indicates that interactions between the dye molecules and adsorbent particles are a van der Waals type and physisorption took place in this adsorption because (ΔH^0) is lower than 20 kJ.mol^{-1}. The values of standard Gibbs free energy change (ΔG^0) are negatives at different temperature, which suggest that the adsorption is favorable, spontaneous and enthalpy controlled. Negative value of standard entropy change (ΔS^0) indicates that the randomness is decreased at the interface solid-liquid when the adsorption occurred **[14, 30]**.

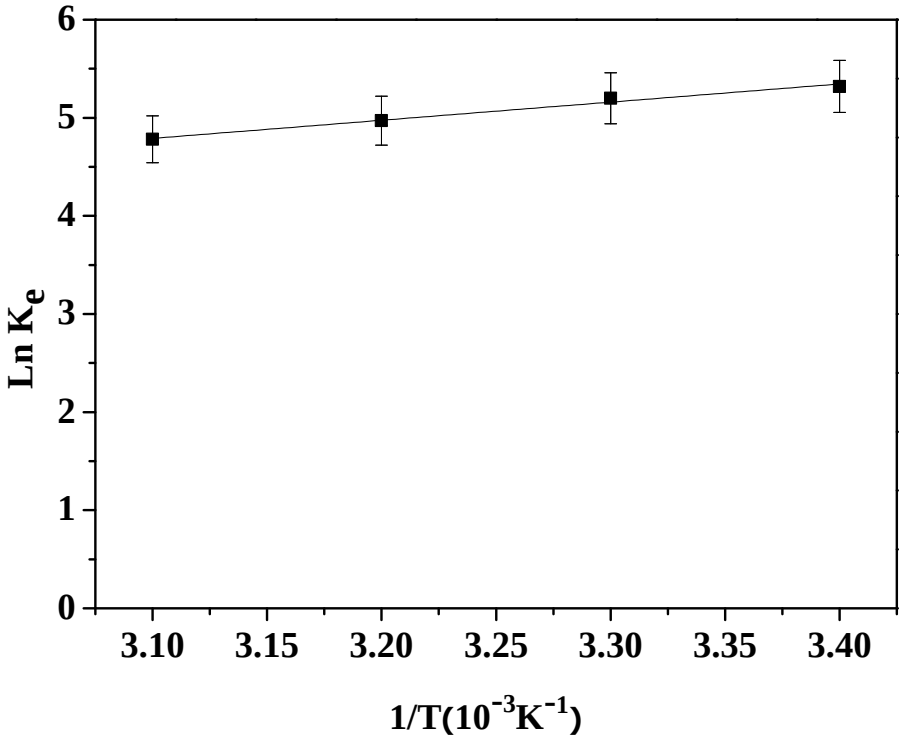

Figure.IV.11. Temperature effect on the equilibrium thermodynamic constant (pH=6; m=20 mg of Fe_3O_4/MWCNTs; 200 mL; 10 mg.L^{-1} of BCP).

Table.IV.6. Thermodynamic parameters.

ΔG^0 (kJ.mol^{-1})				**ΔH^0(kJ.mol^{-1})**	**ΔS^0(J.mol^{-1}.K^{-1})**	**R^2**
293 K	303 K	313 K	323 K	-15.45	-8.09	0.981
-13.08	-13.00	-12.66	-12.84			

IV.4. Efficiency of Fe_3O_4/MWCNTs nanocomposite in the removal of CV via heterogeneous Fenton process

IV.4.1. Spectrophotomtric analysis of Crystal Violet (CV)

IV.4.1.1. Determination of the maximum absorption wavelength

Different samples of CV solution were analyzed via spectrophotometer UV-visible with spectral scanning ranges from 200 to 800 nm and at 20 $nm.s^{-1}$ of rate. The absorbance spectrum of the Crystal Violet shown in figure IV.12 reveals the existence of four absorption bands: three bands in the ultra Violet range (λ=208 nm, λ=249 nm, λ=302 nm) and another band in the visible range (λ_{max}=590 nm). The band at 590 nm is the wavelength characteristic of Crystal Violet **[29]**.

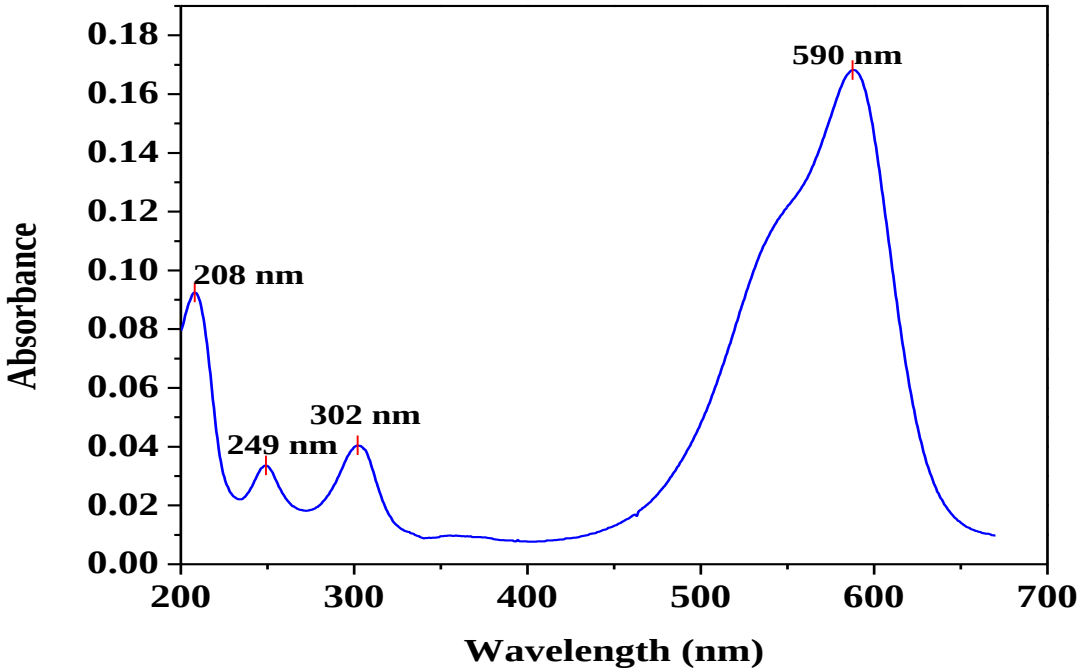

Figure.IV.12. The UV-visible absorption spectrum of CV. [CV] = 6 $mg.L^{-1}$.

IV.4.1.2. Calibration curve

Evolution of the concentration during the degradation process was determined by a calibration curve, obtained from standards with different concentrations (Table.IV.7). A series of samples were prepared to establish the calibration curve from the 100 $mg.L^{-1}$ stock solution. The analysis by UV-visible absorption at λ_{max} = 590 nm was carried out using a diluted solutions in order to verify the Beer - Lambert law.

Table.IV.7. Concentration values and their corresponding absorbance of the calibration curve.

C (mg.L^{1})	0	0.8	1	1.5	2	3	4	5	6	8
A	0	0.1010	0.1674	0.2389	0.3391	0.4876	0.6029	0.7190	0.9030	1.1590

The curve below (figure IV.13) is linear in the range of the selected concentrations; so Beer - Lambert's law is verified.

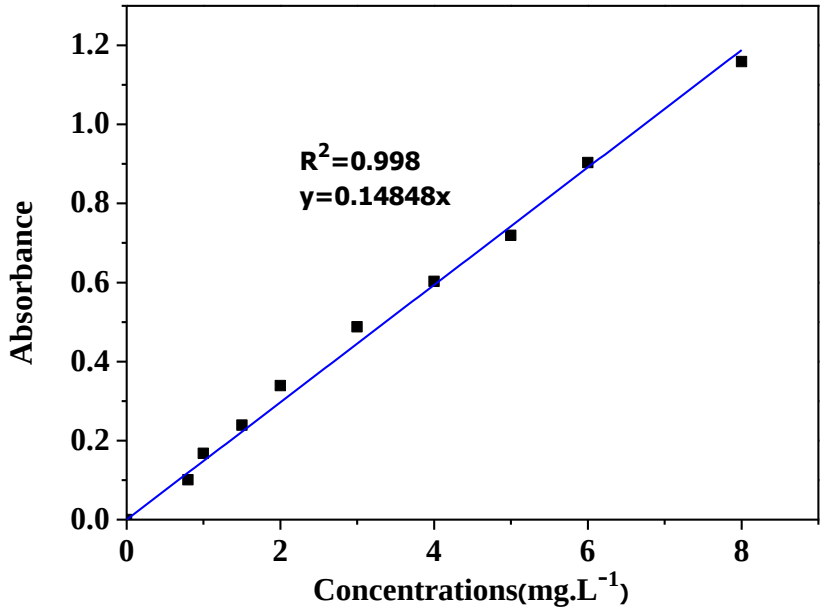

Figure.IV.13. Calibration curve of Crystal Violet.

IV.4.2. Optimization parameters

The removal efficiency R (%) of CV dye was estimated using the following equation **[31]**:

$$R = (1 - \frac{[CV]_t}{[CV]_0}).100 \qquad \text{(eq.15)}$$

$[CV]_t$: CV dye concentration at a given time (t);

$[CV]_0$: Concentration of CV at t=0.

Heterogeneous Fenton reaction was considered as a pseudo-first-order reaction, which is described as follows **[32]**:

$$[CV]_t = [CV]_0 exp(-kt) \qquad \text{(eq.16)}$$

Logarithmic plots of dye concentration of CV as a function of reaction time appear linear, indicating that the degradation reaction fitted pseudo-first-order. The rate constant k (min^{-1}) was obtained from the slope of the line **[33]:**

$$Ln([CV]_0/[CV]_t) = kt \qquad \text{(eq.17)}$$

IV.4.2.1. Effect of Fe_3O_4/MWCNTs weight ratio

Two weight ratios of nanocomposites (Fe_3O_4/MWCNTs: 1/1; 1/3) were synthesized via coprecipitation method. With the aim of obtaining the best catalyst for the degradation of CV dye, an arbitrary concentration of [H_2O_2] equal to 0.2 $mol.L^{-1}$ was chosen for the monitoring of the heterogeneous Fenton process at room temperature and pH around 2.5. According to the curves in figure IV.14 and table.IV.8, the removal efficiency of CV dye is slightly increases when MWCNTs loading increases. After 310 minutes, the degradation of the pollutant is almost complete (98.50% and 98.61%); the rate constants estimated to $1.50.10^{-2}$ and $1.79.10^{-2}$ min^{-1} for Fe_3O_4/MWCNTs: 1/1 and 1/3, respectively. The BET analyses discussed previously are correlated with these results. To conclude, the increase of MWCNTs amount in the nanocomposite leads to little increase in specific surface area and reduce the agglomeration of Fe_3O_4, and improves the stability and the dispersion of catalyst in water. The removal of pollutant is enhanced owing to the synergy between magnetite and MWCNTs via the adsorption and the oxidation of CV dye molecules at the catalyst surface. Herein, the specific surface area plays a critical role, and we can consider the Fe_3O_4/MWCNTs:1/3 as a better catalyst for the heterogeneous Fenton degradation of CV from wastewater and selected it for the subsequent experiments **[34-36]**.

Table.IV.8. Effect of weight ratio on dye removal and rate constant.

Weight ratio	**Removal (%)**	**k(min^{-1})**	**R^2**
Fe_3O_4/MWCNTs: 1/1	98.50	$1.50.10^{-2}$	0.87
Fe_3O_4/MWCNTs: 1/3	98.61	$1.79.10^{-2}$	0.92

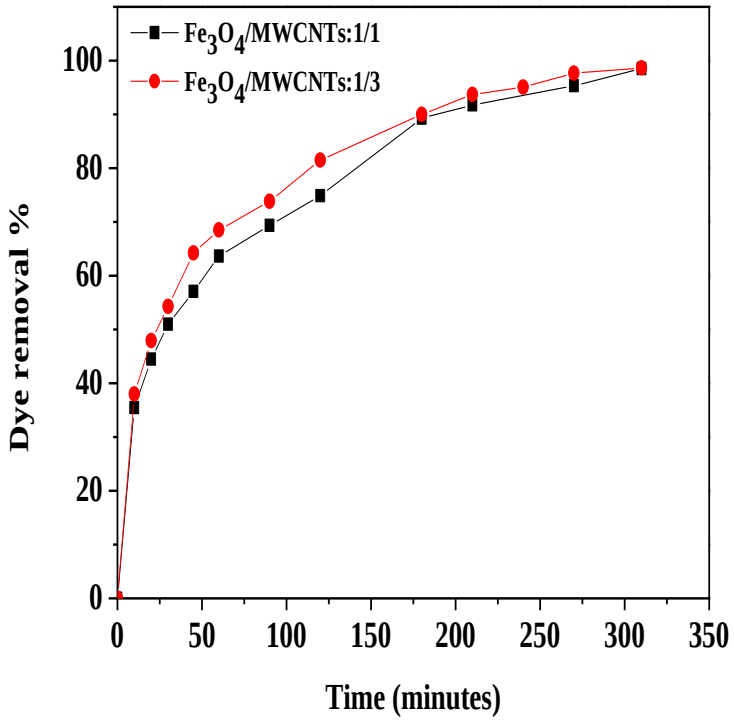

Figure.IV.14. Effect of weight ratio on dye removal: m $_{catalyst}$ =20 mg; pH=2.5, [H_2O_2] = 0.2 mol.L^{-1}; [CV] = 4 mg.g^{-1}; V=200 mL; T= 298 K.

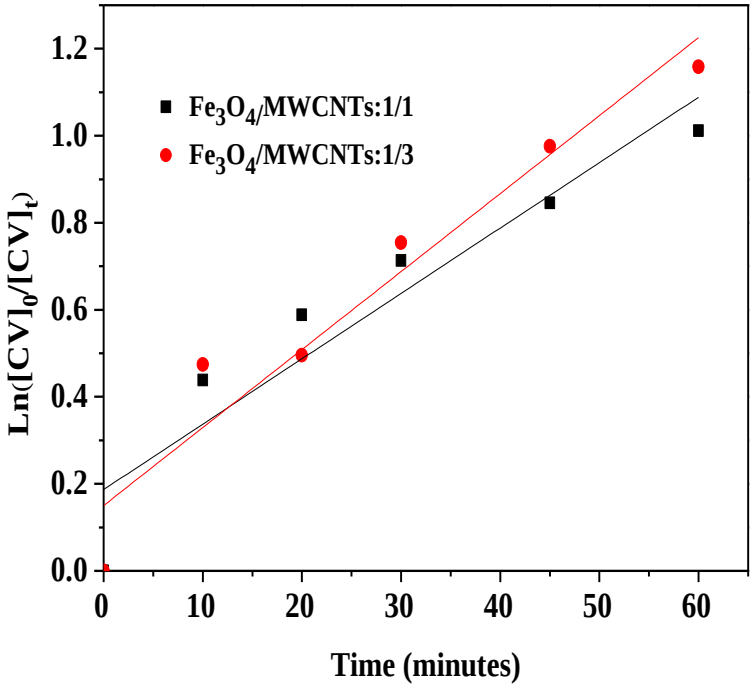

Figure.IV.15. Linearization of the first order kinetic at different weight ratio.

IV.4.2.2. Effect of hydrogen peroxide concentration

It is expected that an increase in hydrogen peroxide concentration leads to higher degradation of CV dye. However, there is no significant enhancement in the degradation of the pollutant at higher concentrations. Figue.IV.16 shows an increase in the removal efficiency from 95 to 97 % when hydrogen peroxide concentration increased from 0.1 to 0.14 mol.L^{-1}. So, 0.14 mol.L^{-1} is considered as the optimum value. At higher concentrations ($[H_2O_2]$ > 0.14 mol.L^{-1}), slight decrease in removal percentage as shown in table.IV.9. The degradation of organic pollutant by heterogeneous Fenton process is mostly related to the hydroxyl radicals produced by catalytic decomposition of hydrogen peroxide. On the other hand, the obtained hydroxyl radicals ·OH can recombine with H_2O_2, which can negatively affect the removal efficiency and rate constant due to the scavenging of hydrogen peroxide following the equations below **[32]**:

$$\cdot OH + H_2O_2 \rightarrow HO_2\cdot + H_2O \quad \text{(eq.18)}$$

$$\cdot OH + HO_2\cdot \rightarrow O_2 + H_2O \quad \text{(eq.19)}$$

$$\cdot OH + \cdot OH \rightarrow H_2O_2 \quad \text{(eq.20)}$$

Table.IV.9. Effect of hydrogen peroxide concentration on dye removal and rate constant.

$[H_2O_2]$ (mol.L^{-1})	Removal (%)	k (min^{-1})	R^2	SE
0.10	95.06	$1.76.10^{-2}$	0.98	$4.99.10^{-4}$
0.14	97.15	$2.41.10^{-2}$	0.95	$8.82.10^{-4}$
0.20	94.27	$1.79.10^{-2}$	0.97	$5.79.10^{-4}$
0.25	95.58	$1.99.10^{-2}$	0.96	$6.69.10^{-4}$

To conclude, the optimum value 0.14 mol.L^{-1} was selected for the subsequent experiments.

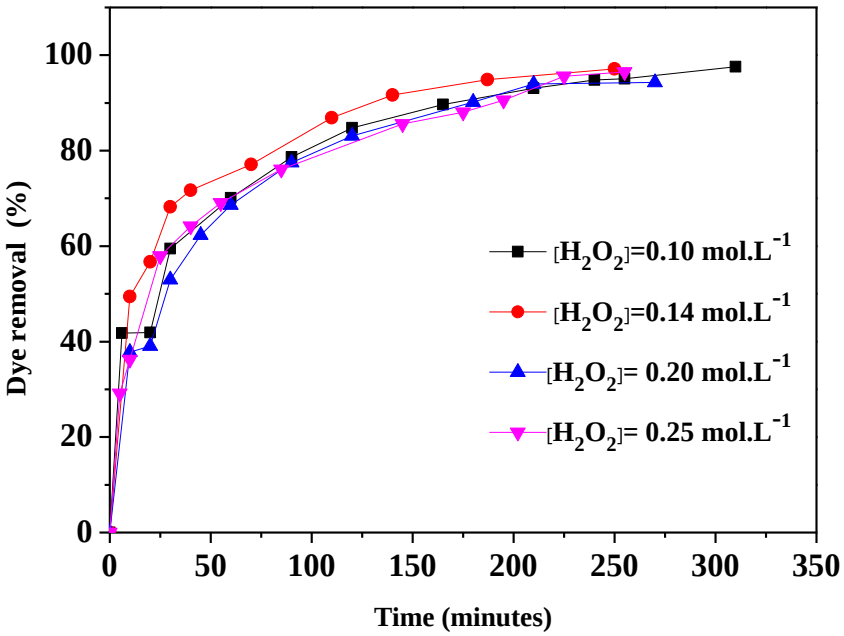

Figure.IV.16. Effect of hydrogen peroxide concentration onto dye removal ($m_{catalyst}$ =20 mg; pH=2.5; [CV] = 4 $mg.g^{-1}$; V=200 mL; T=298 K).

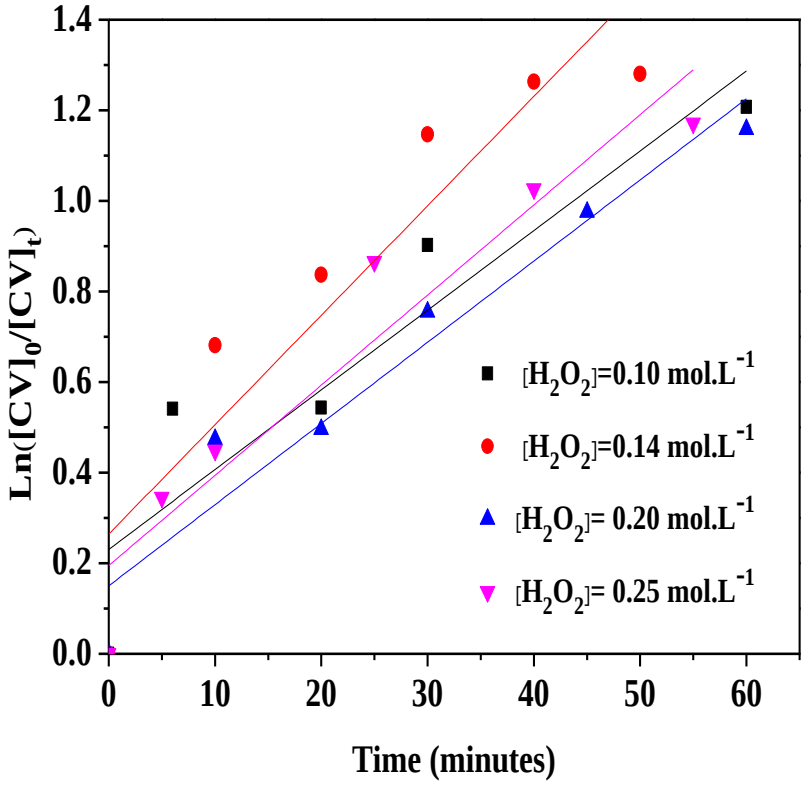

Figure.IV.17. Linearization of the first order kinetic at different H_2O_2 concentrations.

IV.4.2.3. Effect of temperature

Literature has discussed the effect of temperature on the degradation of dyes by Fenton process. Figure.IV.18 shows that the removal efficiency improves at high temperatures from 97% to 99%, and rate constant from $1.28.10^{-2}$ to $3.94.10^{-2}$ min^{-1} for 298 and 318 K, respectively (Table.IV.10). This result can be explained by the faster diffusion of CV molecules toward the Fe_3O_4/MWCNTs surface and the accelerated decomposition of hydrogen peroxide at higher temperatures **[37]**. So, the value 318 K was selected as the optimum temperature and used in further experiments.

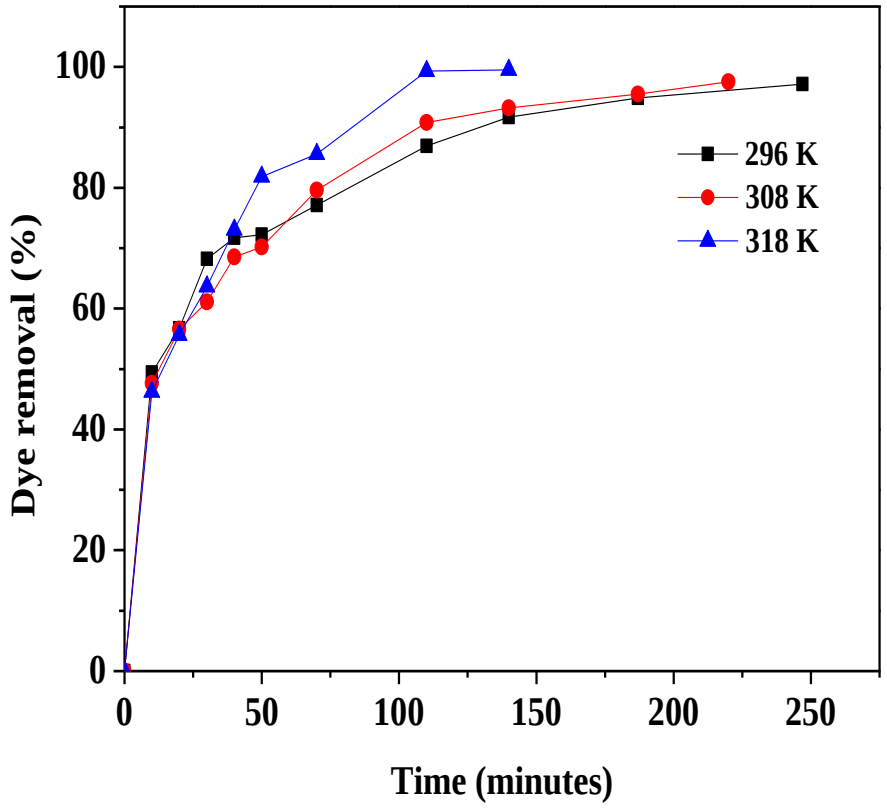

Figure.IV.18. Effect of temperature on dye removal ($m_{catalyst}$ =20 mg; $[H_2O_2]$= 0.14 $mol.L^{-1}$; pH=2.5; V=200 mL; $[CV]_0$ = 4 $mg.L^{-1}$).

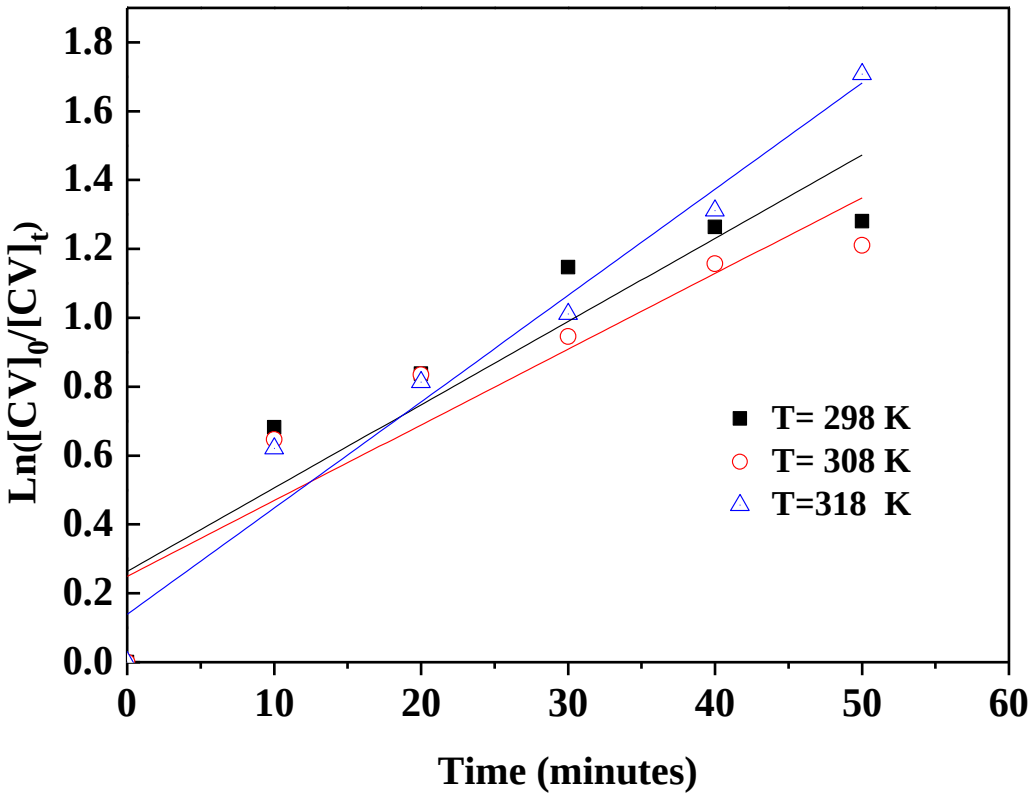

Figure.IV.19. Linearization of the first order kinetic at different temperature.

Table.IV.10. Effect of temperature on removal and rate constant.

Temperature (K)	Removal (%)	k(min^{-1})	R^2	SE
298	97.15	$1.28.10^{-2}$	0.95	$8.90.10^{-4}$
308	97.57	$1.40.10^{-2}$	0.96	$9.48.10^{-4}$
318	99.51	$3.94.10^{-2}$	0.95	$3.16.10^{-3}$

IV.4.3. Determination of activation energy

It is recognized that chemical reactions are dependent on temperature, in heterogeneous Fenton oxidation the relationship between the rate constant k (s^{-1}) and temperature is described using Arrhenius equation (eq.21) as shown in figure.IV.22:

$$Lnk = -\frac{E_a}{R}.\frac{1}{T} + LnA \qquad \text{(eq.21)}$$

Where:

E_a: Activation energy;

A: Frequency factor.

The activation energy was estimated to (42.38 kJ.mol^{-1}) using the slope of the linear plot. It can be considered as the minimum quantity of energy required for the reaction. While, the frequency factor was calculated using the intercept and estimated to (56249.85 s^{-1}). The collision probability between molecules is increased at higher temperatures, which can affect the E_a of the reaction **[38]**. Such value of activation energy proves the catalytic performance of Fe_3O_4/MWCNTs, because it is significantly lower than that of the dissociation of hydrogen peroxide to hydroxyl radicals (213.80 kJ.mol^{-1}) **[35]**.

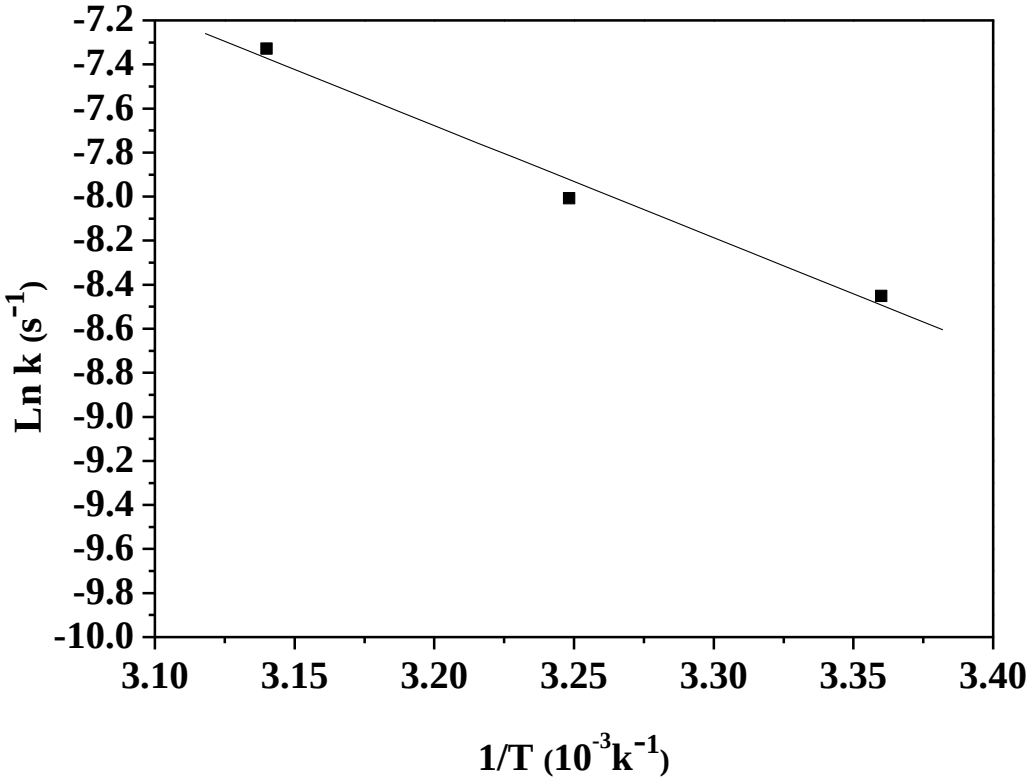

Figure.IV.20. Determination of activation energy.

IV.4.4. The reuse of Fe_3O_4/MWCNTs nanocomposite

Homogeneous Fenton reaction suffers from various drawbacks, that is why the heterogeneous Fenton process was studied and many nanocomposites were developed as an alternative catalysts, with high stability and catalytic performance **[39]**. Figure.IV.23 shows the reuse of catalyst for five successive cycles without any loss in catalytic performance or stability, which makes the Fe_3O_4/MWCNTs a promising catalyst in wastewater treatment **[40]**.

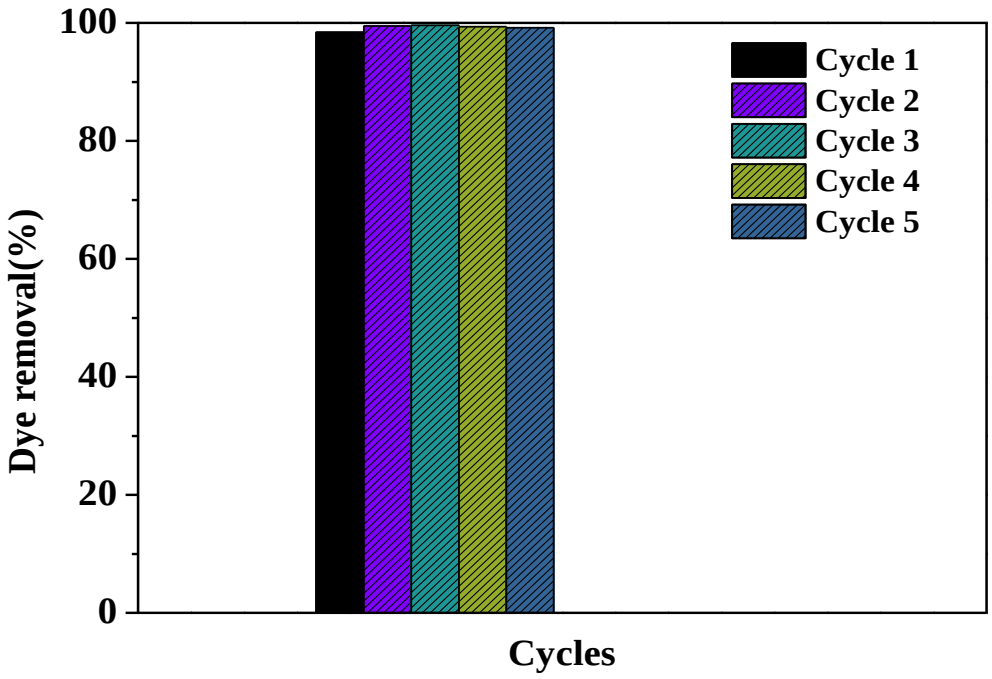

Figure.IV.21. Reuse of the catalyst ($m_{catalyst}$ =20 mg; [CV] = 6 mg.L^{-1}; [H_2O_2] =0.14 mol.L^{-1}; pH=2.5; V=200 mL; T =318 K; t =210 min).

IV.5. Efficiency of Fe_3O_4/MWCNTs catalyst in the removal of CV under polychromatic light

IV.5.1. Photolysis of CV system

According to the curve shown in figure IV.24, the degradation of CV by light in the absence of the catalyst and H_2O_2 is limited. This system is known as the direct photolysis. It consists of exposing the aqueous solution of the dye to polychromatic light. The obtained results indicate that the degradation of the CV dye by direct photolysis has a negligible effect at the initial stage. The organic molecules can be decomposed under the effect of light irradiation by breaking the bonds and producing free radicals, but the decomposition rate was relatively slow (k= $1.53.10^{-3}$.min^{-1}), with modest removal (less than 20%) after a reaction time equal to 180 min (figureIV.25; table IV.12) **[41,42]**.

IV.5.2. Degradation of CV in the presence of H_2O_2 and light irradiation

This system shows the effect of H_2O_2 on the degradation of the dye in the presence of light. When hydrogen peroxide was added (0.14 mol.L^{-1}: which was approximately the optimum value found in the degradation of CV through heterogeneous Fenton degradation).

The rate constant of the reaction reached a value three times higher than that of direct photolysis (k= $5.62.10^{-3}$ min^{-1}). The removal efficiency is increased as well to be about 45% after 180 min. The improvement in the degradation of CV dye is noticed, due to the transformation of hydrogen peroxide to hydroxyl radicals under polychromatic light according to the reaction bellow (eq.22):

$$H_2O_2 + h\upsilon \rightarrow 2HO^{\bullet} \quad \text{(eq.22)}$$

It is likely that hydroxyl radicals react with dye molecules in turn, which leads to the decomposition of organic structure of the pollutant:

$$OH^{\bullet} + CV \rightarrow CV^{\bullet} + H_2O \quad \text{(eq.23)}$$

Presumably, other reactions can take place in the solution as a part of the decoloration process:

$$CV^{\bullet} + O_2 \rightarrow CV{-}O_2^{\bullet} \quad \text{(eq.24)}$$

$$2CV{-}O_2^{\bullet} \rightarrow 2CV{-}O^{\bullet} + O_2 \quad \text{(eq.25)}$$

$$CV{-}O^{\bullet} + O_2 \rightarrow HO_2^{\bullet} + products \quad \text{(eq.26)}$$

Furthermore, peroxy radicals can react also with dye molecules and reproduce hydrogen peroxide as follows **[37, 43]**:

$$HO_2^{\bullet} + CV \rightarrow CV^{\bullet} + H_2O_2 \quad \text{(eq.27)}$$

IV.5.3. Degradation of CV in the presence of Fe_3O_4/MWCNTs and light irradiation

In this system, Fe_3O_4/MWCNTs:1/3 catalyst was introduced to CV solution under polychromatic light irradiation. Slight increase in rate constant (K = 3.74. 10^{-3} min^{-1}), due to relative synergy effect between the composite and light **[44]**. With low removal (35% after 180 min of reaction), which can be explained by the low potential oxidation of Fe^{3+} and Fe^{2+} compared to ·OH radicals produced by the electron accepter H_2O_2 **[45]** .

IV.5.4. Photo-Fenton degradation of CV using Fe_3O_4

This system exhibits a lower rate constant (K = $1.48.10^{-3}$ min^{-1}) and weaker removal percentage (20% after 180 min). This bad result may be due to the agglomeration of magnetite in solution, because the magnetic nanoparticles Fe_3O_4 have high tendency to form aggregates in water, which is resulted by their high surface energy and the interactions of van der Waals **[46, 47]**.

IV.5.5. Photo-Fenton degradation of CV using Fe_3O_4/MWCNTs

This system represents the focus of our study; it is perfectly compatible with the photo-Fenton reaction, which combines Fenton process (Fe^{2+}/H_2O_2) with light energy besides the adsorption of CV molecules onto MWCNTs active sites. Photo-Fenton oxidation consists of two reactions occurred repeatedly and produce radicals in order to attack the organic

structure of dyes; the first one was between Fe^{2+} and H_2O_2, which generates hydroxyl radicals and oxide Fe^{2+} to Fe^{3+}, as shown in (eq.28):

$$Fe^{2+} + H_2O_2 \rightarrow Fe^{3+} + HO^{\cdot} + HO^{-} \qquad \text{(eq.28)}$$

Hydroxyl radicals are considered as the most powerful oxidant, which can completely degrade the organic contaminants to carbon dioxide and water.

The second photo-Fenton reaction occurred between Fe^{3+} and H_2O under polychromatic light. Herein, hydroxyl radicals have been generated and the Fe^{3+} is reduced to Fe^{2+} (eq.29):

$$Fe^{3+} + H_2O + h\upsilon \rightarrow Fe^{2+} + HO^{\cdot} + H^{+} \qquad \text{(eq.29)}$$

On the other hand, the nanocomposite Fe_3O_4/MWCNTs:1/3 combined between photocatalytic activity of magnetite and the great adsorptivity of carbon nanotubes **[45]**, which imparted high and quick degradation of CV dye (more than 90% after 180 min of reaction) with rate constant estimated to $1.28.10^{-2}$ min^{-1}. Therefore, the catalyst Fe_3O_4/MWCNTs in the presence of polychromatic light and H_2O_2 represents the best system.

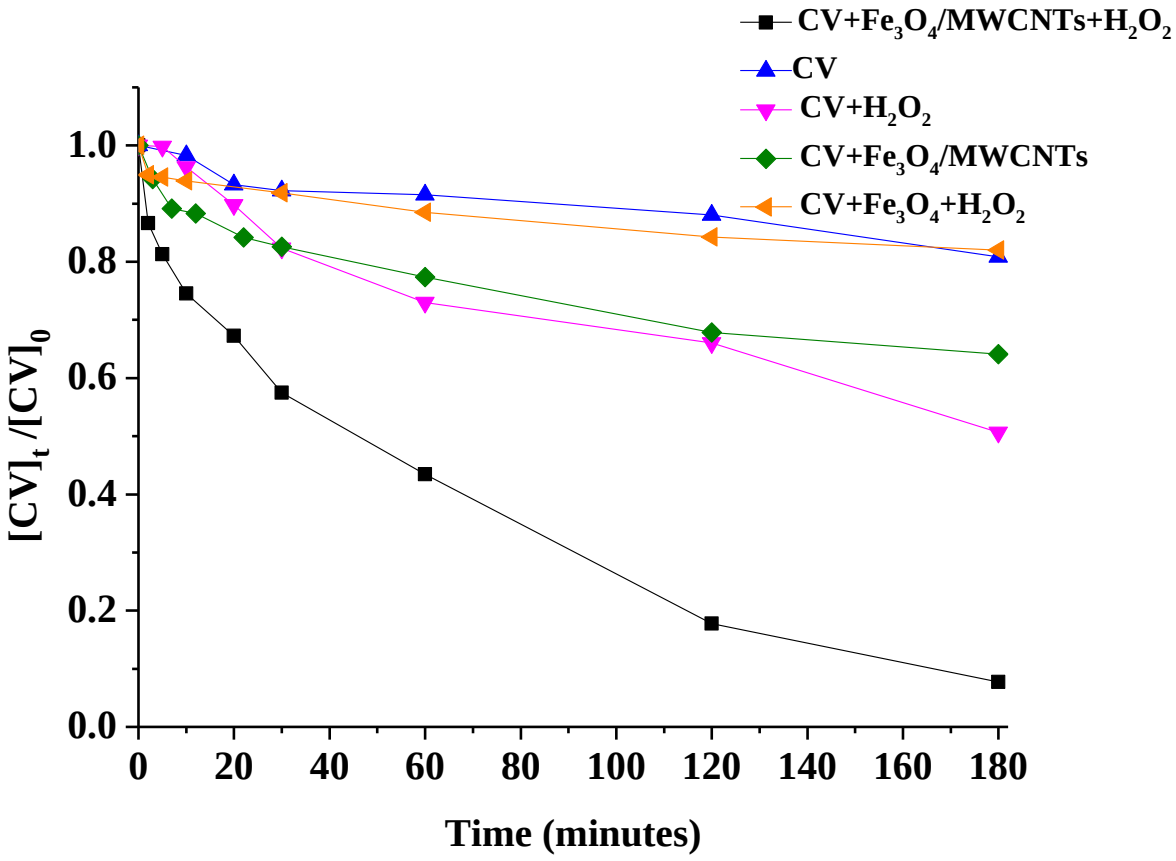

Figure. IV.22. The influence of different systems onto the degradation of CV dye (θ=25 °C; V=100 mL; $[CV]_0$= 4 $mg.L^{-1}$; pH = 2.5; m = 10 mg, $[H_2O_2]$=0.14 $mol.L^{-1}$).

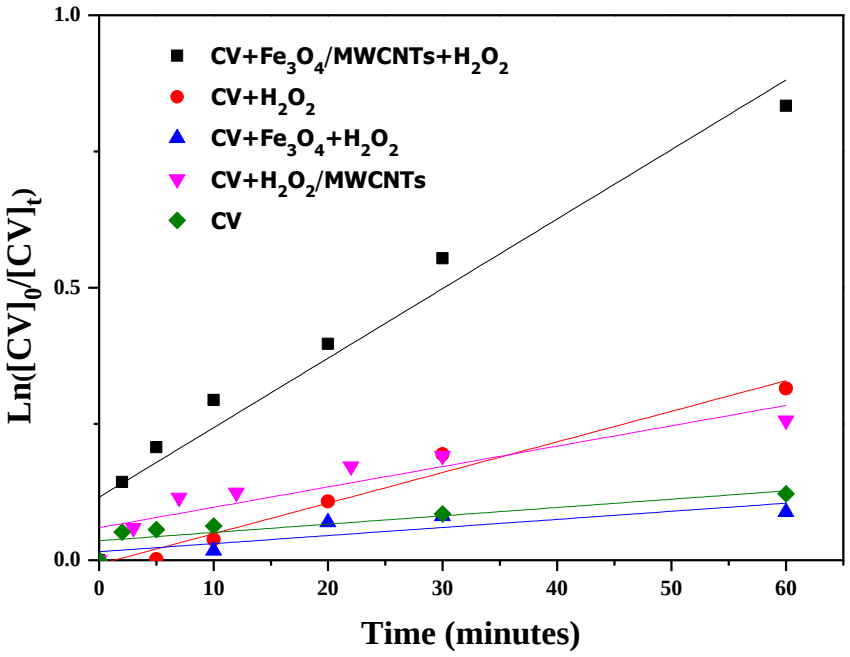

Figure. IV.23. Linearization of the first order kinetic at different systems.

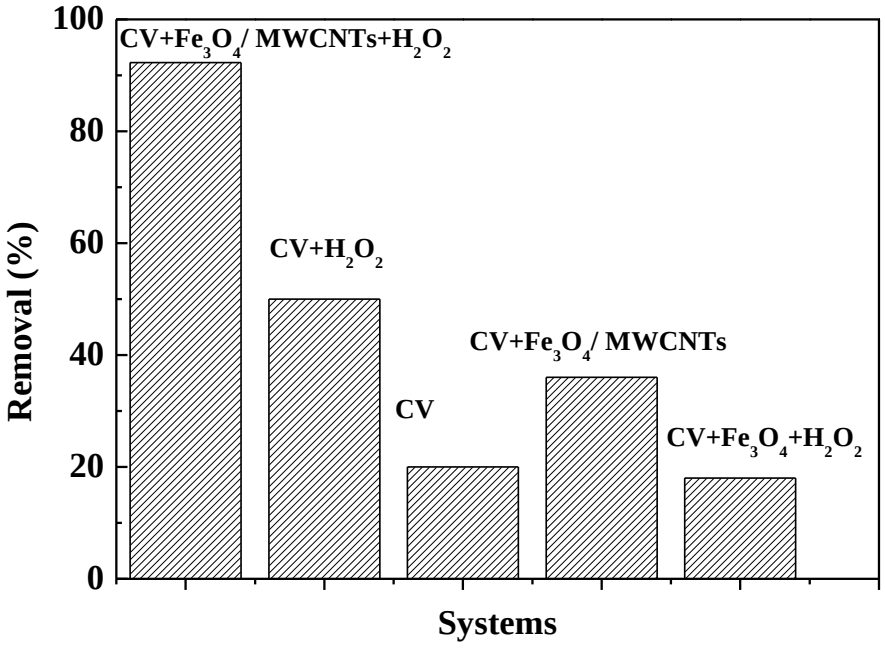

Figure.IV.24. Comparison between the removal rates under polychromatic light obtained by different systems.

Table.IV.11. The rate constant of CV dye degradation.

System	Rate constant k (min^{-1})	R^2	SE
CV+ Fe_3O_4/MWCNTs +H_2O_2	1.28. 10^{-2}	0.94	1.29.10^{-3}
CV+H_2O_2	5.62.10^{-3}	0.97	4.38.10^{-4}
CV	1.53.10^{-3}	0.65	5.13.10^{-4}
CV+ Fe_3O_4/MWCNTs	3.74. 10^{-3}	0.80	7.31.10^{-4}
CV+Fe_3O_4+H_2O_2	1.48.10^{-3}	0.72	4.04.10^{-4}

IV.6. Conclusion

Experimental results revealed that the synthesis of nanocomposite Fe_3O_4/MWCNTs was successful. This material exhibited high adsorption capacity and great catalytic activity in the removal of organic dye from aqueous solution. The huge specific surface area of MWCNTs exhibits high adsorption of Bromocresol Purple dye in short time. Furthermore, the oxidation of Crystal Violet dye via heterogeneous Fenton and photo-Fenton using Fe_3O_4/MWCNTs shows high removal efficiency. The magnetite has transformed the separation from tedious and slower to easier and faster method.

References

[1] X. Duan, H. Sun, Y. Wang, J. Kang, et S. Wang, « N-Doping-Induced Nonradical Reaction on Single-Walled Carbon Nanotubes for Catalytic Phenol Oxidation », ACS Catalysis., vol. 5, nº 2, p. 553‑559, févr. 2015, doi: 10.1021/cs5017613.

[2] X. Hu et al., « Adsorption and heterogeneous Fenton degradation of 17α-methyltestosterone on nano Fe_3O_4/MWCNTs in aqueous solution », Applied Catalysis B: Environmental, vol. 107, nº 3, p. 274‑283, sept. 2011.

[3] V. Cleveland, J.-P. Bingham, et E. Kan, « Heterogeneous Fenton degradation of bisphenol A by carbon nanotube-supported Fe_3O_4 », Separation and Purification Technology, vol. 133, p. 388‑395, sept. 2014, doi: 10.1016/j.seppur.2014.06.061.

[4] L. Houcine, L. Sonia, R. Schneider, et T. B. Chaabane, « Synthesis and Characterizations of ZnS:Cu/ZnS Assisted by 3-Mercaptopropionic Acid », Chemistry Africa, vol. 1, nº 1‑2, p. 37‑42, juin 2018, doi: 10.1007/s42250-018-0007-7.

[5] N. Dalali, M. Habibizadeh, K. Rostamizadeh, et S. Nakisa, « Synthesis of magnetite multi-walled carbon nanotubes composite and its application for removal of basic dyes from aqueous solutions: Removal of basic dyes », Asia-Pacific Journal of Chemical Engineering , vol. 9, no 4, p. 552-56, janv. 2014, doi: 10.1002/apj.1784.

[6] Y. Wei, B. Han, X. Hu, Y. Lin, X. Wang, et X. Deng, « Synthesis of Fe_3O_4 Nanoparticles and their Magnetic Properties », Procedia Engineering, vol. 27, p. 632‑637, 2012, doi: 10.1016/j.proeng.2011.12.498.

[7] M. H. Razali, A. Ahmad, M. A. Azaman, et K. A. M. Amin, « Physicochemical Properties of Carbon Nanotubes (CNT's) Synthesized at Low Temperature using Simple Hydrothermal Method », International Journal of Applied Chemistry, vol. 12, no 3, p. 273-280, 2016.

[8] Gadjah Mada, T. Sulistyaningsih, S. J. Santosa, D. Siswanta, B. Rusdiarso, « Synthesis and Characterization of Magnetites Obtained from Mechanically and Sonochemically Assissted Co-precipitation and Reverse Co-precipitation Methods », international journal of materials, mechanics and manufacturing, vol. 5, nº 1, p. 16‑19, févr. 2017, doi: 10.18178/ijmmm.2017.5.1.280.

[9] R. Shanks, S. Ahmad, et L.-J. Yu, « Multiwalled carbon nanotubes-magnetite reinforced thermoplastic polypropylene-natural rubber blends », World Journal of Engineering, 2013.

[10] N. Fiol et I. Villaescusa, « Determination of sorbent point zero charge: usefulness in sorption studies », Environmental Chemistry Letters, vol. 7, nº 1, p. 79‑84, févr. 2009, doi: 10.1007/s10311-008-0139-0.

[11] Das, R., Leo, B. F., & Murphy, F. The toxic truth about carbon nanotubes in water purification: a perspective view. Nanoscale research letters, 13(1), 1-10., 2018.

[12] Z. Rehimi, H. Ayadi, et S. Halladja, « Synthesis and characterization of Fe_3O_4−MWCNTs adsorbent: application for Bromocresol Purple dye removal in aqueous medium », journal of new technology and materials, vol 10, n° 1 p. 7, 31-37, 2020.

[13] F. M. El-Dars, H. M. Ibrahim, H. A. Farag, M. Z. Abdelwahhab, et M. E. H. Shalabi, « Using bentonite carbon composite material for adsorption of Bromocresol Purple and methylene blue », international journal of science and engineering research., vol. 6, nº 10, p. 188‑197, 2015.

[14] A. Bonilla-Petriciolet, D. I. Mendoza-Castillo, et H. E. Reynel-Ávila, Éd., Adsorption Processes for Water Treatment and Purification. Cham: Springer International Publishing, 2017.

[15] « CiNii Articles - Zur theorie der sogenannten adsorption geloster stoffe ». https://ci.nii.ac.jp/naid/10027970486/.

[16] Y. S. Ho et G. McKay, « The sorption of lead(II) ions on peat », Water Research, vol. 33, nº 2, p. 578‑584, févr. 1999, doi: 10.1016/S0043-1354(98)00207-3.

[17] S. K. Silvanus, « fabrication and characterization of magnetoresponsive carbon nanotube-infused polysulfone (cnt-ipsf) nanocomposites for water purification », p. 170.

[18] N. Rouahna, D. Barkat, A. Ouakouak, et E. Srasra, « Synthesis and characterization of Mg-Al layered double hydroxide intercalated with D2EHPA: Application for copper ions removal from aqueous solution », Journal of Environmental Chemical Engineering, vol. 6, nº 1, p. 1226‑1232, févr. 2018, doi: 10.1016/j.jece.2018.01.036.

[19] V. Rastogi, P. Yadav, S.S. Bhattacharya, A.K. Mishra, N. Verma, A. Verma, & J.K. Pandit, « Carbon Nanotubes: An Emerging Drug Carrier for Targeting Cancer Cells », Journal of Drug Delivery, vol 2014, avr. 24, 2014. https://www.hindawi.com/journals/jdd/2014/670815/.

[20] Sun, Lian-Ming, and Françis Meunier. "Adsorption: aspects théoriques." Techniques de l'ingénieur, technologies de l'eau, vol 2, p 730, 2007.

[21] Langmuir, Irving «The adsorption of gases on plane surfaces of glass, mica and platinum » Journal of the American Chemical society, 1918, vol. 40, no 9, p. 1361-1403, https://doi.org/10.1021/ja02242a004.

[22] Hall, Kenneth R., Eagleton, Lee C., ACRIVOS, Andreas, et al. Pore-and solid-diffusion kinetics in fixed-bed adsorption under constant-pattern conditions. Industrial & Engineering Chemistry Fundamentals, 1966, vol. 5, no 2, p. 212-223, doi: https://doi.org/10.1021/i160018a011.

[23] Hamdaoui, Oualid et Nafferchoux, Emmanuel. Modeling of adsorption isotherms of phenol and chlorophenols onto granular activated carbon: Part I. Two-parameter models and equations allowing determination of thermodynamic parameters. Journal of hazardous materials, 2007, vol. 147, no 1-2, p. 381-394, doi: https://doi.org/10.1016/j.jhazmat.2007.01.021.

[24] Freundlich, H. M. F, Over the adsorption in solution. Phys. Chem, 57(385471), 1100-1107, 1906,dooi: https://doi.org/10.1515/zpch-1907-5723.

[25] Adebowale, K. O., Olu-Owolabi, B. I., & Chigbundu, E. C.. Removal of safranin-O from aqueous solution by adsorption onto kaolinite clay. Journal of Encapsulation and Adsorption Sciences, 4(03), 89, (2014), 10.4236/jeas.2014.43010.

[26] Özcan, A. S., Erdem, B., & Özcan, A. Adsorption of Acid Blue 193 from aqueous solutions onto BTMA-bentonite. Colloids and Surfaces A: Physicochemical and engineering aspects, 266(1-3), 73-81, 2005, https://doi.org/10.1016/j.colsurfa.2005.06.001.

[27] Rouahna, N., Barkat, D., Ouakouak, A., & Srasra, E. Synthesis and characterization of Mg-Al layered double hydroxide intercalated with D2EHPA: Application for copper ions removal from aqueous solution. Journal of environmental chemical engineering, 6(1), 1226-1232, 2018, https://doi.org/10.1016/j.jece.2018.01.036.

[28] W. Konicki, I. Pełech, E. Mijowska, et I. Jasińska, « Adsorption Kinetics of Acid Dye Acid Red 88 onto Magnetic Multi-Walled Carbon Nanotubes-Fe_3C Nanocomposite: Adsorption Kinetics of Acid Dye Acid Red 88 », Clean Soil Air Water, vol. 42, n° 3, p. 284‑294, mars 2014, doi: 10.1002/clen.201200458.

[29] M. Taniguchi et J. S. Lindsey, « Database of Absorption and Fluorescence Spectra of >300 Common Compounds for use in PhotochemCAD », Photochemistry and Photobiology, vol. 94, n° 2, p. 290‑327, 2018, doi: https://doi.org/10.1111/php.12860.

[30] Crini, G., & Badot, P. M. Application of chitosan, a natural aminopolysaccharide, for dye removal from aqueous solutions by adsorption processes using batch studies: a review of recent literature. Progress in polymer science, 33(4), 399-447, 2008, doi : https://doi.org/10.1016/j.progpolymsci.2007.11.001.

[31] V. Cleveland, J.-P. Bingham, et E. Kan, « Heterogeneous Fenton degradation of bisphenol A by carbon nanotube-supported Fe_3O_4 », Separation and Purification Technology, vol. 133, p. 388‑395, sept. 2014, doi: 10.1016/j.seppur.2014.06.061.

[32] L. Zhou, H. Zhang, L. Ji, Y. Shao, et Y. Li, « Fe_3O_4/MWCNT as a heterogeneous Fenton catalyst: Degradation pathways of tetrabromobisphenol A », RSC Advances, vol. 4, p. 24900, juin 2014, doi: 10.1039/c4ra02333a.

[33] M. Nagamine, M. Osial, K. Jackowska, P. Krysinski, et J. Widera-Kalinowska, « Tetracycline Photocatalytic Degradation under CdS Treatment », journal of marine science and engineering , vol. 8, n° 7, p. 483, juin 2020, doi: 10.3390/jmse8070483.

[34] H.-Y. Phin, Y.-T. Ong, et J.-C. Sin, « Effect of carbon nanotubes loading on the photocatalytic activity of zinc oxide/carbon nanotubes photocatalyst synthesized via a modified sol-gel method », Journal of Environmental Chemical Engineering, vol. 8, n° 3, p. 103222, juin 2020, doi: 10.1016/j.jece.2019.103222.

[35] Y. Zhang et al., « Synergistic effect in heterogeneous Fenton degradation of tetrabromobisphenol A by MWCNT and β-CD co-modified Fe_3O_4 », Materials Research Bulletin, vol. 113, p. 14‑24, 2019.

[36] A. R. Dhahawi Ahmad, S. S. Imam, W. D. Oh, et R. Adnan, « Fe_3O_4-Zeolite Hybrid Material as Hetero-Fenton Catalyst for Enhanced Degradation of Aqueous Ofloxacin Solution », Catalysts, vol. 10, n° 11, p. 1241, oct. 2020, doi: 10.3390/catal10111241.

[37] X. Zhang et al., « Fe_3O_4@C nanoparticles as high-performance Fenton-like catalyst for dye decoloration », Chinese Science Bulletin, vol. 59, p. 3406‑3412, sept. 2014, doi: 10.1007/s11434-014-0439-7.

[38] H.-Y. Xu et al., « Heterogeneous Fenton-like discoloration of methyl orange using Fe_3O_4/MWCNTs as catalyst: kinetics and Fenton-like mechanism », Frontiers of Materials Science, vol. 12, févr. 2018, doi: 10.1007/s11706-018-0412-5.

[39] Y. Chen, P. Pötschke, J. Pionteck, B. Voit, et H. Qi, « Fe_3O_4 Nanoparticles Grown on Cellulose/GO Hydrogels as Advanced Catalytic Materials for the Heterogeneous Fenton like Reaction », ACS Omega, vol. 4, n° 3, p. 5117‑5125, mars 2019, doi: 10.1021/acsomega.9b00170.

[40] B. Kakavandi, N. Jaafarzadeh, A. Takdastan, R. Rezaei Kalantary, et S. Jorfi, « Powder activated carbon/ Fe_3O_4 hybrid composite as a highly efficient heterogeneous catalyst for Fenton oxidation of tetracycline: Degradation mechanism and kinetic », RSC Advances, vol. 5, sept. 2015, doi: 10.1039/C5RA17953J.

[41] W. Huang, « Homogeneous and heterogeneous Fenton and photo-Fenton processes: impact of iron complexing agent ethylenediamine-N,N'-disuccinic acid (EDDS) », p. 198, 2012.

[42] M. I. Litter, « Introduction to Photochemical Advanced Oxidation Processes for Water Treatment », in Environmental Photochemistry Part II, P. Boule, D. W. Bahnemann, et P. K. J. Robertson, Éd. Berlin, Heidelberg: Springer, 2005, p. 325‑366.

[43] F. A. Alshamsi, A. S. Albadwawi, M. M. Alnuaimi, M. A. Rauf, et S. S. Ashraf, « Comparative efficiencies of the degradation of Crystal Violet using UV/hydrogen peroxide and Fenton's reagent », Dyes and Pigments, vol. 74, n° 2, p. 283‑287, janv. 2007, doi: 10.1016/j.dyepig.2006.02.016.

[44] L. Houcine, L. Sonia, R. Schneider, et T. B. Chaabane, « Synthesis and Characterizations of ZnS:Cu/ZnS Assisted by 3-Mercaptopropionic Acid », Chemistry Africa, vol. 1, n° 1‑2, p. 37‑42, juin 2018, doi: 10.1007/s42250-018-0007-7.

[45] Kim, Min Il, In, Se Jin, Kim, Hyuk, Kim, Jong-Gyu, et Lee, Young-Seak, « Improved Photo Degradation of Rhodamine B Dye using Iron Oxide/Carbon Nanocomposite by Photo-Fenton Reaction », Carbon letters, vol. 9, n° 3, p. 195‑199, sept. 2008, doi: 10.5714/CL.2008.9.3.195.

[46] S. Feijoo, J. González-Rodríguez, L. Fernández, C. Vázquez-Vázquez, G. Feijoo, et M. T. Moreira, « Fenton and Photo-Fenton Nanocatalysts Revisited from the Perspective of Life Cycle Assessment », Catalysts, vol. 10, n° 1, p. 23, déc. 2019, doi: 10.3390/catal10010023.

[47] W. Konicki, I. Pełech, E. Mijowska, et I. Jasińska, « Adsorption Kinetics of Acid Dye Acid Red 88 onto Magnetic Multi-Walled Carbon Nanotubes-Fe_3C Nanocomposite: Adsorption Kinetics of Acid Dye Acid Red 88 », Clean Soil Air Water, vol. 42, n° 3, p. 284‑294, mars 2014, doi: 10.1002/clen.201200458.

Conclusion

Conclusion

The nanocomposite Fe_3O_4/MWCNTs has been successfully synthesized from oxidized MWCNTs and mixture of iron salts in basic medium via coprecipitation method. The obtained nanomaterial was characterized using different techniques: X-ray diffraction (XRD); Fourier transform infrared spectroscopy (FTIR); Brunauer-Emmett-Teller (BET) and scanning electron microscopy (SEM), which has confirmed the presence of magnetite in the surface of MWCNTs. The BET analysis showed that the specific surface area (SSA) of the nanocomposite is increased with the increase of MWCNTs loading and the best value of SSA (269.38 $m^2.g^{-1}$) was obtained with the ratio 'Fe_3O_4/MWCNTs: 1/3'. This is due to the tendency of magnetite to agglomerate which attributed to the strong interactions (magneto-dipole) among the nanoparticles.

The nanocomposite Fe_3O_4/MWCNTs was used as an adsorbent for the removal of Bromocresol Purple anionic dye from aqueous medium, and exhibited high adsorption capacity equal to 296.52 $mg.g^{-1}$. Kinetic study of the adsorption revealed that pseudo second order fitted well the process. While, isotherm modeling indicated that Langmuir isotherm best suited this adsorption.

For the heterogeneous Fenton process, the removal efficiency of Crystal Violet was about: 98.5% for Fe_3O_4/MWCNTs: 1/1and 98.77 for Fe_3O_4/MWCNTs: 1/3. The optimum values of hydrogen peroxide concentration and temperature were estimated to 0.14 $mol.L^{-1}$ and 318 K, respectively. According to the activation energy value, it did not require high energy to remove CV via heterogeneous Fenton reaction. The study of the stability of the catalyst revealed that it can be reused for five cycles with high efficiency.

The degradation of the CV dye via the heterogeneous photo-Fenton process by the Fe_3O_4/MWCNTs catalyst shows very high efficiency. In order to quantify the effect of the studied nanocomposite on the degradation of the pollutant under polychromatic light, the influence of some systems was discussed. The different systems can be classified according to their removal efficiency and rate constant in the following order:

$CV+ Fe_3O_4/MWCNTs+H_2O_2 > CV+H_2O_2 > CV+Fe_3O_4/MWCNTs > CV > CV+Fe_3O_4+H_2O_2$

Therefore, $CV+Fe_3O_4$/MWCNTs $+H_2O_2$ is the best system with a higher removal efficiency (more than 90%) and a relatively high rate constant estimated to of $1.28.\ 10^{-2}\ min^{-1}$.

As a result, Fe_3O_4/MWCNTs has an outstanding performance in the removal of dye contaminants with low energy, simple devices and fast magnetic separation.

Further studies should be done in the future with this nanocomposite owing to its high reactivity and stability such as:

- Investigate the adsorption efficiency of this nanocomposite towards other organic pollutants, heavy metals and pesticides.
- Implement this work at large scale.
- Evaluate the behavior of Fe_3O_4/MWCNTs in hydrogen storage.

Abstract

تطوير و توصيف مركب نانوي Fe_3O_4/MWCNTs.

التطبيق في إزالة الأصباغ العضوية في محلول مائي .

تتزايد تقنيات تنقية المياه كل يوم إلى جانب تطوير مواد جديدة بحثًا عن تقنيات فعالة للتخلص من الملوثات الضارة. بحثت هذه الدراسة في كفاءة المركب Fe_3O_4/MWCNTs في معالجة مياه الصرف الصحي ضد ملوثات الأصباغ العضوية. لقد تم تصنيع هذه المادة النانوية بنجاح بطريقة الترسيب المزدوج. توصيف Fe_3O_4/MWCNTs تم باستعمال حيود الأشعة السينية (XRD)؛ مطيافية فوريه لتحويل الأشعة تحت الحمراء (FTIR) إلى جانب Brunauer-Emmett-Teller(BET) والفحص المجهري الإلكتروني (SEM) ، وقد تم تأكيد وجود أكسيد الحديد الأسود في المركب النانوي مع انتشار جيد. تم فحص امتزاز صبغة البروموكريسول الأرجواني (BCP) الأنيونية في الوسط المائي من أجل تقييم قدرة الامتزاز للمركب النانوي ، والتي قدرت بحوالي 296,52مغ/غ. تشير الدراسة الحركية إلى أن الزمن اللازم لحدوث التوازن يقدر بـ 90 دقيقة وأن الدرجة الثانية لنموذج الحركة هو الأنسب لهذه العملية. تظهر نمذجة الأيزوثرم أن الامتزاز يتلاءم بشكل جيد مع نموذج لنغمير. كشفت الدراسة الديناميكية الحرارية أن آلية الامتزاز تظهر طبيعة عشوائية ومحررة للحرارة. كما قد تم تقييم كفاءة Fe_3O_4/MWCNTs كمحفز لإزالة صبغة الكريستال البنفسجي (CV). وفقًا للنتائج التي تم الحصول عليها من نسبة إزالة الملون وثابت السرعة ؛يمثل كل من نسبة الوزن 1/3؛ تركيز الماء الاوكسيجني H_2O_2 0,14 مول/ل و درجة الحرارة 318 كلفن الظروف المثلى لتفاعل فنتون غير المتجانس. علاوة على ذلك ، أظهر المحفز ثباتًا عاليًا لأنه يمكن إعادة استخدامه لخمس دورات متتالية دون أي فقد في كفاءته حيث ظلت نسبة إزالته شبه تامة عند كل مرة. تم التحقق أيضا من تأثير بعض الأنظمة ومقارنتها تحت تأثير ضوء متعدد الألوان (450-300 نانومتر) ، وفقًا لنسبة الإزالة وثابت السرعة المحسوب لكل نظام. وقد تم تصنيف تأثير مختلف الأنظمة على إزالة الصبغة بالترتيب التالي:

$CV+Fe_3O_4/MWCNTs+H_2O_2 > CV+H_2O_2 > CV+Fe_3O_4/MWCNTs > CV > CV+Fe_3O_4+H_2O_2$

وقد أظهر النظام $Fe_3O_4/MWCNTs+H_2O_2$ نسبة إزالة للملون CV مرتفعة جدًا (أكثر من 90٪) بالنسبة لبقية الأنظمة. تشير هذه النتائج إلى أهمية المحفز في معالجة المياه ، وتظهر إمكانية استخدامه على نطاق واسع.

الكلمات المفتاحية: الكربون النوني ؛ أكسيد الحديد الأسود؛ أصباغ عضوية ؛ الامتزاز؛ فنتون غير متجانس؛ فنتون الضوئي.

Résumé

Les technologies de purification de l'eau, tout comme le développement de nouveaux nanomatériaux, se développent chaque jour à la recherche de techniques efficaces pour éliminer les polluants récalcitrants. Cette étude a pour objectif d'examiner l'efficacité du nanocomposite magnétique Fe_3O_4/MWCNTs dans le traitement des eaux contaminées par les colorants organiques. Ce nanomatériau a été synthétisé par la méthode de co-précipitation. La caractérisation de Fe_3O_4/MWCNTs a été effectuée par diffraction des rayons X (DRX), spectroscopie infrarouge à transformée de Fourier (IRTR), Brunauer-Emmett-Teller (BET) et microscopie électronique à balayage (MEB). L'adsorption du colorant anionique Pourpre de Bromocrésol (PBC) en milieu aqueux a été étudiée afin d'évaluer la capacité d'adsorption du nanocomposite Fe_3O_4/MWCNTs, qui est estimée à environ 296,52 $mg.g^{-1}$. L'étude cinétique indique que le temps d'équilibre est de 90 minutes et que le pseudo second ordre convient le mieux à ce processus. L'étude des isothermes a montré que l'adsorption est bien adaptée au modèle de Langmuir. L'étude thermodynamique a révélé que le mécanisme de sorption présente une nature spontanée, exothermique et de physisorption. L'évaluation de l'efficacité de Fe_3O_4/MWCNTs comme catalyseur a été également étudiée dans l'élimination du colorant Crystal Violet (CV). Selon les résultats obtenus, le rapport de poids Fe_3O_4/MWCNTs: 3/1, une concentration de H_2O_2 de 0,14 $mol.L^{-1}$ et une température de 318 K, étaient les conditions optimales pour la dégradation hétérogène de Fenton. De plus, le catalyseur a montré une grande stabilité car il peut être réutilisé jusqu'à cinq cycles successifs sans aucune perte de son efficacité puisque le taux de dégradation est quasi-total. L'influence de certains systèmes a été vérifiée et comparée, selon le taux de dégradation et la constante de vitesse calculée avec celle du nanocomposite sous l'irradiation d'une lumière polychromatique (300-450 nm). L'efficacité de la dégradation des systèmes testés est classée dans l'ordre suivant :

$CV+Fe_3O_4/MWCNTs+H_2O_2 > CV+H_2O_2 > CV+Fe_3O_4/MWCNTs > CV > CV+Fe_3O_4+H_2O_2$

Le système Fe_3O_4/MWCNTs $+H_2O_2$ a montré un taux de dégradation très élevé (plus de 90%) par rapport aux autres systèmes. Ces résultats indiquent l'importance du catalyseur Fe_3O_4/MWCNTs dans le traitement des eaux et montrent la possibilité de son utilisation à grande échelle.

Mots clés : MWCNTs ; magnétite ; colorants organiques ; adsorption ; Fenton hétérogène; photo-Fenton.

Abstract

Water purification technology is growing every day along with the developing of new nanomaterials in search of effective techniques to eliminate recalcitrant pollutants. This study investigated the efficiency of synthesized magnetic nanocomposite Fe_3O_4/MWCNTs in wastewater treatment against organic dyes contaminants. This nanomaterial was successfully synthesized via coprecipitation method. The characterization of Fe_3O_4/MWCNTs with X-ray diffraction (XRD); Fourier transform infrared spectroscopy (FTIR); Brunauer-Emmett-Teller (BET) and scanning electron microscopy (SEM) were carried out, which confirmed the presence of magnetite in the nanocomposite with good dispersion. The adsorption of Bromocresol Purple (BCP) anionic dye from aqueous medium was investigated in order to evaluate the adsorption capacity of the nanocomposite, which was around 296.52 $mg.g^{-1}$. Kinetic study indicates that the equilibrium time was estimated to 90 minutes and the pseudo second order best suited this process. Isotherm modeling shows that the adsorption was fitted well by the Langmuir model. Thermodynamic study revealed that the sorption mechanism exhibits a spontaneous, exothermic and physisorption nature. The evaluation of the efficiency of Fe_3O_4/MWCNTs as a catalyst was studied for the removal of Crystal Violet dye (CV). According to the results obtained by rate constants and kinetic studies, the 3:1 weight ratio; the H_2O_2 concentration of 0.14 $mol.L^{-1}$ and temperature of 318 K were the optimum conditions for the heterogeneous Fenton degradation of CV. Furthermore, the catalyst exhibited high stability because it can be reused for five successive cycles without any loss in its efficiency since the degradation rate remains almost complete. We also investigated the efficiency of Fe_3O_4/MWCNTs as a catalyst to eliminate CV in aqueous solution under polychromatic light (300-450 nm). The influence of certain systems on the degradation of CV was verified and compared, by calculating the degradation rate and rate constant. The degradation effect of the different systems is classified in the following order:

$CV+Fe_3O_4/MWCNTs+H_2O_2 > CV+H_2O_2 > CV+Fe_3O_4/MWCNTs > CV > CV+Fe_3O_4+H_2O_2$

The $Fe_3O_4/MWCNT+H_2O_2$ system showed a very high degradation rate (over 90%) compared to the other systems. These results indicate the importance of Fe_3O_4/MWCNTs catalyst in water treatment, and show the possibility of its use at large scale.

Keywords: MWCNTs; magnetite; organic dyes; adsorption; heterogeneous Fenton; photo Fenton.